

MICROWAVE ELECTRONICS

NON-DESTRUCTIVE TESTING OF NON-METALLIC MATERIALS USING MICROWAVES

**A THESIS SUBMITTED BY
P. VENUGOPALAN**

**IN PARTIAL FULFILMENT OF THE REQUIREMENTS
FOR THE DEGREE OF
DOCTOR OF PHILOSOPHY**

**COCHIN UNIVERSITY OF SCIENCE AND TECHNOLOGY
FACULTY OF TECHNOLOGY
DEPARTMENT OF ELECTRONICS
KOCHI - 682 022
INDIA**

AUGUST 1991

*Dedicated
to
my parents*

CERTIFICATE

This is to certify that the thesis entitled "NON-DESTRUCTIVE TESTING OF NON-METALLIC MATERIALS USING MICROWAVES" is a bona fide record of the research work carried out by Mr.P.Venugopalan under my supervision in the Department of Electronics, Cochin University of Science and Technology. The results embodied in this thesis or part of it have not been presented for any other degree.



Dr.K.G.Nair
(Supervising Teacher)
Professor and Head
Department of Electronics
Cochin University of
Science and Technology

Kochi - 682 022

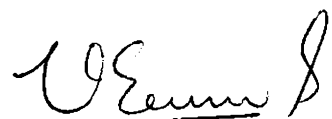
2nd August 1991

DECLARATION

I hereby declare that the work presented in the thesis entitled "NON-DESTRUCTIVE TESTING OF NON-METALLIC MATERIALS USING MICROWAVES" is based on the original work done by me under the supervision of Dr.K.G.Nair, in the Department of Electronics, Cochin University of Science and Technology, and that no part thereof has been presented for the award of any other degree.

Kochi - 682 022

2nd August 1991



P.VENUGOPALAN

ACKNOWLEDGEMENTS

I am extremely grateful to my guide and supervisor, Dr.K.G.Nair, Professor and Head of the Department of Electronics, Cochin University of Science and Technology (CUSAT) for his able guidance and competent advice throughout the progress of this research programme. He has been a source of constant encouragement and inspiration, which ultimately helped me in completing this work.

I wish to express my sincere gratitude to the Director, Naval Physical and Oceanographic Laboratory (NPOL) for providing necessary facilities and for the help and support he has provided during the course of this work. I also wish to thank senior scientific officers of the above laboratory, Mr.M.K.S.Pillai, Sc-'E', Mr.V.Chander, Sc-'F', and Mr.A.V.Prabhu, Sc-'E' for the goodwill and co-operation they have extended to me. I am thankful to all the scientific staff of NPOL, especially Dr.D.Devarajan, Sc-'D', Mr.K.Govindan, Sc-'D', Dr.P.A.Pravinkumar, Sc-'C', Mr.K.G.Ayyappan Pillai, Sc-'C', Mr.Thomas Antony, Sc-'B', and Mr.Thomas Mathew Panicker, Sc-'B', for the keen interest they have shown in the progress of my work.

I have received invaluable help and inspiration from Dr.K.A.Jose, Dr.P.Mohanan, Dr.C.K.Aanandan, Dr.K.Vasudevan and Dr.K.T.Mathew, all members of the

faculty of the Department of Electronics, CUSAT. I acknowledge with pleasure the co-operation from other faculty members and staff of the same department.

My special thanks are due to Mr.V.Ajaikumar, Mr.K.K.Narayanan, Mr.Supriyo Dey, Mr.Stephen Rodrigous and Mr.Wilson Gomez, all research scholars in the microwave laboratory of the Department of Electronics, CUSAT, for providing assistance for the completion of this work.

During the period of this work, I was enjoying fellowships from CSIR, ISRO and DAE. I acknowledge with thanks the financial support provided by these agencies.

I wish to place on record the help and assistance offered by Mr.V.R.Ravindran, Scientist, VSSC, Trivandrum and Mr.P.K.Chaturvedi, Scientist, SPROB, SHAR Centre, Sriharikota for making arrangements for the conduct of experiments at VSSC, Trivandrum.

My sincere thanks to Mr.C.B.Muraleedharan for providing talented technical assistance. Mr.K.P.Sibiraj and Mr.V.M.Peter have helped me to bring out this thesis in the present form. I sincerely acknowledge the assistance offered by them.

Finally, I wish to acknowledge the patience and love of my wife and mother-in-law without which I could not have completed this work. I am also grateful to all who have great concern for me.

CONTENTS

	<u>Page</u>
Chapter 1 INTRODUCTION ..	1
Chapter 2 MEASUREMENT TECHNIQUES AND EXPERIMENTAL ARRANGEMENTS ..	27
Chapter 3 EXPERIMENTAL RESULTS ..	60
Chapter 4 ANALYSIS OF EXPERIMENTAL RESULTS ..	119
Chapter 5 CONCLUSIONS AND SCOPE FOR FURTHER WORK ..	139
Appendix I BANDWIDTH ENHANCEMENT OF MICROSTRIP ANTENNAS BY SHUNT IMPEDANCE TECHNIQUE ..	147
Appendix II A COMPACT DUAL FREQUENCY MICROSTRIP ANTENNA ..	159
Appendix III BANDWIDTH ENHANCEMENT BY A FLARED MICROSTRIP DIPOLE ANTENNA (FMDA) ..	166
REFERENCES ..	172
INDEX ..	179
LIST OF PUBLICATIONS OF THE AUTHOR ..	181

Chapter 1

INTRODUCTION

	<u>Page</u>
1.1 General Introduction ..	2
1.2 Various NDT Techniques ..	3
1.3 Motivation for the Present Work ..	6
1.4 The need for Microwave NDT ..	6
1.5 Essential Test Facilities Required for Microwave NDT ..	9
1.6 Review of Past Work in the Field of Microwave Non-Destructive Testing ..	14
A. Metals: Reflection Technique ..	15
B. Non-metals ..	17
1.7 Scheme of Present Work ..	23

Chapter 1

INTRODUCTION

1.1 GENERAL INTRODUCTION

Manufacturing of an equipment or a subsystem or a part involves certain specifications, with some tolerances, which take into account both the nature of its future use and an estimate of its working life. These specifications may be in respect of the dimension of its components and its electrical and mechanical qualities. Any deviation from the specifications laid down can be considered as a defect and the use of a defective item may prove disastrous in many applications. For example, in a nuclear plant or in an aircraft engine, the use of a defective component may result in serious losses of both life and property. Likewise, in a propellant plant, it is essential to ensure production of a defect-free sample, which otherwise would cause non-uniform burning rate, changing the flight dynamics of the launch vehicle. Hence it is essential to have inspection techniques for assessing the quality and reliability of components and materials. Further the procedure adopted for the inspection of materials and other products should be non-destructive

one. Otherwise the test procedure itself would impair usefulness of the material for future applications.

Non-Destructive Testing, or NDT in short, is the technology by which standards of materials-quality, components-reliability and systems-safety are monitored and maintained. Physical measuring techniques are used to examine materials and parts of constructional assemblies for hidden imperfections and defects. The activity in the field of NDT includes the following:

- a) Fundamental research to understand and describe the ways in which certain imperfection would react to a physical measuring technique.
- b) Use of an optimised physical measuring technique to assess type and grade of imperfections.
- c) Methods to characterize materials and material properties.

1.2 VARIOUS NDT TECHNIQUES

As new materials and products are developed, it is often necessary to develop new techniques for inspecting them. This is because a technique developed may work well

when applied to some materials, but fails to give any information when applied to other materials. There are a wide variety of techniques available to meet the demand for examining a large types of materials such as metals, plastics, rocks as well as different structures and sizes ranging from semiconductor chips, nuclear reactors and off-shore oil platforms. A list of the conventional methods of NDT is given below:

- i) Radiography (X-rays and γ -rays)
- ii) Ultrasonic testing
- iii) Magnetic particle testing
- iv) Liquid penetrant testing
- v) Electromagnetic testing (Flux leakage and eddy-current)
- vi) Neutron radiographic testing
- vii) Leak testing
- viii) Acoustic emission technique
- ix) Visual inspection and holography
- x) Microwave techniques.

Some of the techniques like radiography, ultrasonic testing, eddy-current testing etc., are well developed and are being used frequently in industry. However, methods like microwave-techniques are still in their infancy and a lot of work have to be done if the potential of this techniques are to be exploited fully.

The choice of a particular technique of NDT is based mainly on the material to be inspected and the testing environment. For example, ultrasonic testing method can be employed for inspecting irregularities both on the surface and inside of metallic bodies. But the microwave-technique can help only in the examination of surface defects of metallic bodies since it cannot pass through metallic surfaces. Ultrasonic testing quite often requires a liquid medium for coupling for efficient transfer of energy. But some testing environments may not permit the use of such a coupling medium. In those cases microwaves can offer cheaper and faster solution, if the material to be tested is non-metallic. Otherwise radiographic techniques will have to be used. But in some cases health hazard problems may exclude the use of these techniques. Thus there is no unique solution to the non-destructive testing of materials. Each of the above techniques may prove to be useful in different testing conditions.

1.3 MOTIVATION FOR THE PRESENT WORK

The motivation for the present work is from a project sanctioned by ISRO. The work involved the development of a quick and reliable test procedure using microwaves, for the inspection of cured propellant samples and a method to monitor the curing conditions of propellant mix undergoing the curing process.

Normal testing of the propellant samples involve cutting a piece from each carton and testing it for their tensile strength. The values are then compared with standard ones and based on this result the sample is accepted or rejected. The tensile strength is a measure of degree of cure of the propellant mix. But this measurement is a destructive procedure as it involves cutting of the sample. Moreover, it does not guarantee against non-uniform curing due to power failure, hot air-line failure, operator error etc. This necessitated the need for the development of a quick and reliable non-destructive test procedure.

1.4 THE NEED FOR MICROWAVE NDT

Most of the familiar non-destructive test procedures cannot be applied for the inspection of a

propellant mix. These test procedures quite often fail to give information regarding the internal structure of the material owing to the following factors.

- a) Size and shape of the material
- b) Poor electrical properties of the material
- c) Non-metallic and non-magnetic nature of the material
- d) Poor sonic property of the material.

The use of microwaves, in such cases, can offer a cheaper and faster solution to the testing problem. "Microwaves" are electromagnetic radiations within the frequency range from 1 GHz to 30 GHz which correspond to wavelengths from 30 cm to 1cm in air. Many of the properties of microwaves are a blend of the properties of radiowaves and infra-red radiations because of its location in between the two, in the electromagnetic spectrum.

Microwaves can penetrate through most of the non-metallic materials reflecting and scattering from discontinuities and interacting with molecules. This penetrating property and interaction of microwaves with molecules permit numerous non-destructive test applications

with both on macroscopic and molecular level. The interaction on macroscopic level is similar to the interaction of light waves with microscopic objects and hence can be used for dimensional measurements or flaw-detection. The interaction on molecular level permits measurements of electrical properties like dielectric constant and loss tangent which are functions of material composition, structure, homogeneity, moisture content etc. Apart from these, the use of microwave-technique in NDT has got a number of other advantages also. A few are listed below:

1. Microwave-technique of NDT is a fully non-contact method and does not require liquid coupling as in the case of ultrasonic inspection.
2. It does not pose health hazard problems unlike X-rays, as the power levels used for inspection is only a few milliwatts.
3. Use of high frequency microwaves facilitates detection of very minute defects which otherwise could have detected using ultrasonic means. But in the later case, the energy requirement would be very high due to terrible attenuation.

4. As microwaves can penetrate through the samples almost at the speed of light, measurements will be very fast.

The above factors explain the importance of microwave NDT and its potential as an NDT tool. The only drawback of this inspection technique is that its application in metals is limited to surface defects only.

1.5 ESSENTIAL TEST FACILITIES REQUIRED FOR MICROWAVE NDT

To carry out inspection of a material using microwaves it is important to understand the minimum requirements of a test set up. The essential test facilities required are summarised in the following paragraphs.

1. Microwave generators

A reflex Klystron or a Gunn diode can be used as the source of microwave energy. Klystrons require high voltages for operation and are bulky and fragile. Gunn diodes on the other hand are compact, robust and require only very low voltages (10-20 V) for their operation. Both systems can provide enough power that is required for

most of the NDT applications. The power levels normally used are a few milliwatts. The frequency of these oscillators can be varied within certain limits and can be selected as required by the application.

2. Waveguides

At microwave frequencies the transfer of energy from one point to another is accomplished by the use of hollow structures (or waveguides). At lower frequencies, transmission lines such as a coaxial line can be used. But at microwave frequencies they are highly attenuated along these lines. The waveguides used may be either rectangular or circular and are normally made of copper with its inner side coated with silver to keep losses minimum. The dimension of the waveguides selected should be such that they support only the dominant mode of propagation at the frequency of operation.

3. Detectors and amplifiers

Detection of microwaves is usually accomplished by the use of crystal detectors. Because of the non-linearity of the crystal structure at the origin, any

alternate voltage applied across it gets rectified. At some occasions, the source will be frequency modulated by a few KHz so that by using standard techniques, weak signals can be amplified and thereby sensitivity of the system can be improved.

4. Wavemeters or frequency meters

Quite often in a microwave test set up there is a need for measuring or changing the frequency of the waves employed. Thus a wavemeter or a frequency meter also form a part of the test set up. The frequency meter employed normally is of cavity type. It's micrometer reading is calibrated to give the frequency directly.

5. Attenuators

An attenuator is used for controlling the microwave power transmitted. There is a moving vane (bakelite coated with carbon) the position of which can be changed to control the attenuation. The attenuator is calibrated in dB.

6. Isolators

This component protect the microwave source from changing load conditions. Any change in the load-condition can cause reflections which travel backwards and interact with the source causing a change in the operating frequency. Use of isolators take care of this undesirable effect by allowing transmission only in the forward direction. Reflected waves are severely attenuated by them. This is normally accomplished by the use of ferrites.

7. Matched loads or terminators

To avoid reflections from the ends of a waveguide, it is normally terminated to a matched load. The reflection from the ends of the waveguide will be absorbed by them and does not allow to interfere with the main waves.

8. Magic tee

The magic tee is a waveguide junction of four arms. These are commonly designated as E and H arms and the two side arms. The function of this component is analogous to bridge circuits in ordinary electrical

measurements. Any unbalance in power in the two side arms can be measured by monitoring the power either in the E-arm or H-arm. This property makes it useful in many applications.

9. Probes or antennas

For directing energy to a material and also for receiving the energy reflected, transmitted or scattered from the sample, microwave-antennas or probes are used. This could either be an open ended waveguide or, for more directivity, a microwave horn. Apart from these, there are many other useful antenna structures and selecting an antenna for an application is decided by its radiation characteristics in the presence of the samples to be tested.

Most of the equipment described above are simple and a microwave non-destructive test-set up can be developed using them. However, the advancement of technology in the field of microwave integrated circuitry and computers has resulted in the development of many sophisticated equipment for detection and analysis of

microwave signals. A network analyzer system is one such equipment. A completely automated microwave non-destructive test set up can be developed using these sophisticated equipment and a few other components. An automated test set up employing HP 8510 B network analyzer system is described in the next chapter.

1.6 REVIEW OF PAST WORK IN THE FIELD OF MICROWAVE NON-DESTRUCTIVE TESTING

The use of microwaves for NDT is relatively recent and the first papers describing such techniques appeared only in 1950's. Bulk of the papers were published after 1960. This was mainly because of lack of appropriate instrumentation. The application of this technique in metals is limited to examination of surface irregularities by reflection technique as microwaves cannot penetrate more than a few micron-thickness of a conducting body. However, the situation is different with non-metallic materials which reflect, absorb, transmit, change the phase and or polarisation of, scatter and otherwise interact with incident microwave radiation in ways which are characterised by the properties of the material involved. These tests therefore provide a means for examining the different properties of non-metallic materials.

Following is the summary of the work carried out so far in the field of microwave NDT and applied to metallic and non-metallic bodies.

A. METALS: REFLECTION TECHNIQUE

Ryan and Summers [1] have used microwave NDT technique to observe and record the surface irregularities of commutators and slip rings during the operation of associated machines. Surface irregularities of the order of 0.5 mil or less were detected by them using this technique.

A method of measuring non-destructively the resistivity of a semi-conductor in the form of an epitaxial layer has been described by Bichara and Poitevin [2] by using microwaves at 70 GHz. The principle employed consists of measuring the attenuation and phase changes, which are functions of sample resistivity and thickness, undergone by microwaves upon reflection by the sample under test.

Hruby and Feinstein [3] have described a novel method of measuring depth of ultra thin deep slots in metal

surfaces. Their experiments have shown that waves propagating in TM_{01} mode is more likely to provide larger sensitivity for magnetic materials while for non-magnetic materials TE_{01} mode would be more practical.

Owston [4] has described a microwave eddy current technique which is useful in testing thin protective coating on suitable materials. The instrument employed could detect 2% change in the resistivity of the surface layers and coating about 1μ thick.

Beyer et al. [5] measured the thickness of conducting sheets and plates by comparing the amplitude or phase of the signals reflected from both surfaces of the specimen under test. The amplitude measurements were found to give satisfactory results and a thickness change of 0.025 mm could be measured with a specimen moving at a speed of 0.5 m/sec. and placed in between the transmitter and receiver.

A microwave interferometer for measuring dynamic clearance between moving surfaces has been described by Wort [6]. Using 3 cm waves clearances of the order of

0.01 mm were measured accurately. A method of detecting fatigue cracks in steel has been described by Hussain and Ash [7]. The instrument employed was a microwave scanning microscope. The method can be applied only to materials with flat surfaces and can be modified to suit for other surfaces as well.

B. NON-METALS

(i) Reflection Technique

Lavelle [8] has used the principle of microwave interferometry for thickness Gauging of non-metallic materials and structures bounded by parallel surfaces. He found that for a given material and test frequency, changes in the thickness of the material can be directly correlated with the amplitude of the reflected signal. Lavelle was successful in measuring thickness to a resolution of 0.1 mm in a 6 inch block of epoxy resin. A similar technique has been employed by Whistlecroft [9] for thickness gauging of radomes.

A magic Tee reflection technique at 35 GHz was employed by Lavelle for detection of voids and delamination

in epoxy resin [8]. Cylindrical flaws of dimension varying from 5.8 mm to 1.02 mm were detected on a 1 inch x 1.5 inch square epoxy resin block. Delaminations in adhesive bonded honeycomb structure were also detected by using this technique. The frequency used was 9.4 GHz.

Turi et al. [10] used a microwave set up for the measurement of small inhomogenities in super calender rollers and other dielectric materials. The technique involved the measurement of variations in the dielectric constant over the surface of the super calender rollers by recording the amplitude of the reflected microwave energy. Experiments showed that variations of the order of 0.1% in the dielectric constant can be recorded reliably.

Rockowitz and McCurire [11] used radiations at 69 GHz and were able to detect defects with dimensions as small as 1/8 inch in one direction in a 2 inch thick glass fibre honeycomb structure filled with ablative materials.

Stinebring and Harrison [12] have used microwave NDT for checking the delamination of rocket components. They were able to detect 1 inch delamination more than 2 feet deep in a solid rocket propellant.

A high resolution microwave instrumentation system was used by Dean and Green [13] for measuring burning rate of solid propellant rocket motors. The method could be applied to measurement of erosion or burning rate of any other layer of material where access is not available to the eroding surface. The position of burning surface could be measured with an accuracy of ± 0.2 mm by this technique.

Forssell [14] has described a reflection technique employing microwaves for the measurement of fibre content in reinforced plastics.

For ATIRA (Ahmedabad Textile Industries Research Association), Space Application Centre has conducted a feasibility study of using microwave reflection technique for measuring the moisture content in textile yarn [15]. The results indicated that a measurement accuracy of 1% at about 12% moisture content can be obtained by this technique.

Non-destructive test methods for measuring the complex permittivity of the dielectric materials have been described by Eiji Tanobe and William T. Joines [16],

Dereton and Ramachandrah [17] and Itoh [18]. The method described by Itoh employs a microstrip resonator and dielectric constant of materials were measured accurately upto 1 GHz. By the other technique mentioned, dielectric constant measurements were possible upto 4 GHz.

Hashimoto and Shimizu [19] have studied the reflecting characteristics of anisotropic rubber sheets and used the results for the measurement of complex permittivity.

Reza-Zoughi and Sasan Bakhtiari [20] have described a reflection technique for non-destructive detection of disbonding and delamination in layered dielectric slabs. The results obtained from these measurements were used for dielectric constant calculations. Very good agreement have been reported between the theory and experiments. Marianne Gex Fabry et al. has described methods of evaluating dielectric constant of the materials by using open ended circular waveguides in the TM_{11} mode [21] and open ended coaxial lines [22]. In all these test methods for dielectric constant measurement, there should be a small flat surface available for contact between the open ended resonator and the material.

(ii) Scattering techniques

Lavelle [8] has conducted studies on the scattering of microwaves by epoxy resin samples embedded with glass spheres at their centres. Hollow and solid glass spheres were used to simulate voids and inclusions. Eventhough detection of glass spheres were possible, a correlation could not be established between the scattered wave amplitude and the dimension of the sphere.

Dean and Green [13] were able to detect a cavity of 4 mm diameter in the centre of a rubber material 25 cm in diameter. By the use of microwaves at 35 GHz, they were able to detect defective areas in a 10 mm cube containing 0.5 mm diameter pores at about 2 mm spacing.

(iii) Transmission technique

Stinebring and Harrison [12] used microwave transmission technique for the detection of flaws inside a solid rocket propellant sample and for measuring the degree of cure of an epoxy material. The effect of microwave on undercured propellant grains and aged propellant samples were also studied. Two open ended waveguide sections were used as transmitting and receiving antennas.

Lavelle [8] used transmission technique for the estimation of thickness of material and the same degree of resolution in the thickness measurement as in the reflection technique could be achieved. He also studied the effect on the passage of microwaves during the curing of an epoxy resin. It was seen that the received microwave energy increases as the curing period increases and levels off to a constant value after a certain period.

Summerhill [23] and Taylor [24] have used similar microwave transmission techniques for the measurement of moisture content in materials. The accuracies of measurements were $\pm 2\%$ for low moisture content and $\pm 1\%$ for materials with a moisture content of 60% or above.

A summary of the general techniques employed in microwave non-destructive testing has been briefly dealt with in reference [25]. Hochschild [26] has discussed in detail, various applications of microwaves in non-destructive test measurements. Wittig and Bam [27] have discussed the different types of antenna systems for Microwave NDT applications. Their experiments showed that estimation about the signal shape to be expected from an

inhomogeneity and the resolution of measurements are controlled by the beam cross-section of the transmitting and receiving antennas. For testing a flat shaped plastic specimen with holes drilled on it, the authors found that two waveguide sections with one of it filled with the material, can be used as transmitter and receiver to get good results.

1.7 SCHEME OF PRESENT WORK

The potential of microwaves as an NDT tool and the role played by it in the inspection of materials is evident from the review of literature presented in the previous section. The main objective of the present study is to explore the possibility of developing a non-destructive test facility using microwaves to monitor the curing conditions of solid rocket propellant, if a non-uniform curing portion is detected, then the engineer can take necessary steps to rectify it before removing the sample from the oven. The following feasibility studies were planned and performed in detail in this research work.

- a) Development of microwave NDT methods for testing non-metallic materials and free standing propellant samples.

- b) Development of a microwave method for studying the phases of curing of real-time propellant samples.

In the first part of the study experiments were carried out,

- a) to detect and locate flaws inside cured propellant samples of different types.
- b) to find the minimum detectable flaw size in the directions both parallel and perpendicular to the direction of propagation of microwaves.
- c) to study variations in the phase and amplitude of the signal with flaw-size and shape for defect characterization.

In the second part of the study, the following parameters were studied experimentally,

- a) change in electrical property (dielectric constant) of a propellant sample at various stages of curing by reflection of microwaves.
- b) variation in the absorption properties of the propellant samples of different compositions during the process of curing.

c) correlation between mechanical property (tensile strength) and electrical property (dielectric constant).

The thesis has been organised into different chapters with contents as detailed below:

Chapter 2 gives the methodology adopted and descriptions of the experimental set up used. A free space transmission technique is described for the detection and location of flaws inside a cured propellant sample. An automated test set up used for the same employing an HP 8510 B network analyzer is presented. Waveguide transmission and reflection techniques for the measurement of material properties for a propellant sample undergoing curing process are also presented.

The results obtained from various investigations are presented in chapter 3. Minimum detectable defect size and its estimated location are presented along with variations in the phase and amplitude patterns for defects of different size and geometry. Results obtained by the dielectric measurements for two propellant compositions are also given.

Chapter 4 analyzes the results in detail. The conclusions drawn from the analysis are also brought out in this section.

The limitations of the methods used and the possible extensions of the technique in testing of other materials are presented in chapter 5. Results obtained from an experiment conducted in the laboratory on vehicular tyres is cited as an example for the validity of the test set up used.

In addition to the main work on NDT, the author has carried out investigations on the development of microstrip antennas with enhanced bandwidth capabilities using modern antenna test facilities. The results obtained from these investigations are presented in the Appendices. A short description of an Anechoic Chamber facility used for recording the radiation patterns of the antenna is also presented. Design of a dual frequency antenna and its radiation characteristics are also presented in the Appendix. Finally, design parameters for a flared dipole microstrip antenna (FMDA) for operation over a larger bandwidth is given.

Chapter 2

MEASUREMENT TECHNIQUES AND EXPERIMENTAL ARRANGEMENTS

	<u>Page</u>
2.1 Introduction ..	28
2.2 Measurement Techniques ..	28
2.3.1 Free-space Transmission Technique for Detecting Non-uniformities in Cured Propellant Samples: Experimental Arrangements Used ..	37
2.3.2 Measurement Procedures ..	41
(a) Detection of Flaws ..	41
(b) Location of Defects ..	45
2.4 Measurement of Dielectric constant and Loss Tangent--Waveguide Method ..	49
(a) Measurement set up and Experimental Procedure ..	49
(b) Theoretical Considerations ..	52
(c) VSWR Variation ..	56
2.5 Attenuation Measurements ..	56
2.6 Conclusion ..	59

Chapter 2

MEASUREMENT TECHNIQUES AND EXPERIMENTAL ARRANGEMENTS

2.1 INTRODUCTION

The measurement techniques adopted and the experimental arrangements used for the investigations are presented in this chapter. A simple formula for locating defects inside a non-metallic material of cylindrical geometry has been derived. Theoretical formula for calculating the dielectric constant and loss tangent of the propellant samples undergoing curing process are also presented. An attenuation measurement system used for the absorption studies of the propellant samples as it undergoes curing is also described.

2.2 MEASUREMENT TECHNIQUES

Measurements by microwave methods can be made by the following three basic techniques.

1. Reflection
2. Scattering and
3. Transmission.

In the reflection technique the signal reflected from the surface or interior of the test samples are measured and analysed for the presence of inhomogenities. The basic test set up is shown in Fig.2.2(A). A defect of many wavelengths wider will reflect microwave energy. When the defect is very small, energy is scattered in all directions and the detection becomes difficult. The mechanism of reflection from an internal defect is illustrated in Fig.2.2(B).

This method would also be useful for the thickness measurements, especially when the material is coated on one side of the metal film. As metals give rise strong reflections, this method is also useful for detecting metallic inclusions within a non-metallic media. This method would be useful for measuring surface irregularities and internal defects provided their dimensions are of the order of operating wavelength.

Scattering, can be used for detecting inhomogenities like porosity inside a non-metallic medium. A typical test set up is shown in Fig.2.2(C). When there is no porosity within the medium all the energy passes through

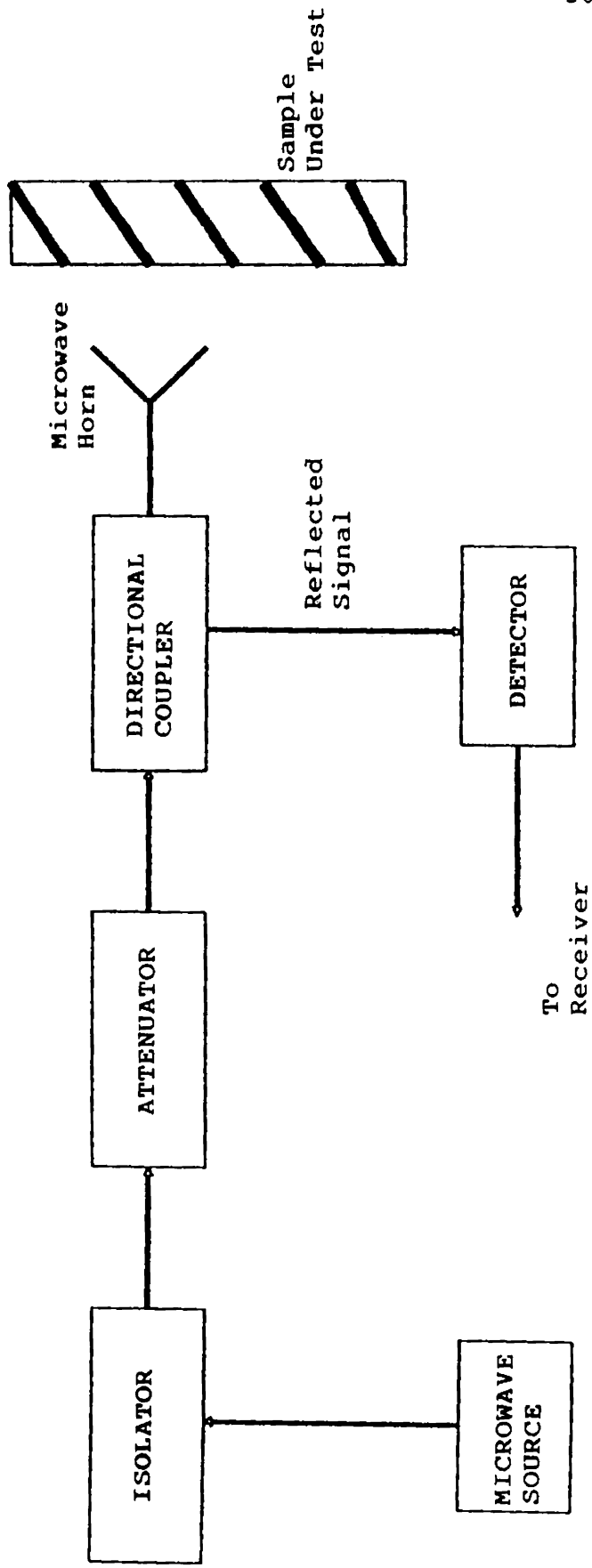


Fig.2.2(A) A typical microwave reflection measurement system

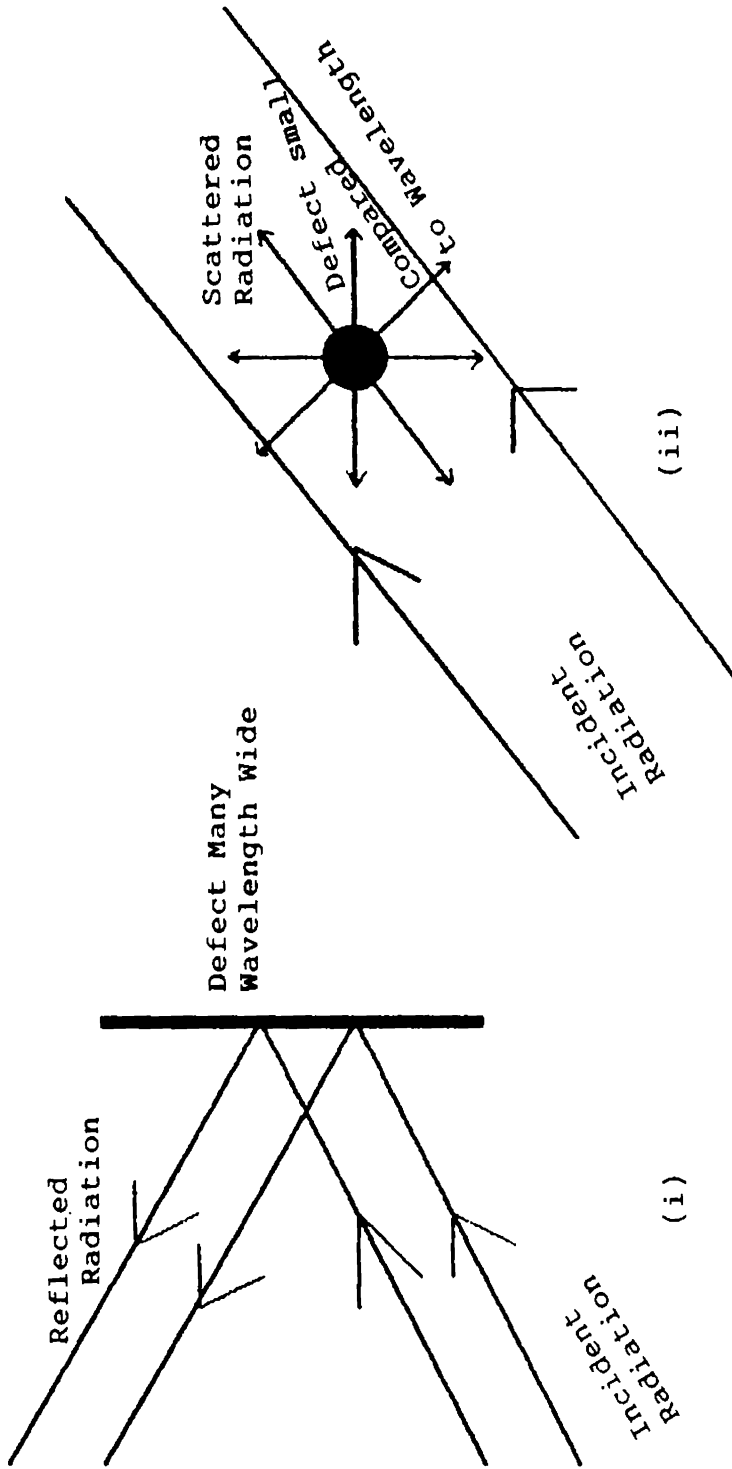


Fig.2.3(B) Mechanism of reflection of microwaves from an internal defect:

- (i) Defect many wavelenght wide
- (ii) Defect small compared to wavelenght

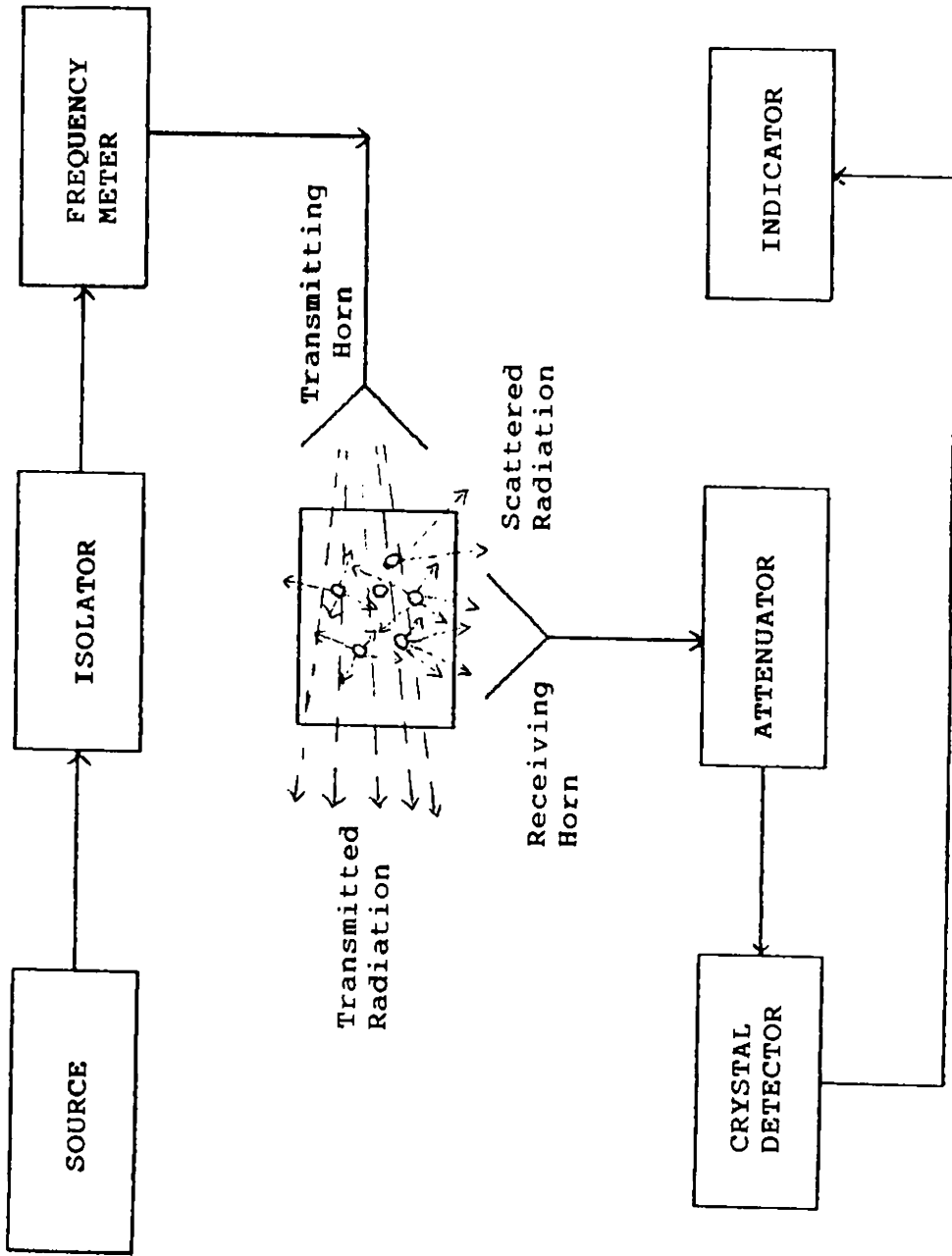


Fig.2.2(C) Microwave scattering measurement set-up for porosity detection.

the material and no energy will be available in the receiver. If the test sample contain porosity, they act as scattering centres resulting in some energy directed towards the receiving horn.

Transmission technique is a simple and most widely used technique for detection of non-uniformities within a non-metallic medium. The technique involves irradiating the sample with microwaves and then analysing the amplitude and phase of the signal coming out after transmission through the sample. The presence of a defect can be observed as a reduction in intensity of received power or as a diffraction pattern as it passes through the signal beam. The measurement set up normally employed is shown in Fig.2.2(D). This method is also useful for studying absorption properties of the samples, and hence in monitoring the degree of curing or moisture content within the samples.

Investigations during the initial phase of this research work have shown that a free space transmission technique yields better results compared to either the reflection or scattering techniques. Hence for detecting

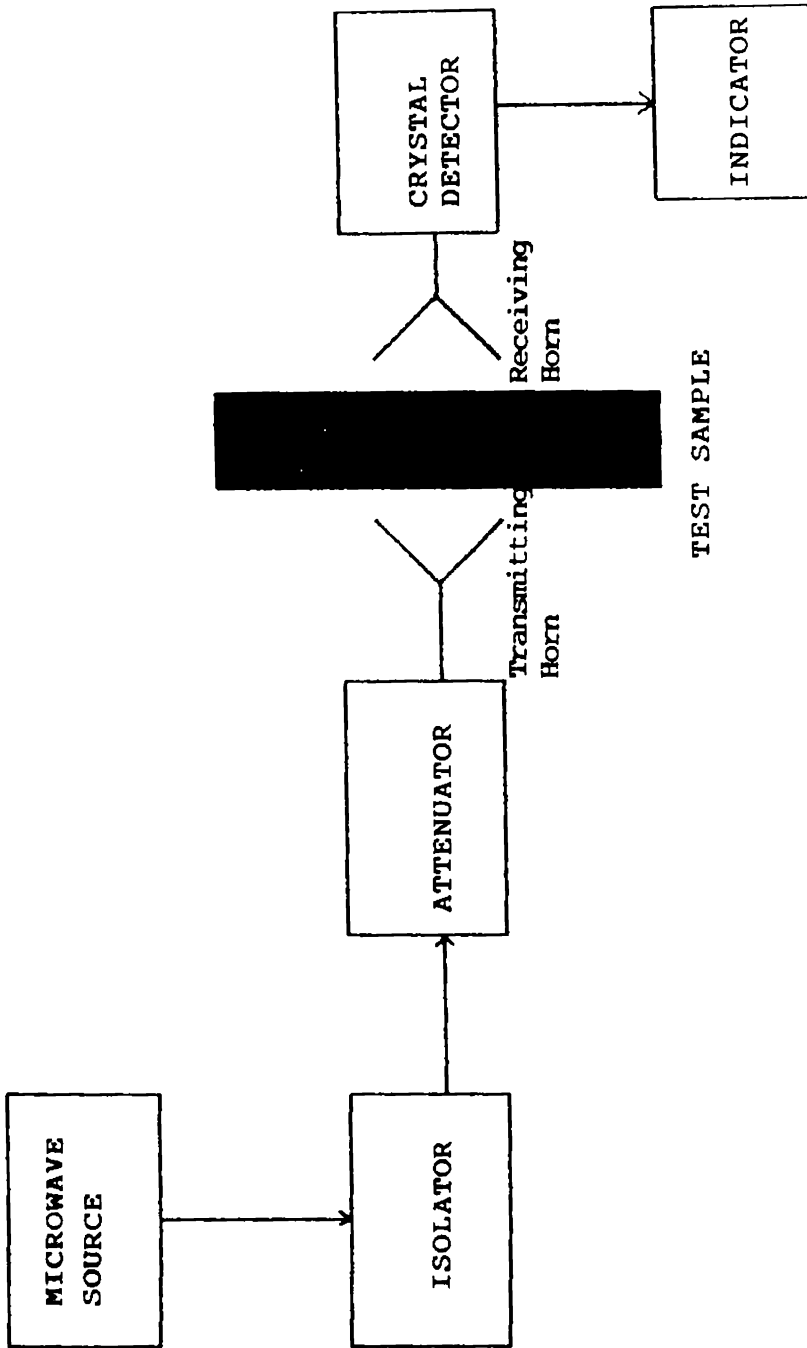


Fig.2.2(D) Basic test set-up for microwave transmission measurements

flaws inside cured propellant samples and for estimating their approximate location, a transmission technique was employed. A detailed description of this technique along with the experimental set up and measurement procedure is given in section 2.3.

The process of curing of a sample involves physical change of the material along with changes in its electrical properties. A measure of the changes in the electrical property of the material can give information regarding its degree of cure.

The electrical parameters involved are dielectric constant of the material and its loss tangent (or $\tan \delta$, as it is popularly known). These parameters for a non-conducting medium can be obtained from the characteristics of the electromagnetic waves passing through them. In general, both dielectric constant and loss tangent are functions of frequency.

The methods available for measuring these electrical parameters fall into two groups [28]. They are:

1. Free wave method/technique and
2. Guided wave method/technique.

In the free-wave method of investigating a material, there are inherent uncertainties like effect of boundaries, reflections etc., and hence the results obtained are less reliable compared to other techniques.

The guided wave method can be further classified into cavity method and waveguide method. In the cavity method, the changes in the frequency of the cavity are recorded as a measure of the permittivity of the material, when the cavity is filled with the material. The waveguide method, on the other hand is based on the travelling waves set up by reflections from the sample-face introduced into a waveguide section.

In this study a waveguide method has been adopted for measuring the dielectric constant and loss tangent of a propellant sample undergoing curing process. This is brought out in section 2.4. Section 2.5 describes the waveguide attenuation measurements carried out for studying the changes in absorptive property of the sample as the curing progresses.

2.3.1 Free-space transmission technique for detecting non-uniformities in cured propellant samples: Experimental arrangements used

The measurement set up used for initial investigations is shown in Fig.2.3(A). An HP 8620 C sweep oscillator was used as the source of microwave energy. The frequency of the source can be varied from 8 to 12.4 GHz (X-band). It gives levelled output for all the operating frequencies. The power level employed in the present study was 10 dBm at all frequencies. The source was followed by an isolator and an attenuator, the requirements of which have already been discussed in chapter 1. A reflection transmission test unit (HP 8734 B) was used for splitting the main signal into a reference signal and a test signal. The reference signal goes directly to a network analyzer system, while the test signal after passing through the sample also end up in the network analyzer (HP 8410 C). Both open ended waveguides and microwave horns were used for directing microwave energy on to the sample and for receiving it after transmission through the sample. The test sample was mounted on a turn-table which can be rotated in clockwise and anticlockwise directions using

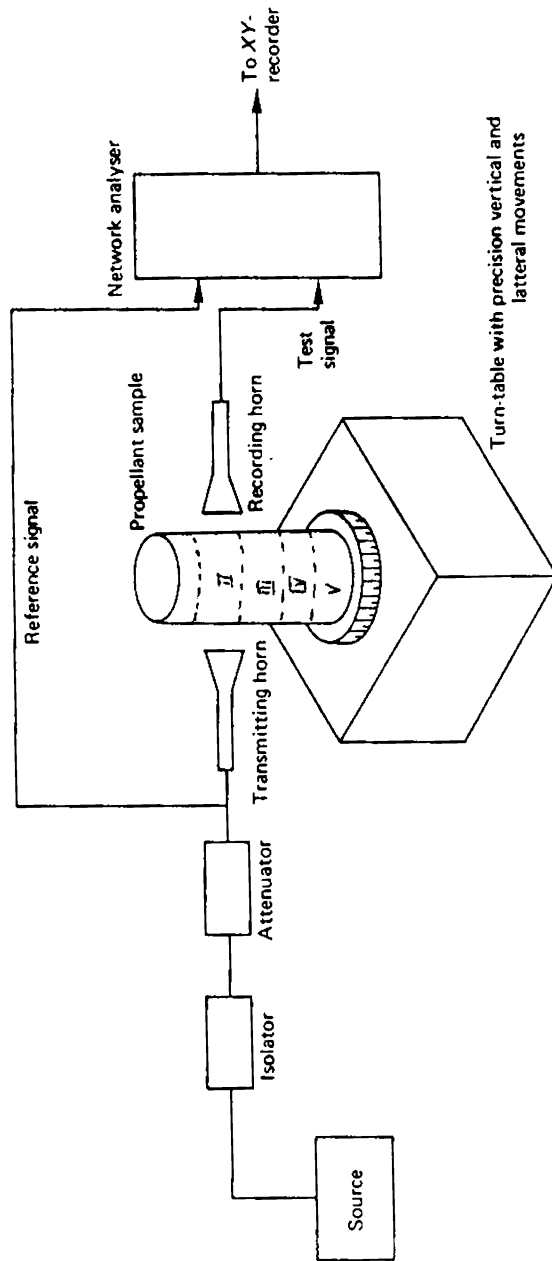


Fig.2.3(A) Microwave transmission set up to locate defects or flaws.

push-button controls. To get the angular position of the sample, a potentiometer was attached to the rotating axis of the sample and it was fed with a d.c. voltage. As the table rotates the d.c. voltage will vary and this was calibrated for angle measurements. The network analyzer compares amplitude and phase of the reference signal with that of the test signal and gives an output. An XY-recorder was used for recording the informations on a graph sheet.

Apart from the experimental set up just described, an automatic 8510 B network analyzer test facility was also employed in this study. Using this system a semi-automated inspection test facility was set up for carrying out fast and accurate measurements on cured propellant samples. The test set up is shown in Fig.2.3(B). All the subsystems like sweep oscillator, reflection transmission test unit or S-parameter test unit, network analyzer, turn-table positioner controller etc., are interfaced to an HP 9000 series computer through HPIB interface controller. The frequency can be varied from 10 MHz to 26 GHz. By the use of a user-interactive software developed in the laboratory, all the parameters like frequency, power level to be used, angular position of turn-table, its speed and direction etc., can

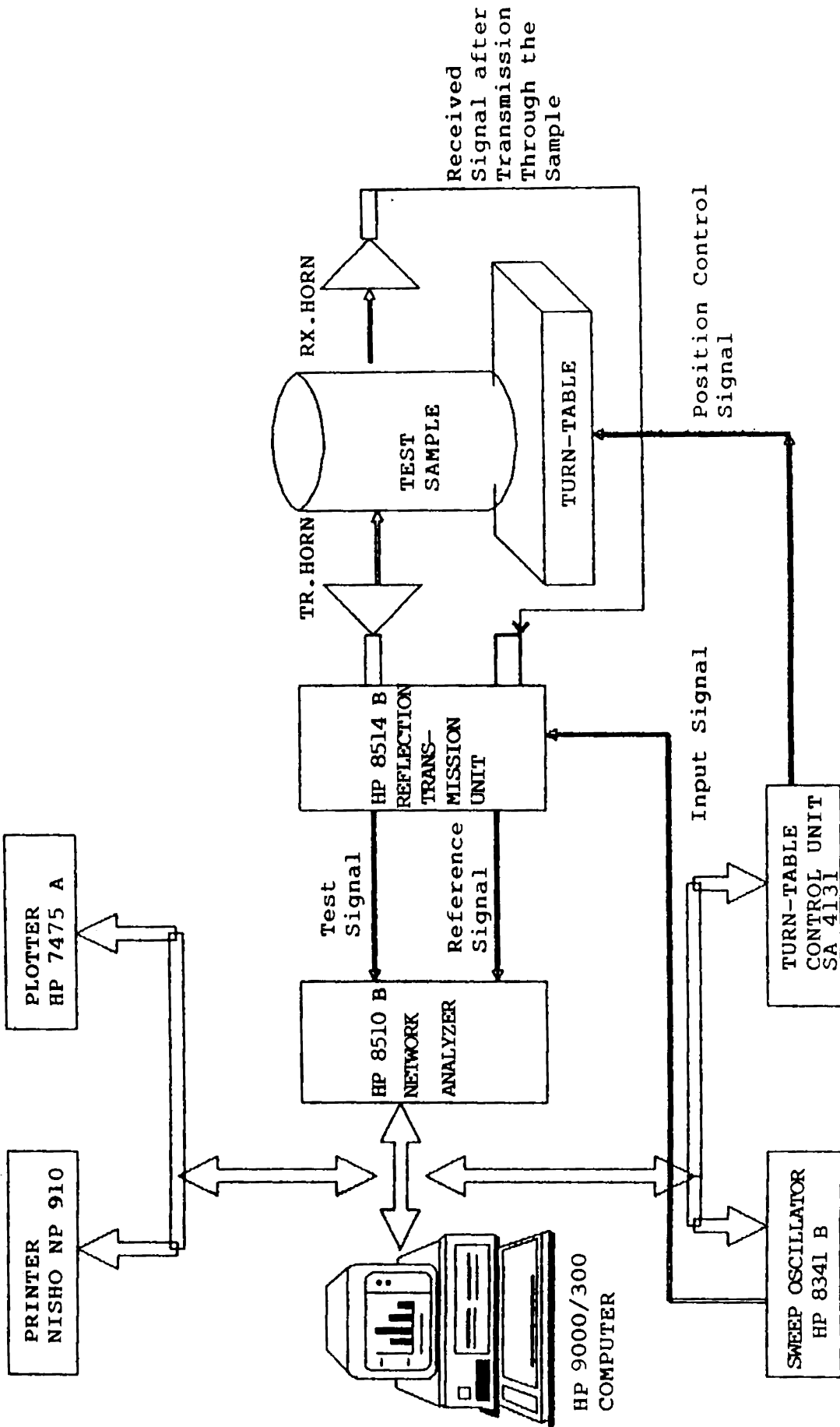


Fig.2.3(B) Automatic network analyzer (8510 B) test set up employed for detecting inhomogeneities in a cured propellant sample.

be selected and measurements can be carried out in one shot. Using the same set up, experiments can be performed either in the reflection mode or in the transmission mode. Single frequency measurements or swept frequency measurements can be carried out during a single scan of the test sample. The data collected by the network analyzer can be stored in a disc for future use. After each measurement a plot of the amplitude and or phase versus angle of rotation of the turn-table will be displayed on the monitor and the same can be transferred to a plotter (HP 7475 A) for further analysis. If the data for a standard (or reference) sample is available then it can be stored in the computer memory and by comparing the data, a decision whether to accept or reject the sample under test, could be made. Thus, this set up facilitate an on-line inspection of materials. Apart from this, simultaneous measurement of both phase and amplitude were possible using this test set up at multiple frequencies.

2.3.2 Measurement procedures

(a) Detection of flaws

A cured propellant sample was selected and the total exposure area was divided into a number of zones

along the length of the sample as indicated in Fig.2.3(A). Each zone measured 10 cm in height. The sample was then mounted on the turn-table with its vertical axis collinear with that of the turn-table. The system was then placed symmetrically between the transmitting and receiving antennas. The frequency was set at 9 GHz and the power level was set at 10 dBm. Using a lifting mechanism provided to the turn-table, the sample was lifted so that the first zone is exposed to the narrow pencil beam of transmitting horn. The turn-table was then rotated through 270 degrees. The use of the potentiometer did not permit rotation through 360° in the earlier set up. (But the automatic measurement employing 8510 B network analyzer has overcome this limitation) Now a plot of the amplitude versus angle of rotation was made using an XY-recorder. The phase of the transmitted signal was also plotted in the same manner. By lifting the sample in steps of 10 cm and by rotating the turn-table, the whole length of the sample was scanned and in each case the amplitude and phase patterns were recorded. To check the capability of the system in detecting flaws, an artificial flaw was introduced into the sample by drilling a hole. The sample with artificial flaw is depicted in Fig.2.3(C). This part of the sample alone was irradiated with microwaves and the amplitude and phase patterns were again recorded.

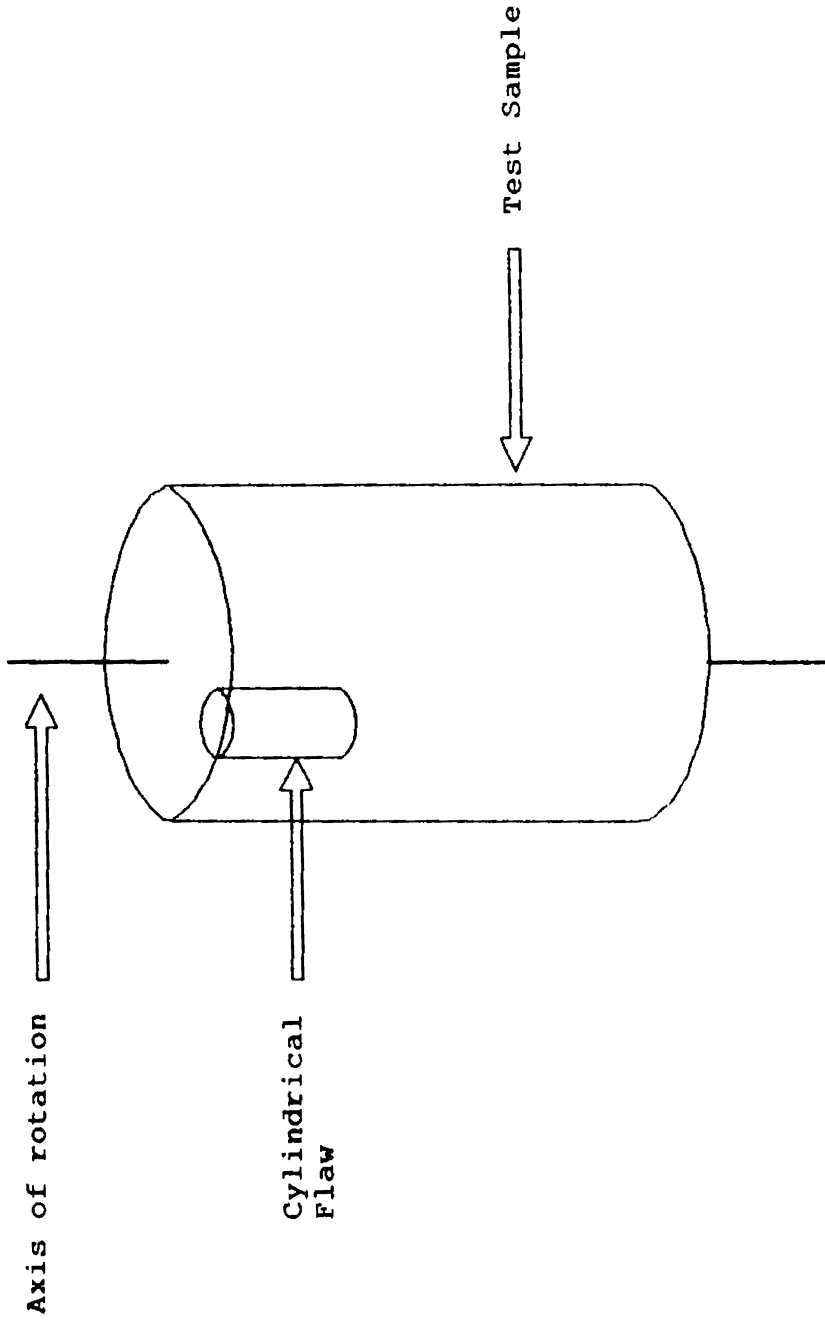


Fig.2.3(C) Propellant sample with an artificial cylindrical flaw.

To study the effect of flaw-size, holes of different sizes were drilled in the specimen and in each case the phase and amplitude patterns were recorded. The experiments were repeated with a rectangular flaw cut inside the sample. This was done to see the effect of flaw-shapes on signal transmission. The minimum detectable size, both parallel and perpendicular to the direction of propagation, was also found out using the same experimental procedure.

The signal characteristics corresponding to a particular flaw-size and shape may also vary with the frequency. Hence the experiments were repeated for different frequencies from 8 to 12 GHz at intervals of 1 GHz.

The presence of a material in front of an antenna can distort the electromagnetic field, and for a given test set up this distortion will be a function of the spacing of the transmitter and receiver from the test sample. Hence experiments were repeated for different spacings between the transmitter and receiver, to see the effect on the amplitude and phase patterns.

In the preliminary tests carried out, the samples used were without a mandrel which will normally be present in a real sample. This is to eliminate reflections from irregular cross-sections of mandrel as microwaves pass through them. In the later studies using the HP 8510 B network analyzer, samples with mandrel were also tested. The propellant samples tested in this study were RH 125, RH 200 and RH 250.

(b) Location of defects

The inference from the previous experiment was that the defect within a non-metallic material can be detected and the line along which the defect lies can be marked. However, pin-pointing its location was not possible. The following technique has been adopted for finding the approximate position of the non-uniformity from the centre of the sample.

The presence of a flaw was observed as a change either in the phase or amplitude of the signal passing through the sample. For the arrangement shown in Fig.2.3(D) the result obtained will be like the pattern (solid line)

shown in Fig.2.3(F). Here two peaks are observed separated by 180° as the flaw in the sample intercept in the transmitter-receiver path twice. The sample along with the turn-table is given a lateral shift so that the arrangement now looks like as shown in Fig.2.3(E). For the same direction of rotation, the two peaks in the pattern will be closer than in the previous case, because the sample has to be rotated only through a smaller angle for the flaw to intercept the transmitter-receiver path twice. The new result is showed as dotted lines in the Fig.2.3(F). Let 'd' be the lateral shift given and D the position of the flaw from the centre of the sample. Then from the Fig.2.3(D&E), it is clear that,

$$\frac{d}{D} = \cos \theta \quad \text{or}$$

$$D = \frac{d}{\cos \theta}$$

where 2θ is the angular separation between the peaks. Now, if the sample was given a shift in the opposite direction or if the direction of rotation is changed, then the angular separation between the two peaks will be more

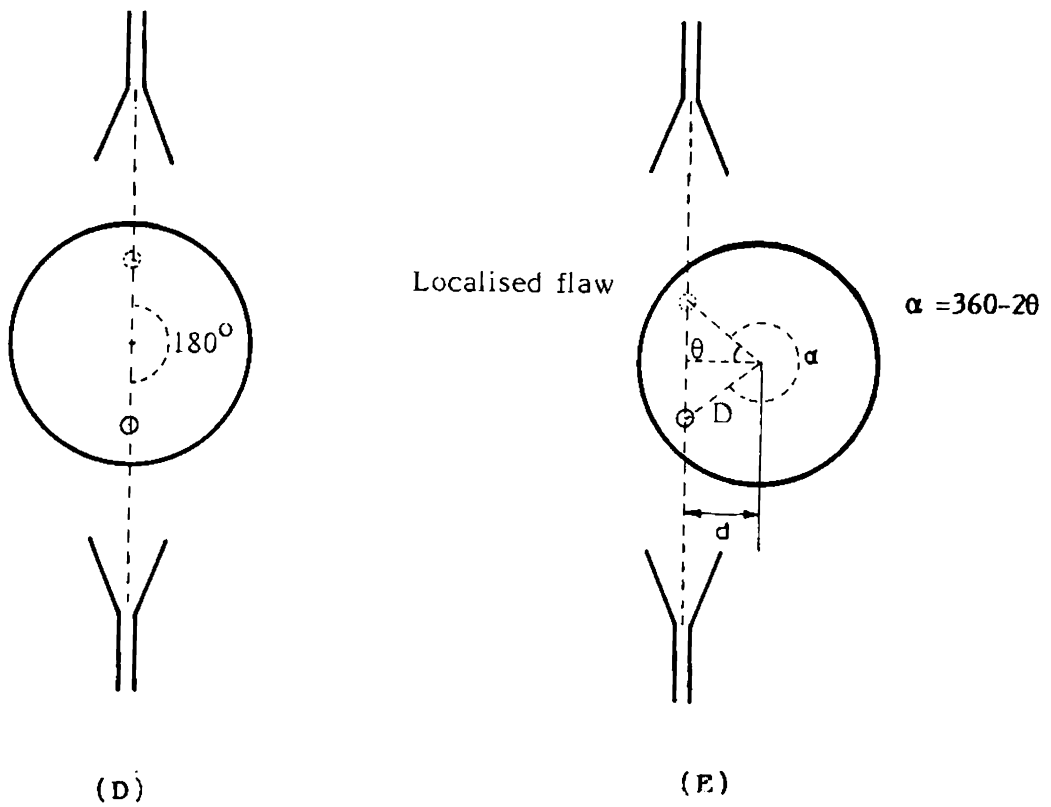


Fig.2.3(D) Propellant sample mounted symmetrically with respect to transmitter and receiver
(E) Sample is given a lateral displacement

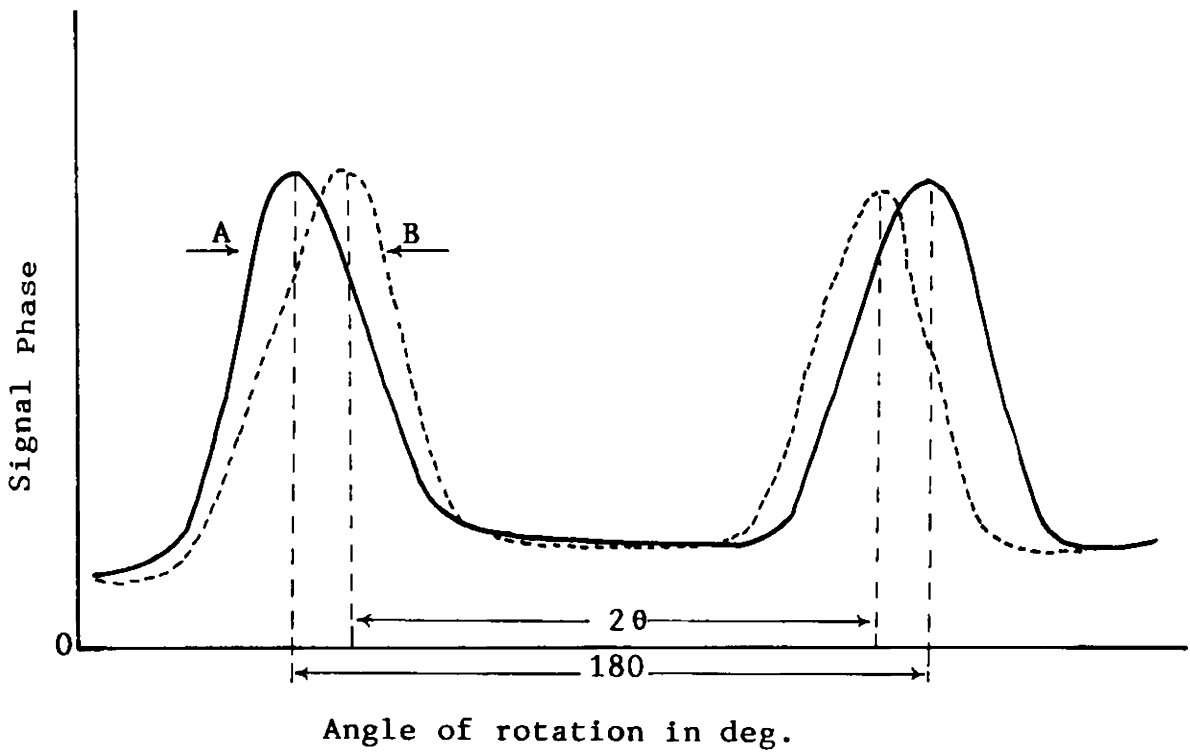


Fig.2.3(F) Phase patterns of transmitted signal at the sample is rotated about the vertical axis.
 — (A) When sample is mounted symmetrically
 ---- (B) When sample is given a lateral displacement.

compared to the first case. If α is the measured angular separation in the later case then,

$$2\theta = 360 - \alpha$$

and again the above formulae is applied to calculate value of 'D'.

To check the validity of this formula experimentally, tests were carried out in the following way. A cylindrical flaw of diameter 0.9 cm was made inside a cured propellant sample at a distance of 6.9 cm from the centre of the sample. The sample was given lateral displacement of 1.2 cm, 1.4 cm and 1.6 cm. The patterns were plotted and in each case, D was calculated using the value of '2 θ ', the angular separation between the peaks. Experiments were repeated for flaws of different sizes at different distances from the centre of the sample. The results obtained are tabulated in the next chapter.

2.4 MEASUREMENT OF DIELECTRIC CONSTANT AND LOSS TANGENT- WAVEGUIDE METHOD

(a) Measurement set up and experimental procedure

The experimental set up employed for the measurement of dielectric constant is shown in Fig.2.4(A).

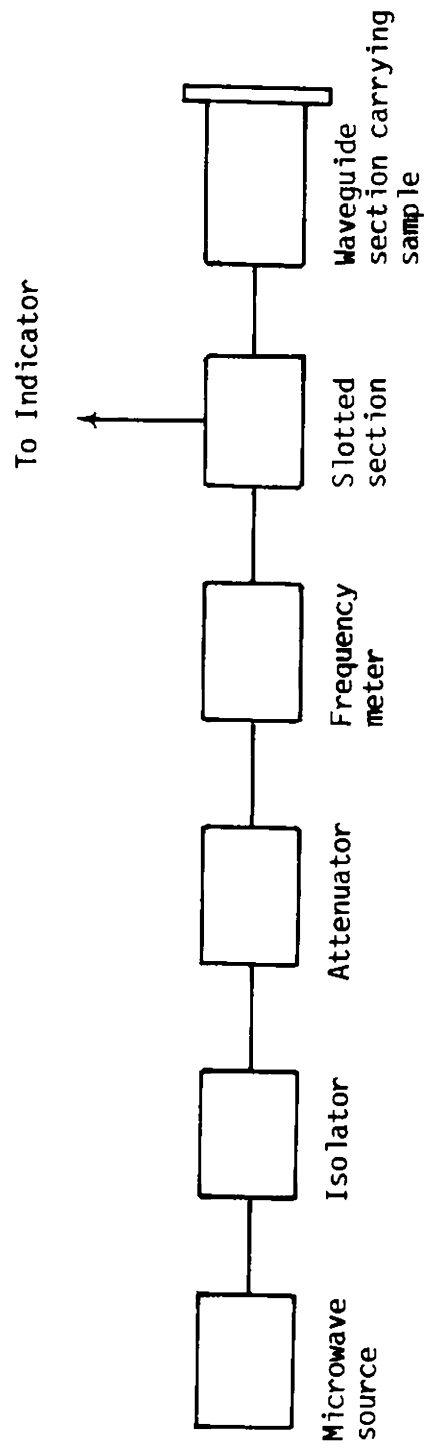


Fig. 2.4(A) Experimental set up for the determination of dielectric properties of the prope llant sample.

A slotted section with a probe carriage was employed for standing wave measurements. The sample can be introduced or taken out from the terminating waveguide section. A short circuiting metal plate is attached to one end of the waveguide section. The microwave power intercepted by the probe is detected using a crystal detector and fed to a micrometer for measurements.

To start the measurement, the waveguide section with the short-circuiting plate was connected and by moving the probe the position of the minimum from the side of the waveguide section was measured. Now the waveguide was filled with propellant mix in slurry form and one end of it was closed with the short-circuiting plate. The waveguide section was again connected to the system as before and the shift in the first minimum was observed. The sample was then placed in an oven maintained at the curing temperature. The sample was taken out at definite intervals, and after connecting to the system, measurements were made. The experiment was repeated till the sample is completely cured. Observations were taken for samples of different lengths and two different compositions. From the measured value of shift in the first minimum the dielectric constant and loss tangent were calculated using the following theory.

(b) Theoretical considerations

The introduction of the sample into the waveguide raises dielectric constant of the medium and this will result in a change of the guide wavelength. This change in guide wavelength, which is a function of sample dielectric constant and its thickness, resulted in the shift of the minimum in the slotted section. This shift can be measured precisely and it is sufficient for calculating the dielectric constant of the sample and its loss tangent.

A general solution of the transmission line equation for a dielectric filled line has been given by Roberts and Von Hippel [29]. A modified version of the same technique was developed by Dakin and Works [30]. This theory has been used here for the calculation of dielectric constant.

The waveguide section employed and the standing wave patterns within the waveguide section with and without the sample are illustrated in Fig.2.4(B), 2.4(C) and 2.4(D) respectively. The separation of the first minimum of the standing wave from the face of the sample is given by [31].

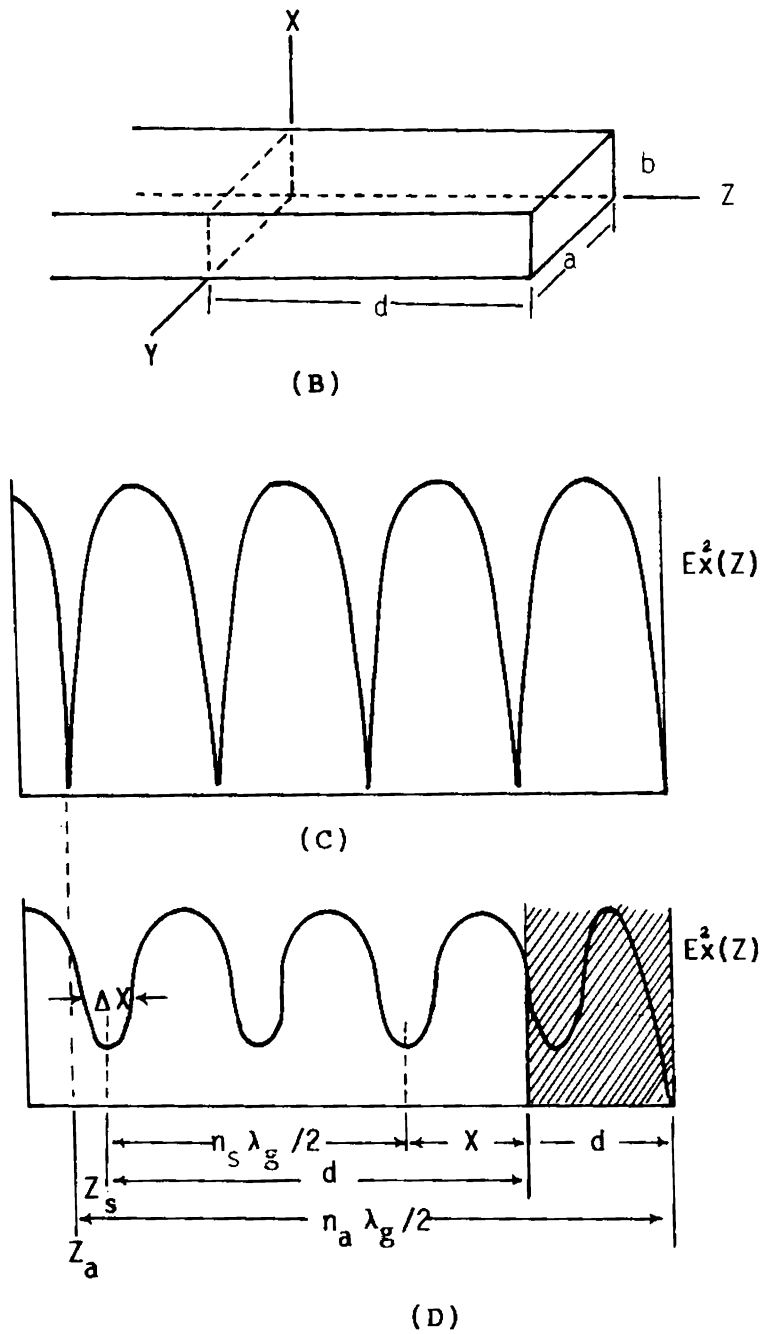


Fig.2.4(B) Short-circuited rectangular waveguide with dielectric sample of length d at the shorted end
 (C) & (D) Voltage standing-wave patterns in an empty and dielectric filled waveguide.

$$\chi_o = (n_a - n_s) \lambda_g / 2 - [d + z_a - z_s] \quad (2.1)$$

where,

χ_o = distance of the first minimum from the face of the sample

d = thickness of the sample

λ_g = guide wavelength in free-space

n_a , n_s , z_a and z_s are the distances illustrated in the figure.

The dielectric constant of the sample is related to the attenuation constant and the standing wave ratio (SWR) by the relation

$$\frac{\frac{E_{\min}}{E_{\max}} - i \tan[360 \chi_o / \lambda_g]}{1 - i \frac{E_{\min}}{E_{\max}} \tan[360 \chi_o / \lambda_g]} \frac{\lambda_g}{2\pi d i} = \frac{\tan \gamma_2 d}{\gamma_2 d} \quad (2.2)$$

where, $\gamma_2 = \alpha_2 + j \beta_2$; is the propagation constant. The above transcendental equation can be solved by putting $\gamma_2 = \alpha_2 + j \beta_2$ and separating it into real and imaginary parts. Equating the real part we have,

$$\frac{\tan \beta_2 d}{\beta_2 d} = \frac{-\lambda_g \tan\left(\frac{360 X_0}{\lambda_g}\right)}{2 \pi d} \quad (2.3)$$

The equation is solved for $\beta_2 d$ and the dielectric constant is calculated using the relation,

$$\epsilon = \frac{1/\lambda_c^2 + (\frac{\beta_2 d}{2\pi d})^2}{1/\lambda_c^2 + 1/\lambda_g^2} \quad (2.4)$$

Equation (2.4) gives several values for the dielectric constant since, $\beta_2 d$ is a multivalued function. To obtain a correct value for ϵ either previous knowledge about the sample property is required or the experiment has to be repeated for different values of d , the sample thickness. In this study the later procedure has been adopted, as there was no data available as regard to the dielectric constant of the sample.

Equating imaginary parts of equation and applying the conditions that α_2 and E_{\min}/E_{\max} are small, the equation will reduce to

$$\alpha_2 d = \frac{\beta_2^2 d^2 \lambda_g}{2 \pi d} \frac{E_{\min}}{E_{\max}} \left[\frac{1 + \tan^2\left(\frac{360 X_0}{\lambda_g}\right)}{\beta_2 d (1 + \tan^2 \beta_2 d) - \tan \beta_2 d} \right] \quad (3.5)$$

Substituting for $\frac{E_{\min}}{E_{\max}} = \frac{\pi \Delta x}{g}$ where Δx is the width of minimum of the standing wave to the double points from equation (2.5) we have,

$$\tan \delta_2 = \frac{\Delta x}{d} \frac{(1/\lambda_c^2 + 1/\lambda_g^2) - 1/\lambda_c^2 \cdot \epsilon}{(1/\lambda_c^2 + 1/\lambda_g^2)} + \frac{\beta_2 d (1 + \tan^2 \frac{360 X_0}{\lambda_g})}{\beta_2 d (1 + \tan^2 \beta_2 d) - \tan \beta_2 d} \quad (2.6)$$

(c) VSWR variation

Variations in the VSWR due to propellant samples at different curing stages has also been recorded using the above set up. The procedure involved reading the values of maxima and minima by moving the probe carriage. The ratio of E_{\max}/E_{\min} was calculated and the results were plotted against curing time.

2.5 ATTENUATION MEASUREMENTS

Another technique employed to study the degree of cure of the material was the attenuation measurements. Microwave absorption property of the sample undergoes

changes during the process of curing and hence by monitoring the power at the sample output, it is possible to get an idea regarding the states of cure of the propellant sample.

The measurement set up adopted for this technique is shown in Fig.2.5(A). A directional coupler was used to tap a part of the transmitted energy for reference. This power is monitored to ascertain constant input power. An HP 346 A powermeter was used for measuring the microwave power at the input and output of the material under test. A waveguide cell was constructed for holding the sample and oil at the curing temperature (70°C) was circulated through its output jacket.

Sample in paste form was introduced into the cell and the power at the sample output was measured. The waveguide cell was maintained at 70°C by circulating oil through the jacket and measurements were taken at different intervals or at different curing stages. This was continued till the expiry of curing period. Experiment was repeated for a sample of another composition. The results (output power vs curing time) were plotted.

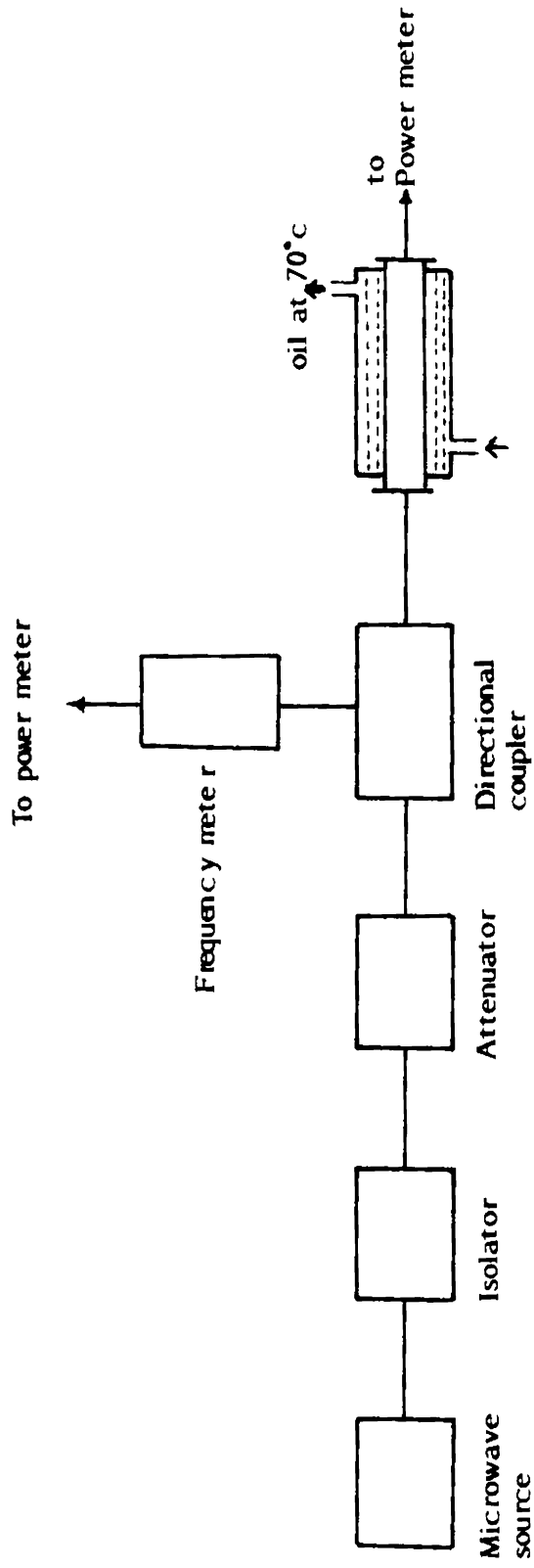


Fig - 2.5(A) Experimental set up for attenuation measurements

2.6 CONCLUSION

In this chapter, different experimental techniques adopted and facilities used during the course of this study has been described. A free space transmission method and an automatic network analyzer measurement system for quick and reliable inspection of materials have been brought out. Importance of dielectric constant measurement to understand the state of cure of a propellant sample and different techniques employed for the same were described. Attenuation measurements carried out to study the absorptive property of a propellant sample undergoing curing process has also been described in this chapter.

Chapter 3

EXPERIMENTAL RESULTS

	<u>Page</u>
3.1 Introduction	61
3.2 Detection of Flaws by Microwave Transmission Technique	63
3.3 Locating the Defects	70
3.4 Variation in Phase and Amplitude with Defect Size and Geometry	76
3.5 Multiple Defects: Defect Resolution	87
3.6 Effect of Changing the Frequency	99
3.7 Variation of Dielectric Constant of a Propellant Mix Subjected to Curing	99
3.8 Variation of Loss Tangent	106
3.9 Correlation between Mechanical and Electrical Properties	106
3.10 Attenuation Measurements	112
3.11 Variation of VSWR	115
3.12 Conclusion	115

Chapter 3

EXPERIMENTAL RESULTS

3.1 INTRODUCTION

The results obtained from various studies carried out on propellant samples are presented in this chapter. The first part of the results presented are related to the observations on cured propellant samples. These results can be grouped into the following three categories.

1. Detection of flaws
2. Locating the flaws and
3. Flaw characterization

The presence of a flaw or a void within a cured propellant sample was detected by comparing the changes in phase and amplitude of the transmitted microwave signal corresponding to a defective sample with that of a reference sample. Results are presented both for samples with single localized defects and those with multiple defects. Changes in signal characteristics corresponding

to flaws of rectangular and cylindrical cross-sections are also presented. The samples tested include those with and without a cavity along its central or axial line.

After the detection of a defect, the next task would be to locate it. Hence, following the detection results pertaining to detection of the location of flaw are presented. The test method and the procedures involved in the measurements have already been discussed in chapter 2. A comparison of the actual distances of flaw-position from the centre of the sample and its location experimentally determined is presented in a tabular form.

The characterization of defects aim at classifying them in size and shape from the observed amplitude and phase patterns. Therefore, experimental curves are given for defects of various sizes and with rectangular and cylindrical cross-sections.

The second part of the results are the outcome of the experiments carried out on propellant samples undergoing curing process. The results presented include changes in the dielectric constant with curing time of propellant

samples of two different compositions. The other results presented are changes in loss-tangent, VSWR and attenuation of the propellant samples undergoing curing with curing-cycle. The main aim of this experiment was to predict the cure-state of the propellant sample from the changes observed in the electrical properties.

Using the data from RPP Division, VSSC, Trivandrum, the changes in the mechanical property (tensile strength) of propellant sample were plotted against curing time. In the same graph, the changes observed in electrical properties were also plotted to study the correlation between the mechanical property and the electrical property. This curve is also incorporated in this chapter.

3.2 DETECTION OF FLAWS BY MICROWAVE TRANSMISSION TECHNIQUE

The first sample tested was (RH 200), without a mandrel and having a rubber sheathing on its periphery. The mandrel was avoided for reasons explained in chapter 2. The diameter of the sample was 20 cm. The test set up shown in Fig.2.3(A) was employed in this study. The experiment was carried out at 9 GHz.

The amplitude and phase of the transmitted signal were plotted against the angular positions of the sample. The curves obtained for a reference sample are shown in Figs.3.2(A) and 3.2(B). The amplitude pattern for a defective sample, with a cylindrical flaw of diameter 3.2 cm, is shown in Fig.3.2(C). In Fig.3.2(D) changes observed in the phase pattern for a sample with a flaw of rectangular cross-section and size 3x3 cm is shown. The broken curve in the same plot is obtained when the gap was filled with undercured paste.

Similar results have been observed for the tests carried out using an automatic network analyzer system, the HP 8510 B. The results obtained for a propellant sample with a cylindrical cavity of diameter 1.25 cm is shown in Fig.3.2(E). The sample was 24 cm in diameter (RH 250) and was without rubber covering.

The above experiment was repeated using samples with a central star shaped cavity which will be present in a real-time sample. The samples subjected to the study were RH 200 and RH 125 with diameters 20 cm and 11 cm respectively. Both samples were having an outer rubber sheathing.

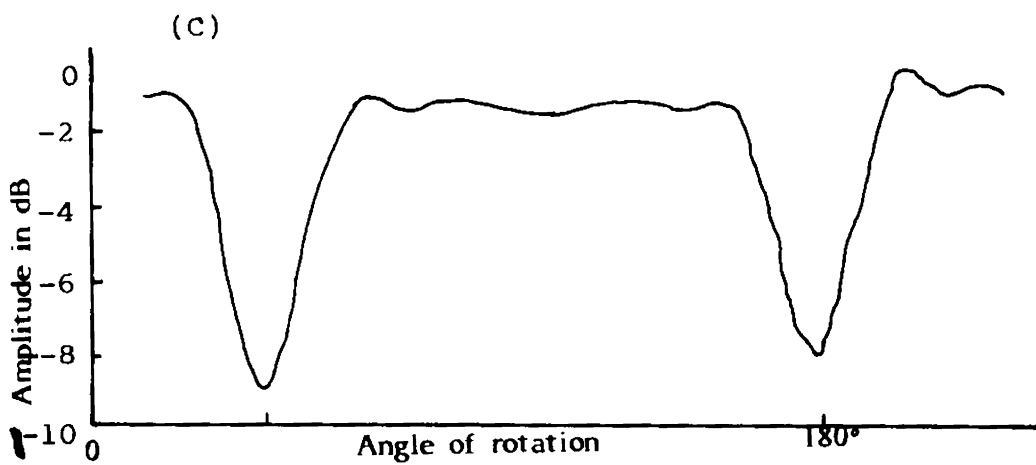
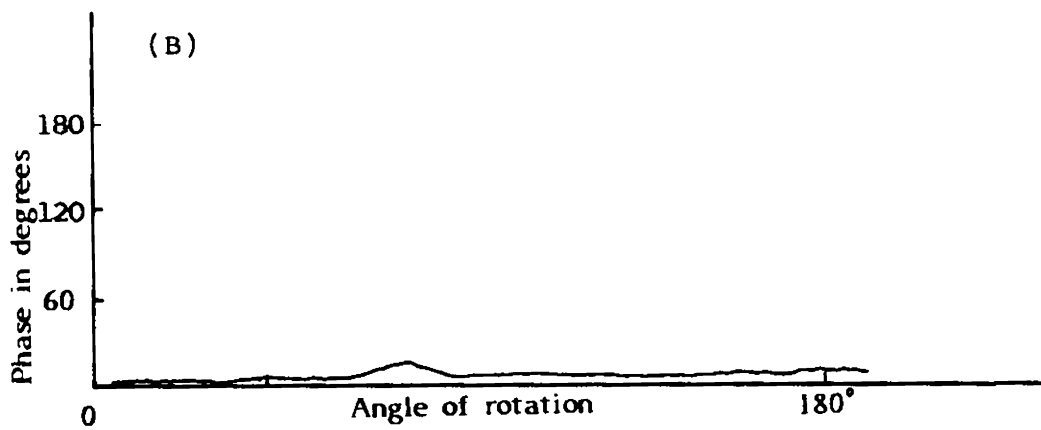
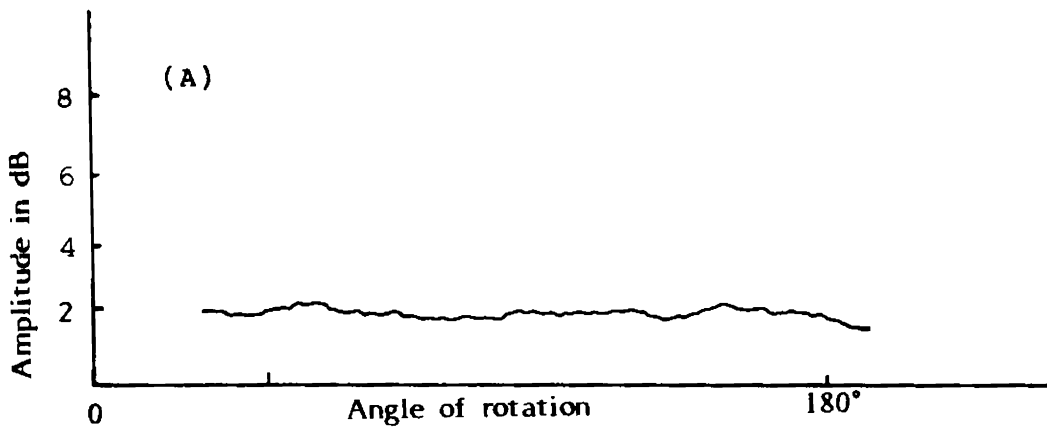


Fig.3.2(A) Amplitude patterns of flawless homogeneous sample
 (B) Phase pattern of a flawless homogeneous sample
 (C) Amplitude pattern of propellant sample with a cylindrical flaw.

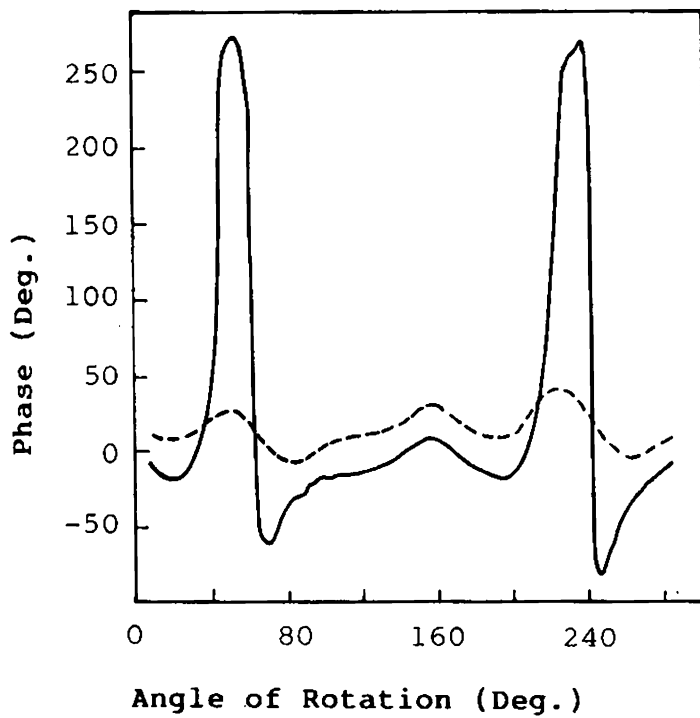


Fig.3.2(D) Changes recorded in the phase pattern for a defective propellant sample.

———— rectangular cavity of size 3x3 cm

----- cavity filled with under cured paste

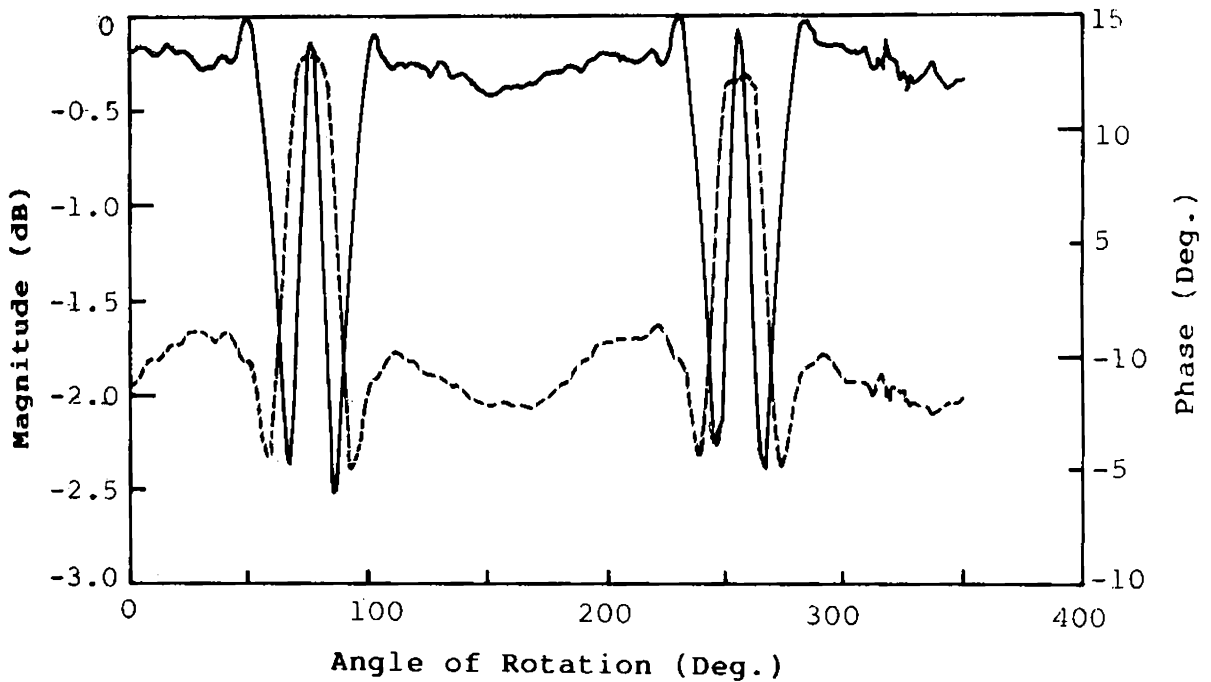


Fig.3.2(E) Amplitude and phase pattern recorded for an KH 250 propellant sample with an artificially created cylindrical flaw, using HP 8510 B network analyzer system.

—— Amplitude; - - - - - Phase
 Frequency 8.5 GHz; Flaw dia. 1.25 cm

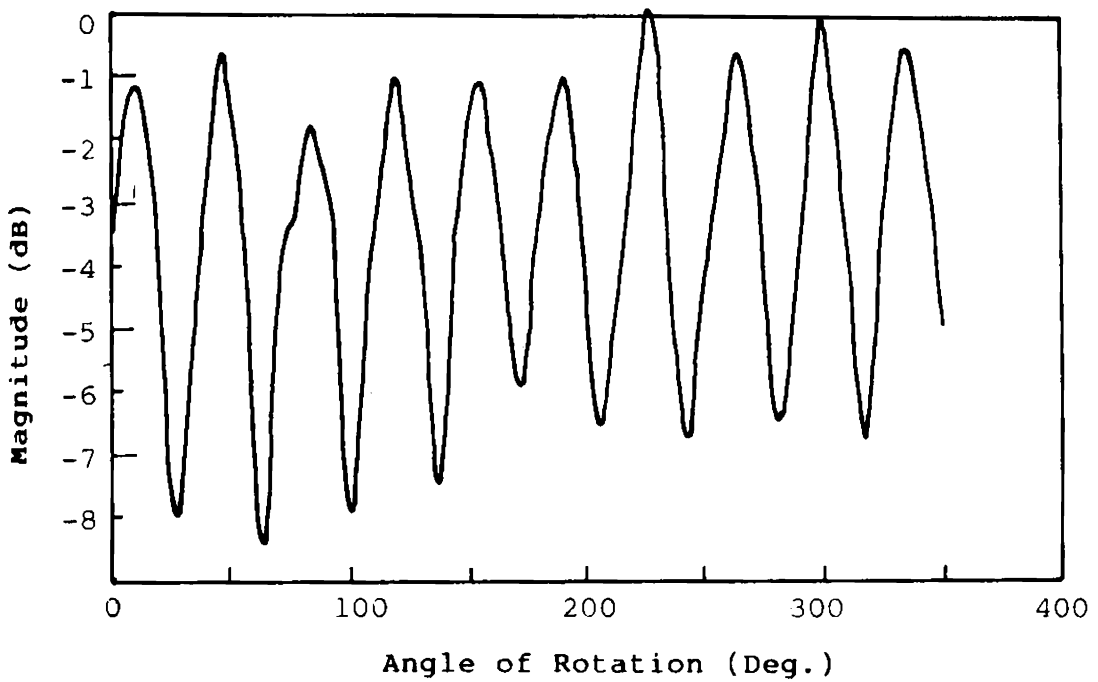


Fig.3.2(F) Amplitude plot for a RH 200 reference sample (sample without any artificially created defect). The ups and downs in the curve is due to a star-shaped cavity along the axis of the test sample. Pattern recorded at 7 GHz.

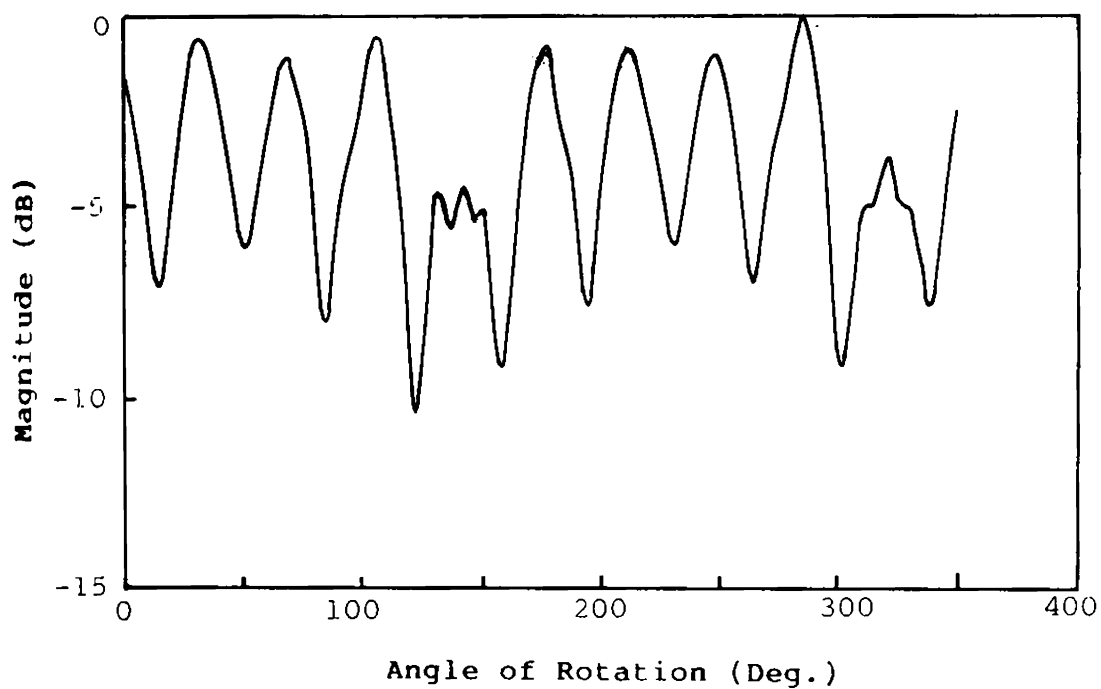


Fig.3.2(G) Amplitude pattern corresponding to a defective RH 200 propellant sample. The defect was an artificially created cylindrical cavity of diameter 1.25 cm. Experiment was performed at 7 GHz.

The recorded amplitude pattern for the RH 200 reference sample is shown in Fig.3.2(F). In Fig.3.2(G) the changes recorded in the amplitude pattern for the same sample, but with an artificially created cylindrical cavity of diameter 1.25 cm is shown. The positions of defects are marked in the plot. Experiment was performed at 7 GHz.

Recordings were carried out for the RH 125 sample also and the results are summarised in Figs.3.2(H) & 3.2(J). The frequency employed was 9 GHz. The positions of defects can be easily recognised from the plots.

The experiments have been carried out at different frequencies and similar results have been observed.

3.3 LOCATING THE DEFECTS

The results presented in the previous section showed that the presence of a defect within a cured propellant sample can be detected as well-marked changes both in phase and amplitude of the transmitted signal. However, the method is useful only in finding out the line

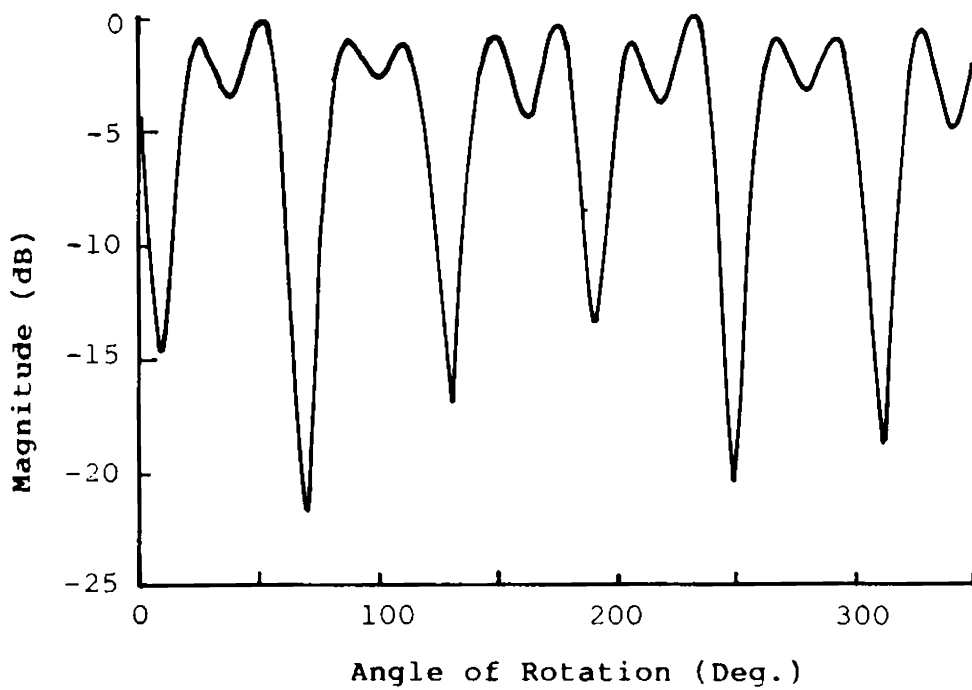


Fig.3.2(H) Amplitude plot for a RH 125 propellant sample without any artificially created flaws (reference sample). The sample was having an axial star-shaped cavity. Pattern recorded at 9 GHz.

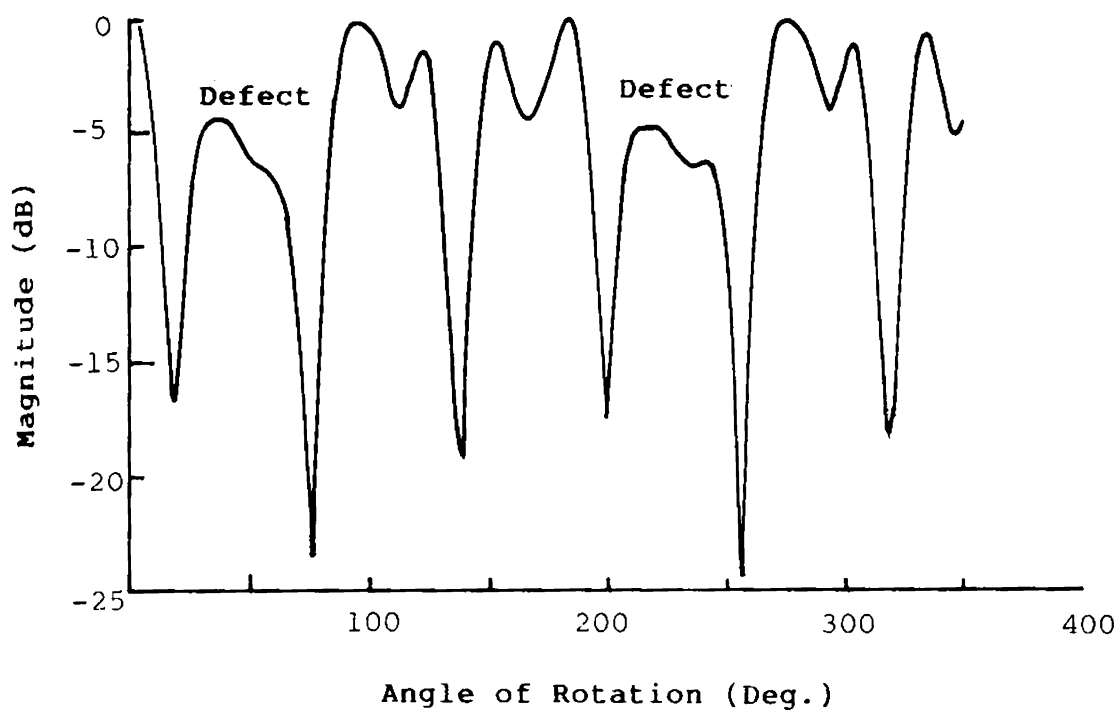


Fig.3.2(J) Amplitude pattern corresponding to a defective RH 125 propellant sample. The defect was an artificially created cylindrical cavity of diameter 1.25 cm. Experiment was performed at 9 GHz.

along which the flaw lies. The position of the defect from the centre of the sample can be determined by using a method already outlined in section 2.3.2(b) of chapter 2. The results obtained using this method is presented in this section.

The observed phase pattern for a defective sample symmetrically mounted between the transmitter and receiver is shown by the solid line in Fig.3.3(A). The sample tested was RH 250 and without a mandrel. The defect was located at 9.25 cm from the centre of the sample. The phase patterns recorded corresponding to different lateral displacements of the sample are illustrated by broken lines in the same. Similar recordings were carried out for a defective sample of the same type but with flaws located at 9 cm and 6.9 cm respectively from the centre of the sample.

From each of the recorded phase patterns the value of ' 2θ ' was measured and using the equation $D = d/\cos \theta$, the position of the defect from the centre of the sample was calculated as explained in chapter 2. The values were tabulated and is shown in table 3.3.

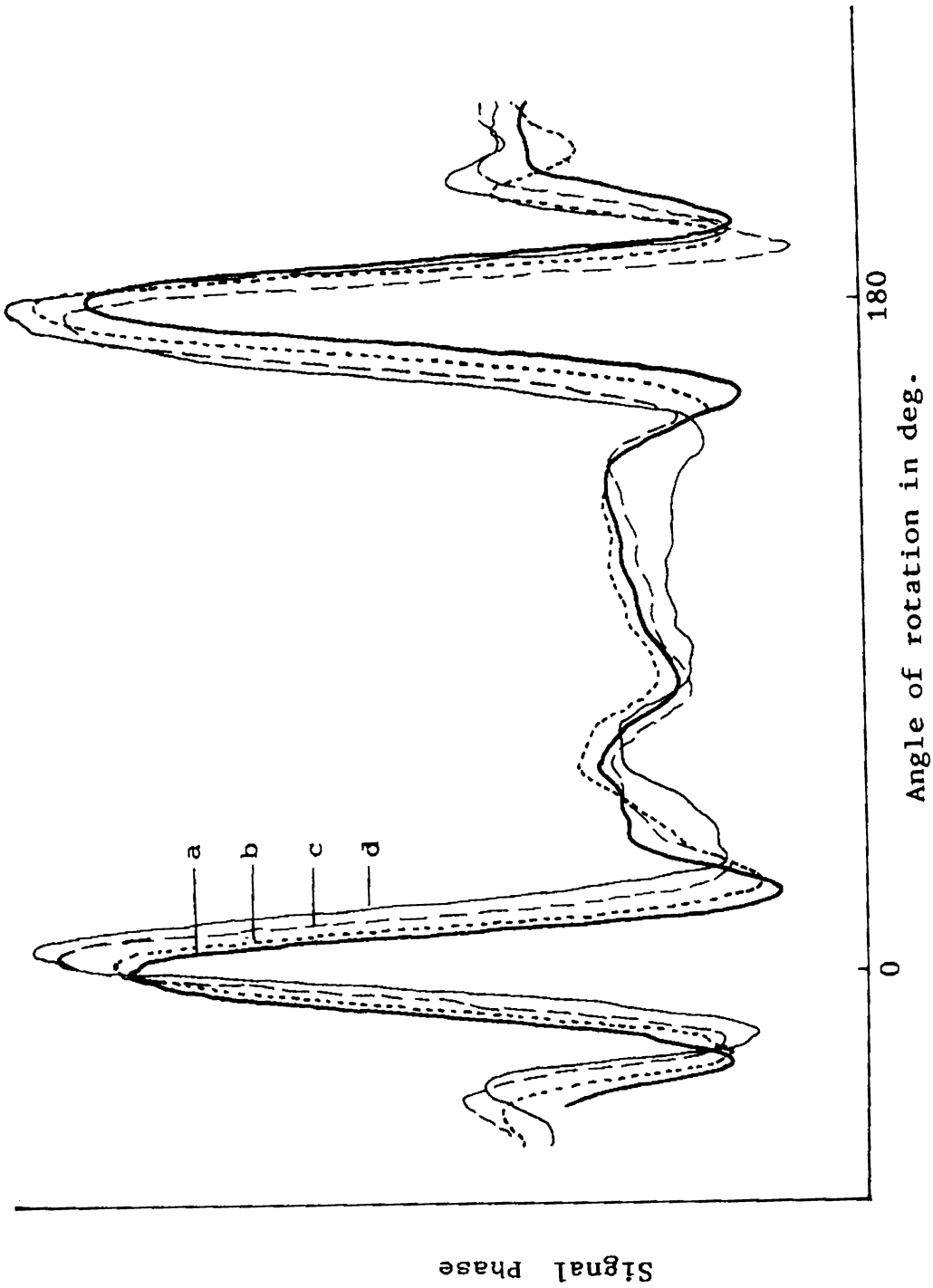


Fig. 3.3(A) Experimentally recorded phase patterns of a rocket propellant sample. (RH 250)
 (a). Sample is mounted symmetrically., (b). with a lateral shift of 0.3 cm., (c) & (d). with a lateral shift of 0.6 and 0.9 cm respectively.

Table 3.3: Table showing the actual defect location and the experimentally determined value.

Sl. No.	Flaw size (Dia-meter) (cm)	Actual distance from the centre D (cm)	Displacement of motor axis d (cm)	2θ	Estimated value of D $D = \frac{d}{\cos \theta}$	% of variation
1.	1.5	9.25	0.3	176.14	8.90	3.78
			0.6	172.28	8.91	3.67
			0.9	168.42	8.92	3.56
2.	1.1	9	0.4	174.90	8.99	0.11
			0.8	169.85	9.04	0.44
			1.2	165.40	9.45	5.00
			1.6	159.70	9.08	0.88
3.	0.9	6.9	1.2	159.01	6.59	4.40
			1.4	155.24	6.53	5.30
			1.6	155.13	7.43	7.60

3.4 VARIATION IN PHASE AND AMPLITUDE WITH DEFECT SIZE AND GEOMETRY

After the defect was detected and its position approximately located, the next step was to see whether the recorded signal characteristics give any information as regard to the size and shape of the defect. Further, for a defect of rectangular geometry there are two dimensions, one parallel and the other perpendicular to the direction of propagation, which define the defect size and the minimum detectable defect size is decided by these flaw dimensions. Hence it was necessary to carry out studies on flaws of different sizes and shapes. In this study only flaw shapes of rectangular and cylindrical cross-section have been considered.

Fig.3.4(A) shows the recorded amplitude patterns for cylindrical flaws of different diameters drilled within a cured propellant sample. For reference, the plot also include the recording of a flaw-free sample.

Figs.3.4(B) to 3.4(E) show amplitude and phase patterns of transmitted signals corresponding to rectangular slots of different dimensions cut in the cured propellant

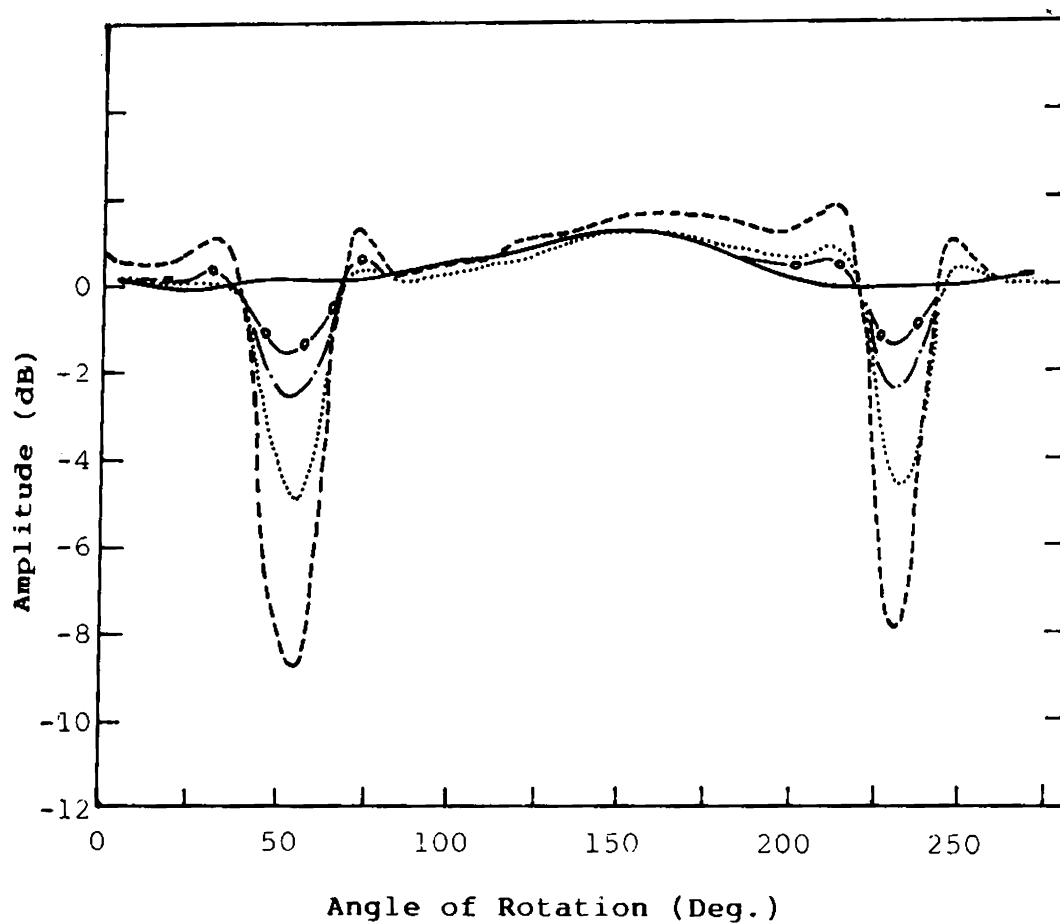


Fig.3.4(A) Changes in the amplitude pattern with defect size recorded for a defective sample. The defect was cylindrical in shape and the pattern was recorded at 10 GHz.

————— reference ; -o-o-o-o- 0.75 cm dia
 0.85 cm dia; - - - - - 1.25 cm dia
 1 cm dia

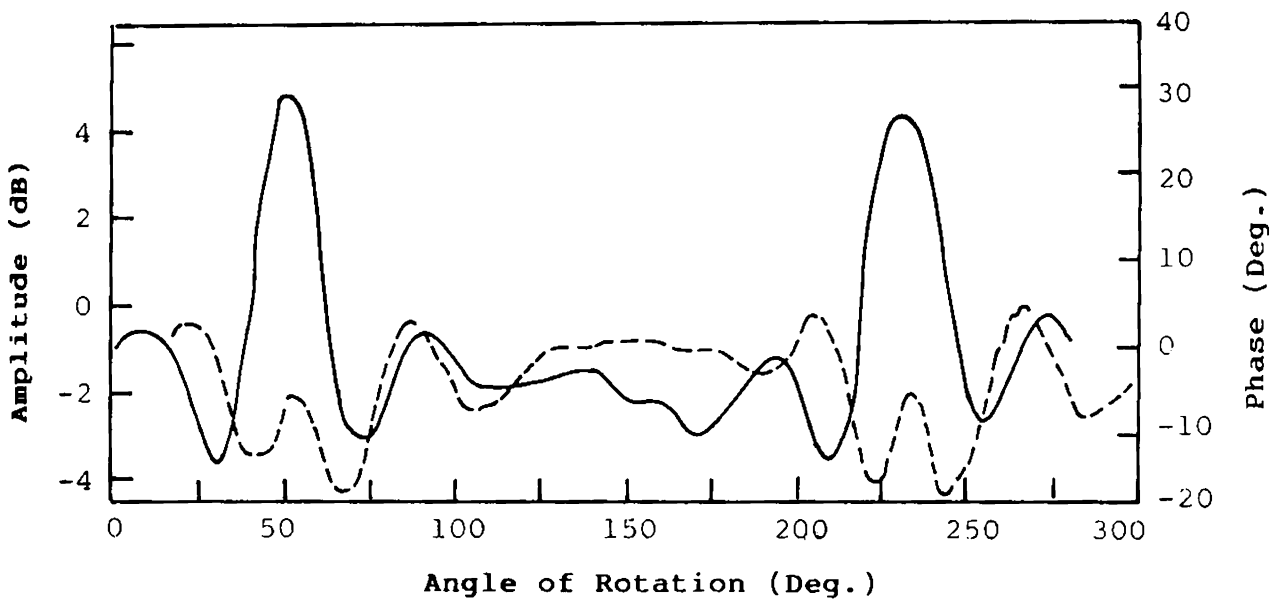


Fig.3.4(B) Amplitude and phase pattern recorded for a cured propellant sample having a rectangular flaw of size 0.5x0.9 cm, with shorter dimension being parallel to the direction of propagation. Pattern recorded at 9 GHz.

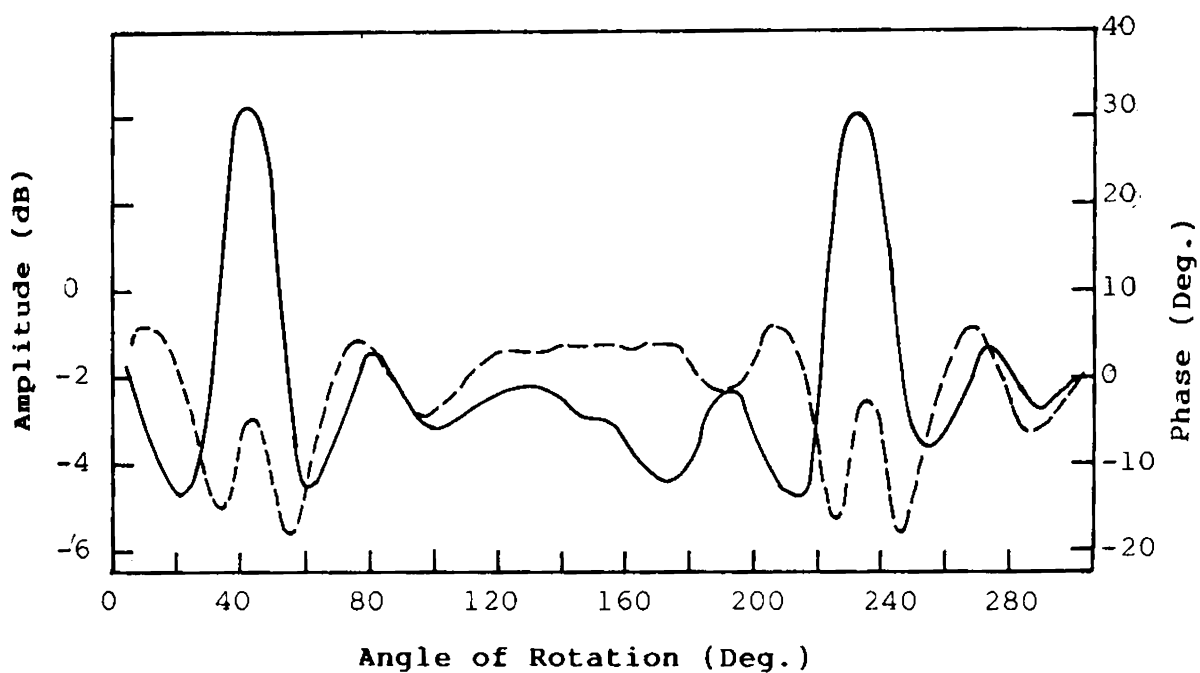


Fig.3.4(C) Amplitude and phase patterns for a defective propellant sample with rectangular flaw. Flaw size 0.9×0.5 cm, with shorter dimension being perpendicular to the direction of propagation. Pattern recorded at 9 GHz.

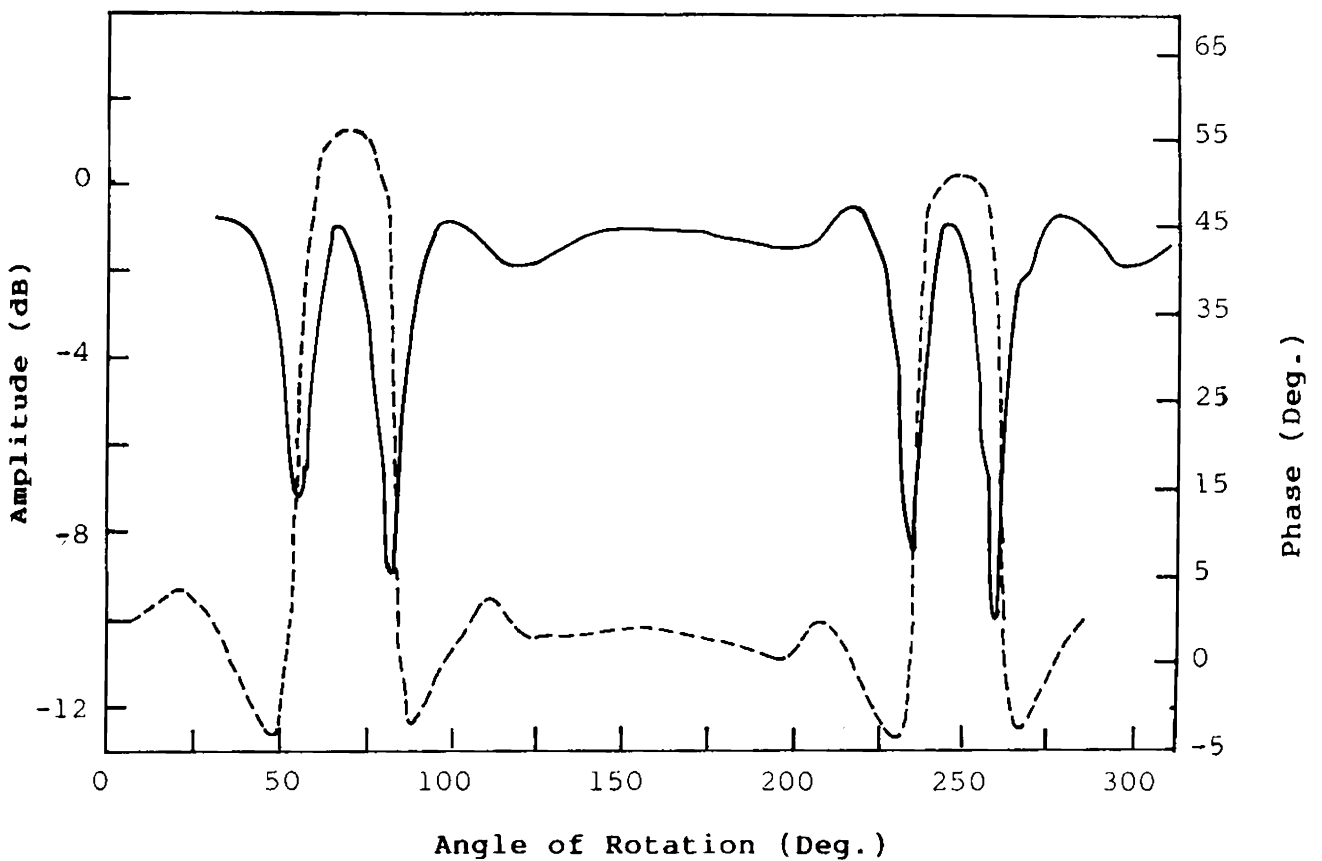


Fig.3.4(D) Amplitude and phase patterns for a defective propellant sample with a rectangular flaw. Flaw size were: 2.8 cm - perpendicular to the direction of propagation; 0.9 cm - parallel to the direction of propagation. Frequency employed - 9 GHz.

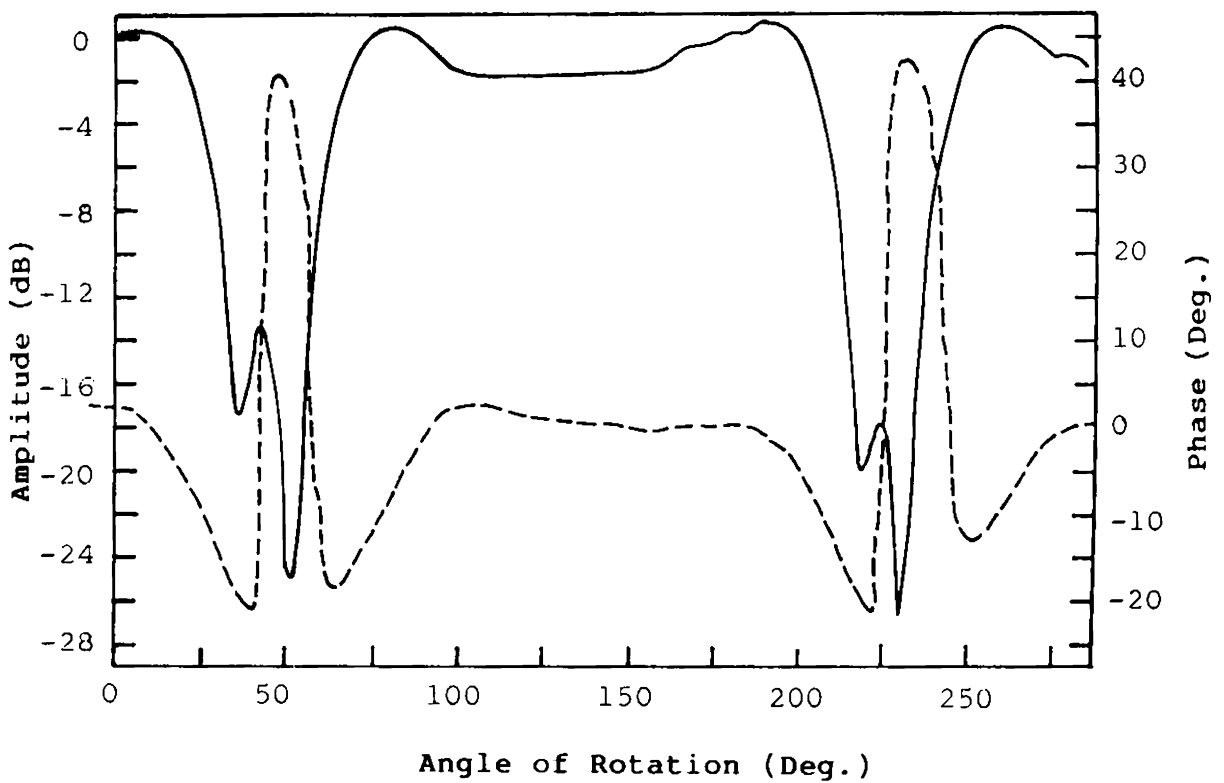


Fig.3.4(E) Amplitude and phase patterns for a defective propellant sample with a rectangular flaw of dimensions 2.8 cm parallel and 0.9 cm perpendicular to the direction of propagation. Frequency used was 9 GHz,

sample. Fig.3.4(F) shows the amplitude pattern corresponding to the minimum detectable defect size in directions both parallel and perpendicular to the direction of propagation in the operating frequency band (ie., X-band).

Similar measurements have been carried out using the 8510 B automatic network analyzer system. The amplitude obtained for cylindrical flaws of different dimensions are summarised in Fig.3.4(G). The frequency used was 9 GHz. The experiment was repeated at different frequencies and the results were reproducible.

Effort has also been made to characterize the defect-type from the recorded patterns. For this purpose both rectangular and cylindrical flaws were cut into the same sample and the amplitude and phase patterns were plotted.

In Fig.3.4(H), one such recorded amplitude pattern is shown. The defect dimensions were 1 cm x 1.75 cm for rectangular type and 1.75 cm diameter for cylindrical type. Another recording was done for a second sample with

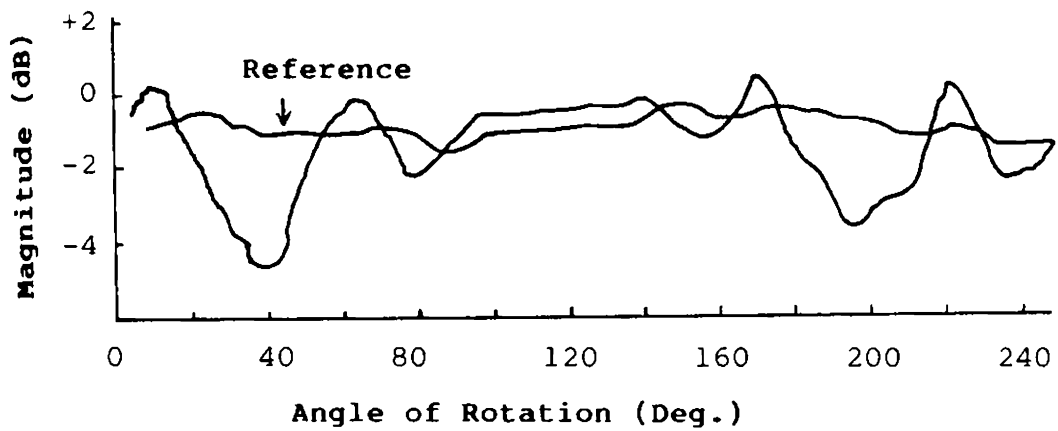


Fig.3.4(F) Amplitude pattern for a defective propellant sample. The defect size was 0.45x0.45 cm which turned out to be the minimum detectable defect size. The plot also include the reference curve.

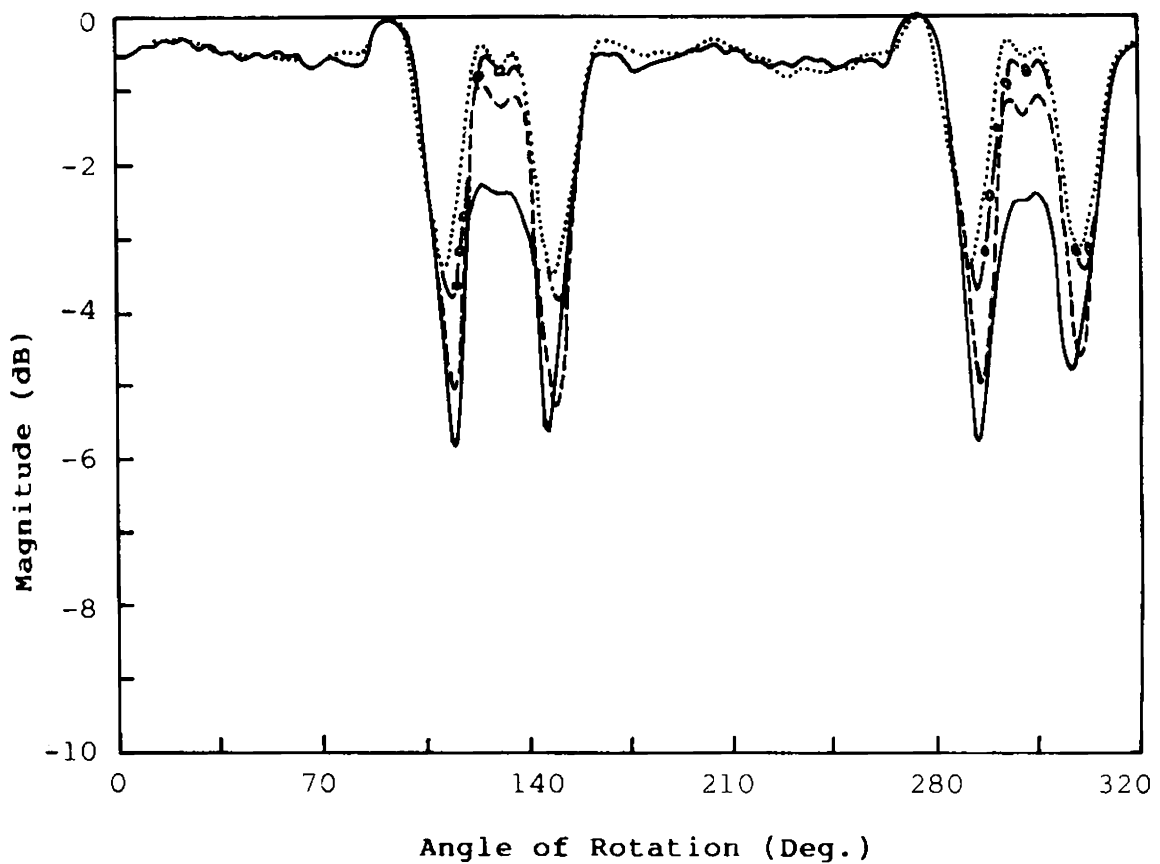


Fig.3.4(G) Changes recorded in the amplitude patterns for a cured propellant sample having defects of different sizes. The defect was cylindrical in shape and the patterns were recorded at 9 GHz.

..... 9 mm ; -o-o-o-o-o- 11.1 mm
 ----- 12.5 mm ; ————— 17 mm

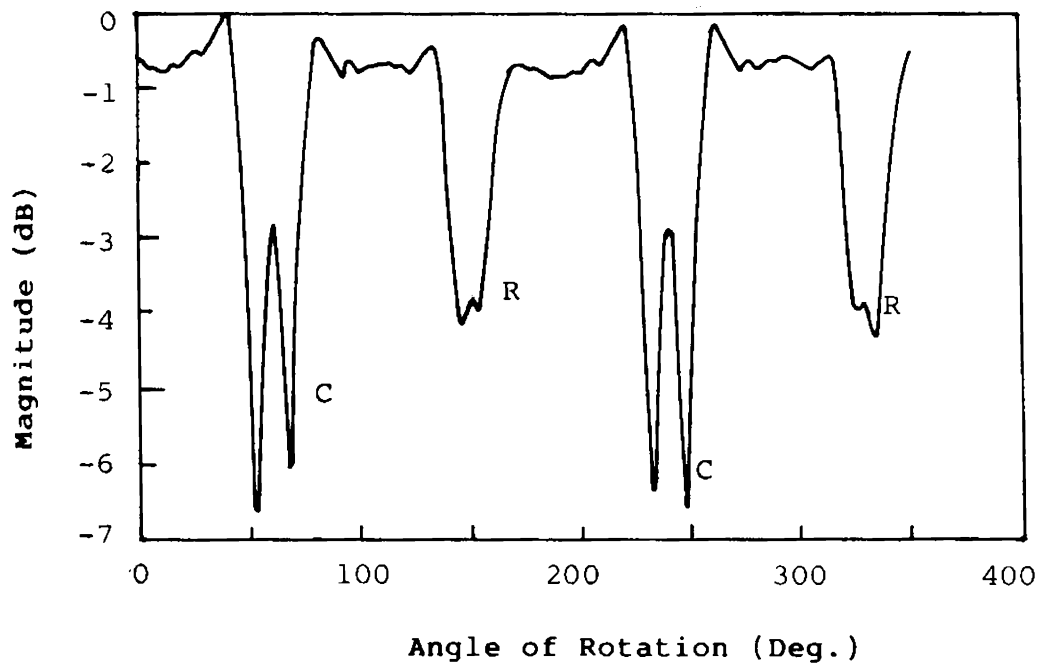


Fig.3.4(H) Recorded amplitude pattern for a cured propellant sample with two defects of different geometry.

C - Cylindrical (1.75 cm dia)

R - Rectangular (1x1.75)cm

Test frequency - 12 GHz.

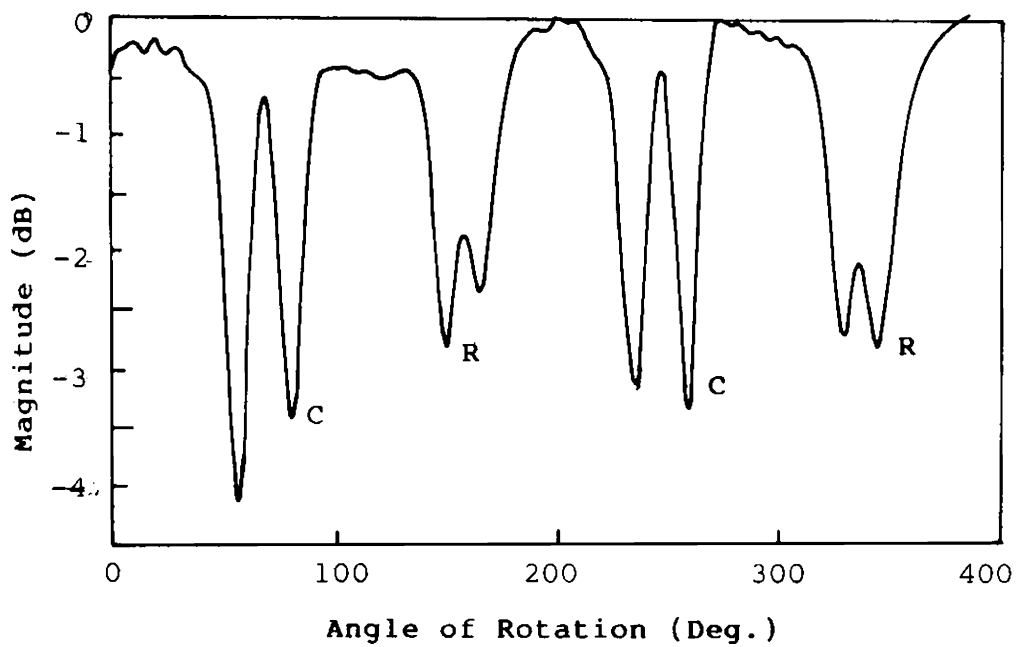


Fig.3.4(J) Amplitude plot for a cured propellant sample with defects of two different geometry.

C - Cylindrical (1.5 cm dia)

R - Rectangular (2x1.5) cm

Pattern was recorded at 10 GHz.

defect dimensions 2 cm x 1.5 cm for rectangular type and 1.5 cm diameter for cylindrical type. The recorded pattern is shown in Fig.3.4(J). Similar recordings were observed at different operating frequencies.

3.5 MULTIPLE DEFECTS: DEFECT RESOLUTION

So far, detection and location of single localized flaws have been dealt with. In this section results obtained from experiments carried out on a cured propellant sample with multiple defects are presented. One problem often associated with a sample having multiple flaws is the defect resolution ie., how well one defect can be distinguished from the other. The major parameters which decide the defect resolution are:

- i) width and shape of the microwave beam
- ii) defect size and shape, and
- iii) defect location, (if flared beam is employed)

For a parallel beam all the defects of the same size and shape, will lie within the beam for a fixed time and hence the angular displacement over which the changes can be observed

will be the same irrespective of the defect location. Here the only parameter which decides the resolution is the width of the beam. However, for a flared beam, defects which are close to the periphery of the sample will lie for a shorter duration (or over a smaller angular displacement) while those at the interior of the sample will be in the beam over a longer period. Hence the location of the defects also plays a role in deciding the resolution. Other factors which will have a direct effect on the width of the beam are the operating frequency and the spacing between the sample and the transmitting and receiving horns. Increasing the frequency reduces the beamwidth and hence resolution will improve. Similarly closer spacings of the transmitting and receiving horns will also result in an improvement of resolution.

In the following investigation, defects lying only on the periphery of the sample and along the same circumference, have been considered. Defects of cylindrical shapes were analyzed. Due to shortage of samples patterns were recorded only for limited cases.

Artificial defects of cylindrical types were created within the samples at different angular spacings

and the transmitted signal characteristics were recorded. Fig.3.5(A) shows the amplitude pattern recorded for a sample with two cylindrical flaws of diameters 2.2 cm and 1.25 cm respectively at an angular spacing of 100 degrees between them and with the defects located at a distance of 9.5 cm from the centre of the sample. In Fig.3.5(B) the amplitude pattern recorded for the same sample at a different frequency is shown. Another amplitude pattern recorded for two defects much more closely spaced (angular spacing of 30 degrees) is shown in Fig.3.5(C). This was recorded at 8 GHz. Plots corresponding to frequencies of 10 GHz and 12 GHz are shown in Figs.3.5(D) & 3.5(E) respectively. Experiments were repeated for a sample with three cylindrical flaws. The recorded patterns for two different cases at different frequencies are illustrated in Figs.3.5(F) to 3.5(J). In the first case (Fig.3.5(F) & 3.5(G)) the three defects were equally spaced at 30 degrees between them while for the second case (Fig.3.5(H) & 3.5(J)) the first two defects are spaced at 30 degree angle while the third defect is at an angular spacing of 20 degree from the second (or centre) defect. These results have been analyzed in more detail in the succeeding chapter.

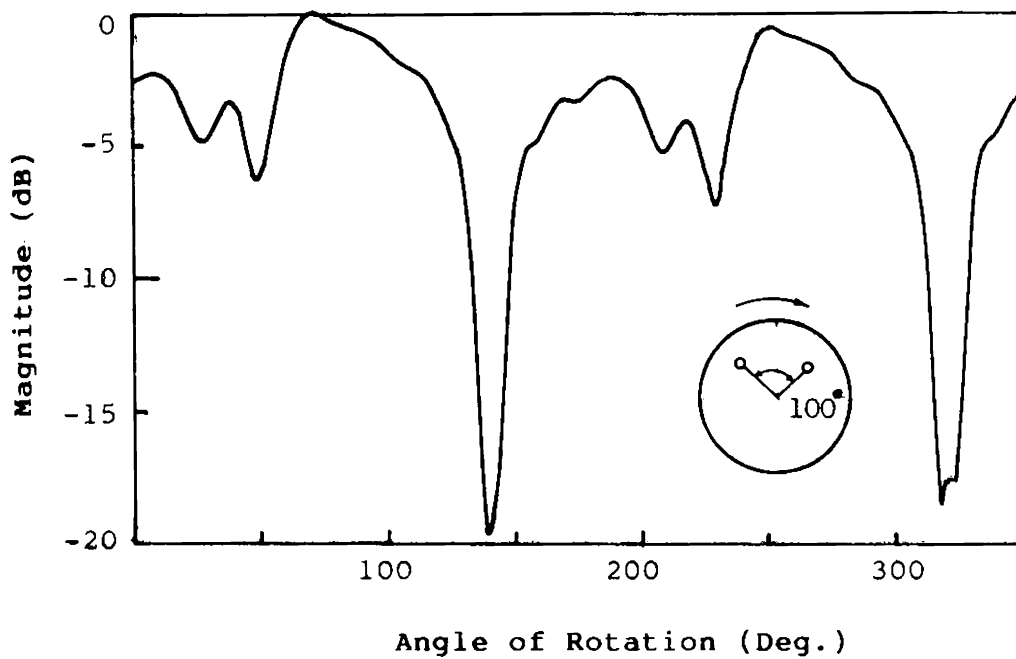


Fig.3.5(A) Amplitude plot for an RH 250 sample with two cylindrical flaws artificially created. Test frequency was 8 GHz. Top view of the sample given in inset.

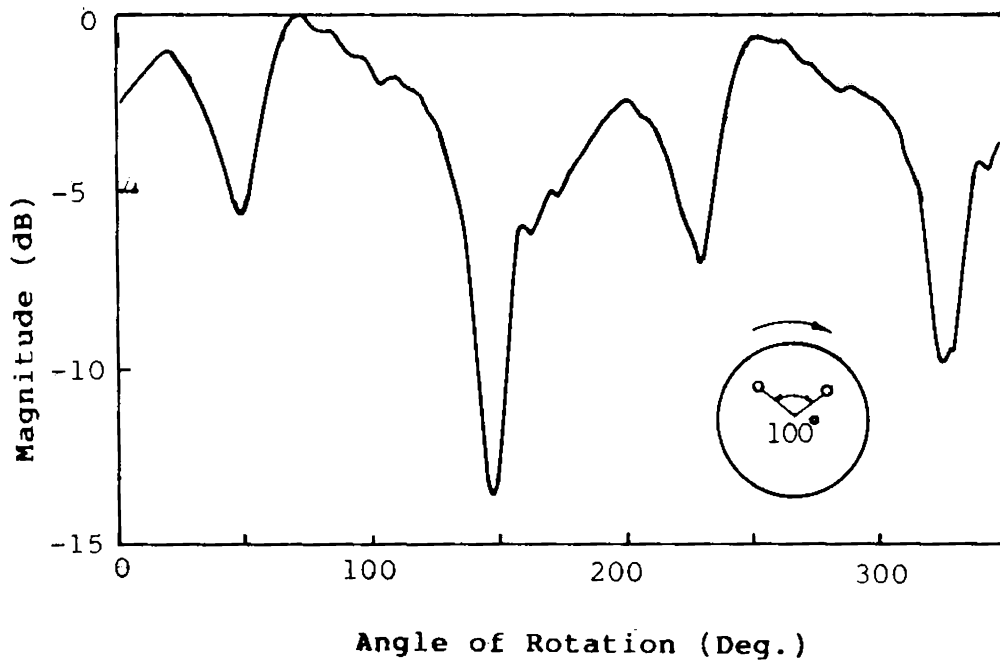


Fig.3.5(B) Amplitude pattern recorded for a cured propellant sample (RH 250) with two artificially created flaws separated by 100 deg. Top view of test sample shown in inset. Test frequency was 12 GHz.

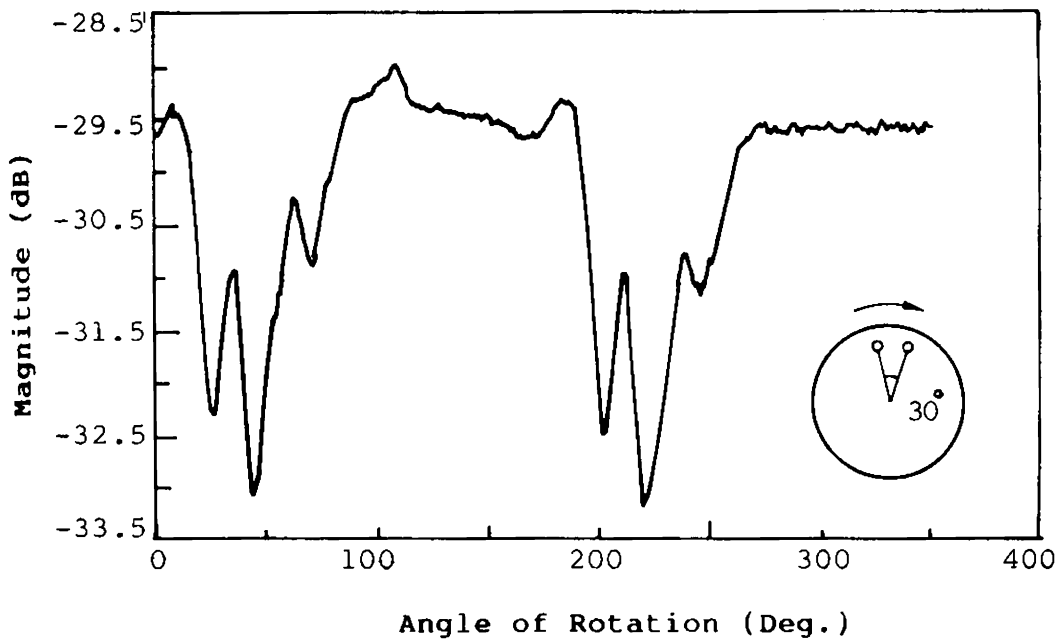


Fig.3.5(D) Amplitude pattern for an RH 250 defective sample with two artificially created flaws as shown in inset (top view). The experiment was done at a frequency of 8 GHz.

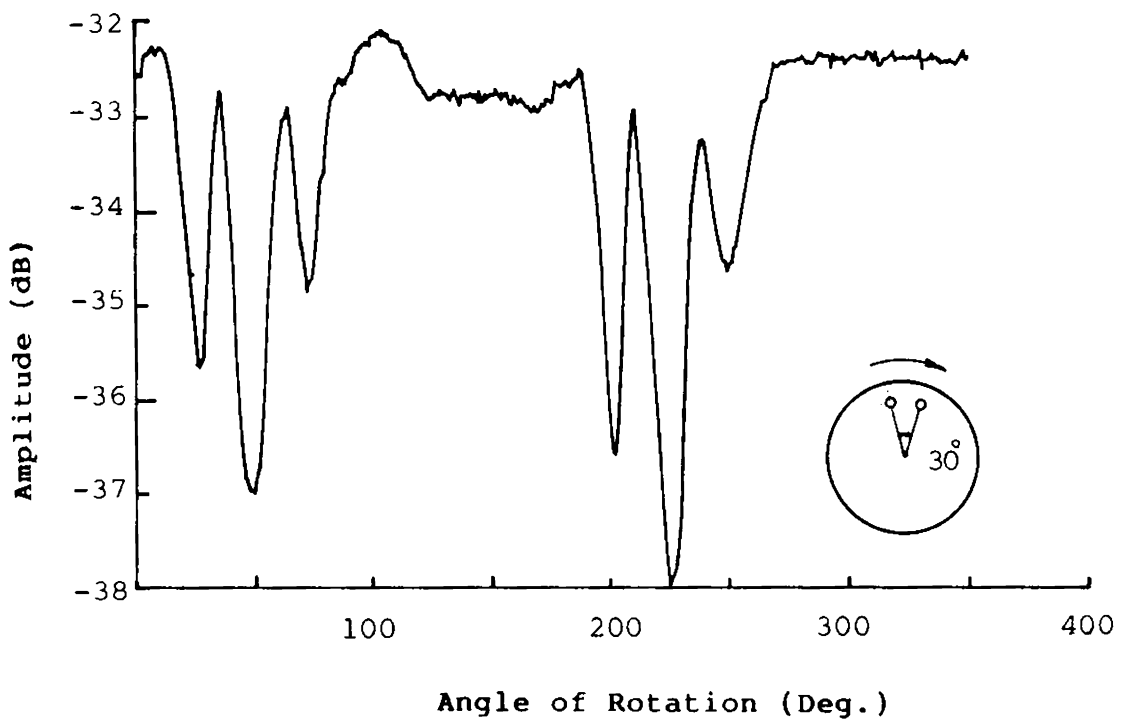


Fig.3.5(D) Amplitude pattern for a defective propellant sample with two cylindrical flaws separated by 30 degrees. Frequency used - 10 GHz.

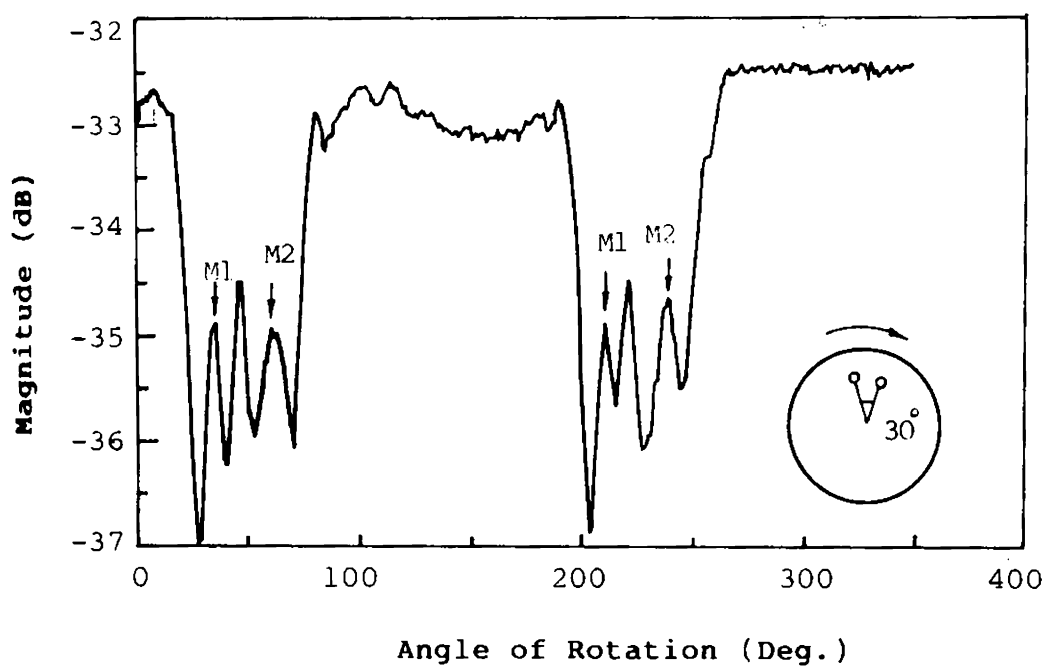


Fig.3.5(E) Recorded amplitude pattern for a defective sample at 12 GHz with test sample (top view) shown in inset.

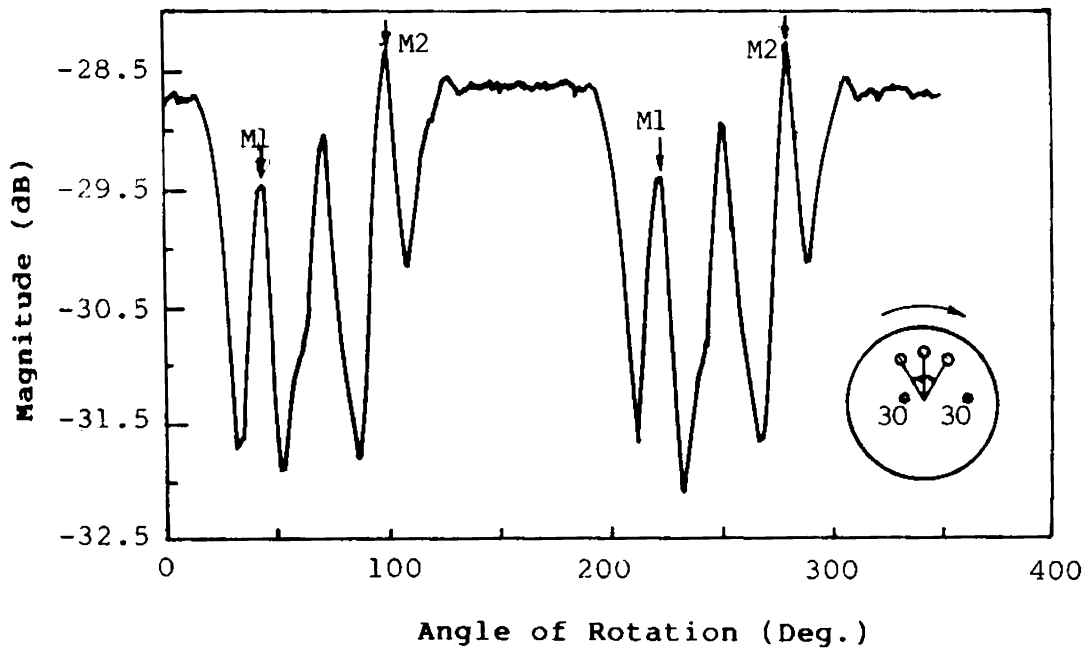


Fig.3.5(F) Recorded amplitude pattern along with top view of the test sample. The pattern was recorded at 8 GHz.

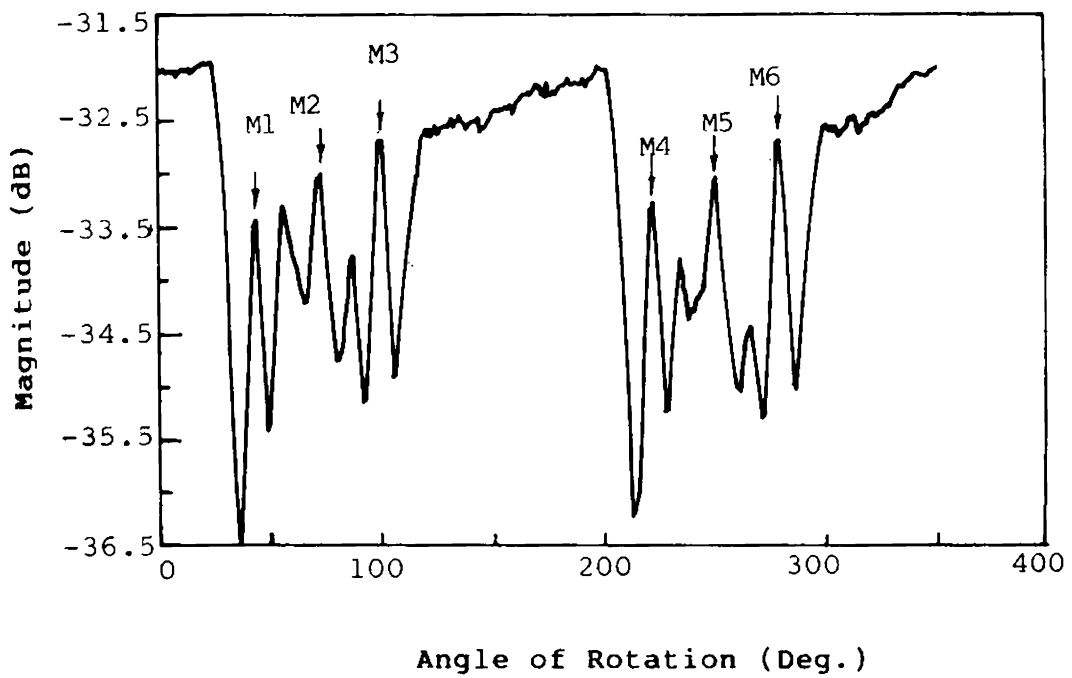


Fig.3.5(G) Amplitude pattern recorded at 12 GHz for the same defective sample shown in inset , Fig.3.5(F).

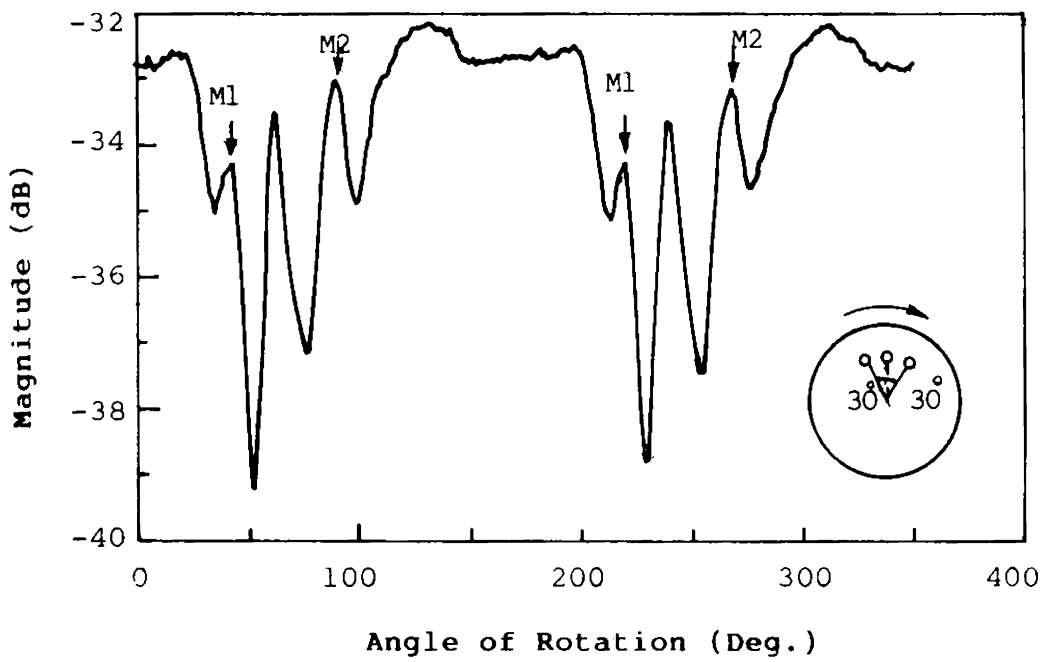


Fig.3.5(H) Amplitude pattern for an RH 250 sample with three defects. Test frequency was 10 GHz.

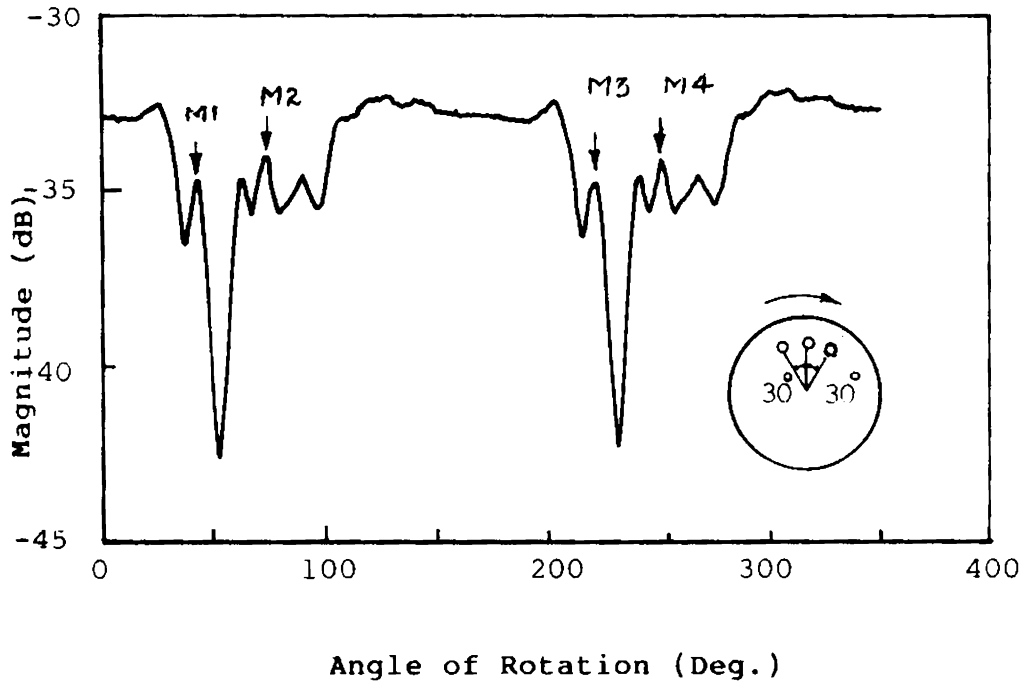


Fig.3.5(J) Amplitude pattern for the test sample (top view shown in inset) at 12 GHz.

3.6 EFFECT OF CHANGING THE FREQUENCY

Experiments were conducted to study the response of an artificially created flaw within a non-metallic material to changes in frequency of operation. The results are summarised in Figs.3.6(A) to 3.6(E). Figs.3.6(A) depicts the changes in both amplitude and phase of the transmitted signal corresponding to a flaw of 15 mm diameter created artificially within a solid propellant sample. The flaw location was close to the periphery of the sample. In Figs.3.6(B) and 3.6(C) similar patterns are shown for flaw-size of 12.5 mm diameter and the flaw being created closer to the centre of the sample. Another result is shown in Figs.3.6(D) and 3.6(E) for a flaw size of 17 mm.

3.7 VARIATION OF DIELECTRIC CONSTANT OF A PROPELLANT MIX SUBJECTED TO CURING

As outlined in chapter 2, a guided wave method was used to study the variations in the dielectric constant of a propellant mix at different stages of curing. Two different propellant compositions have been studied. These are designated as composition I (IPP 40-LIVE) and

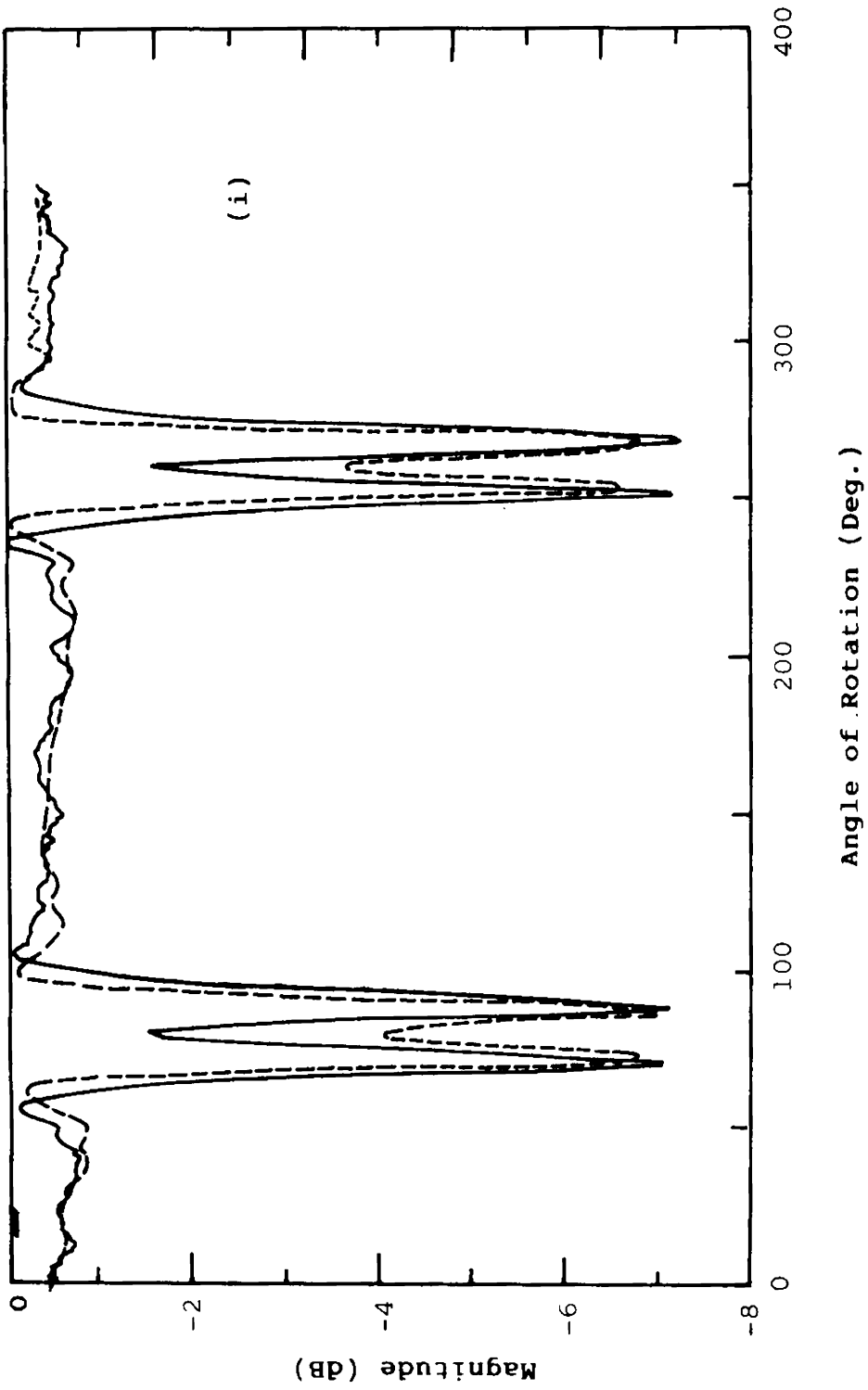


Fig.3.6(A) (i) Amplitude pattern recorded for a defective sample with a cylindrical flaw (dia - 15 mm) at two different frequencies.
—— 9 GHz ; - - - - - 10.5 GHz

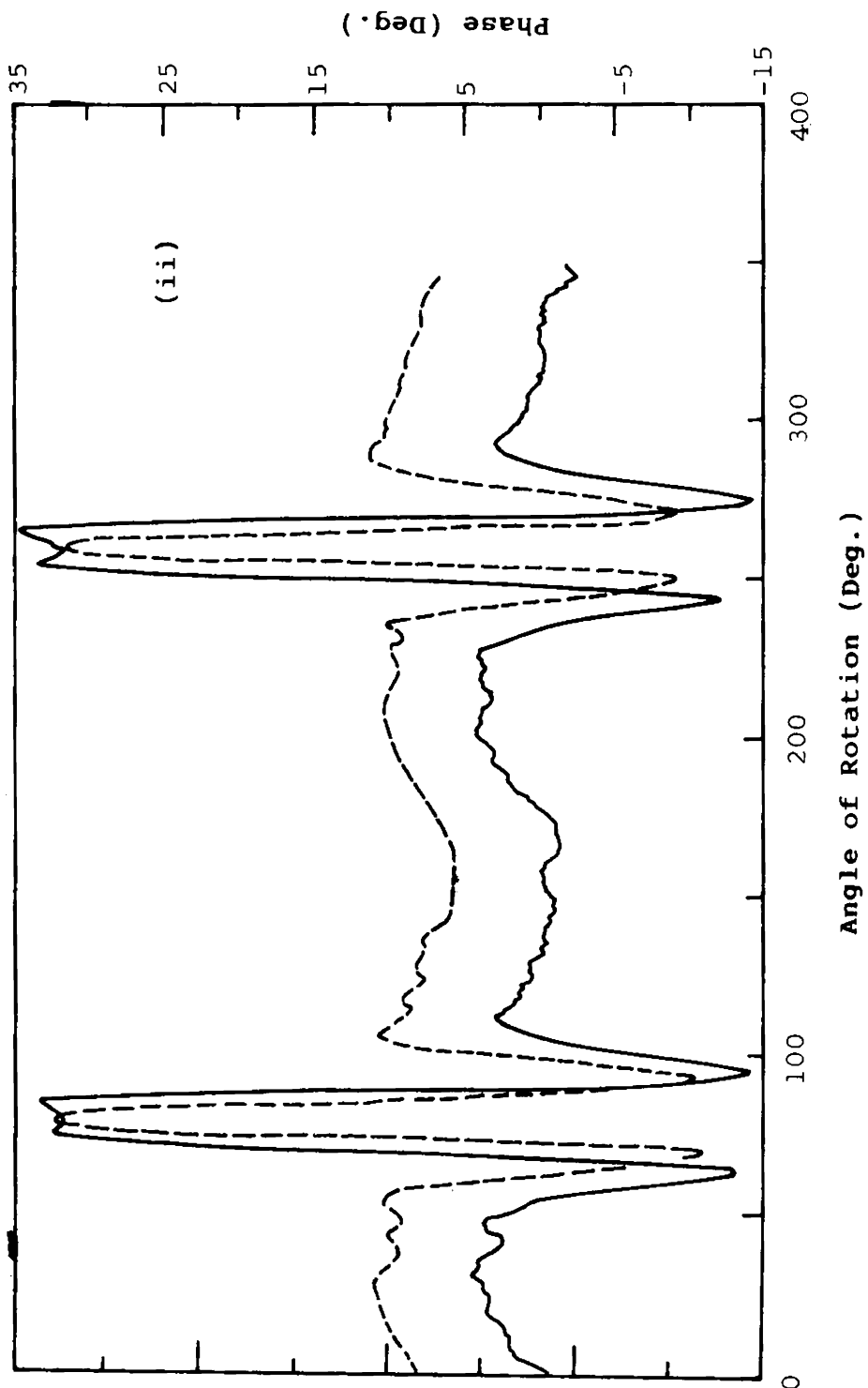


Fig.3.6(A)(ii) Phase pattern recorded for a defective sample with a cylindrical flaw (dia - 15 mm) at two different frequencies.

— 9 GHz ; - - - - 10.5 GHz

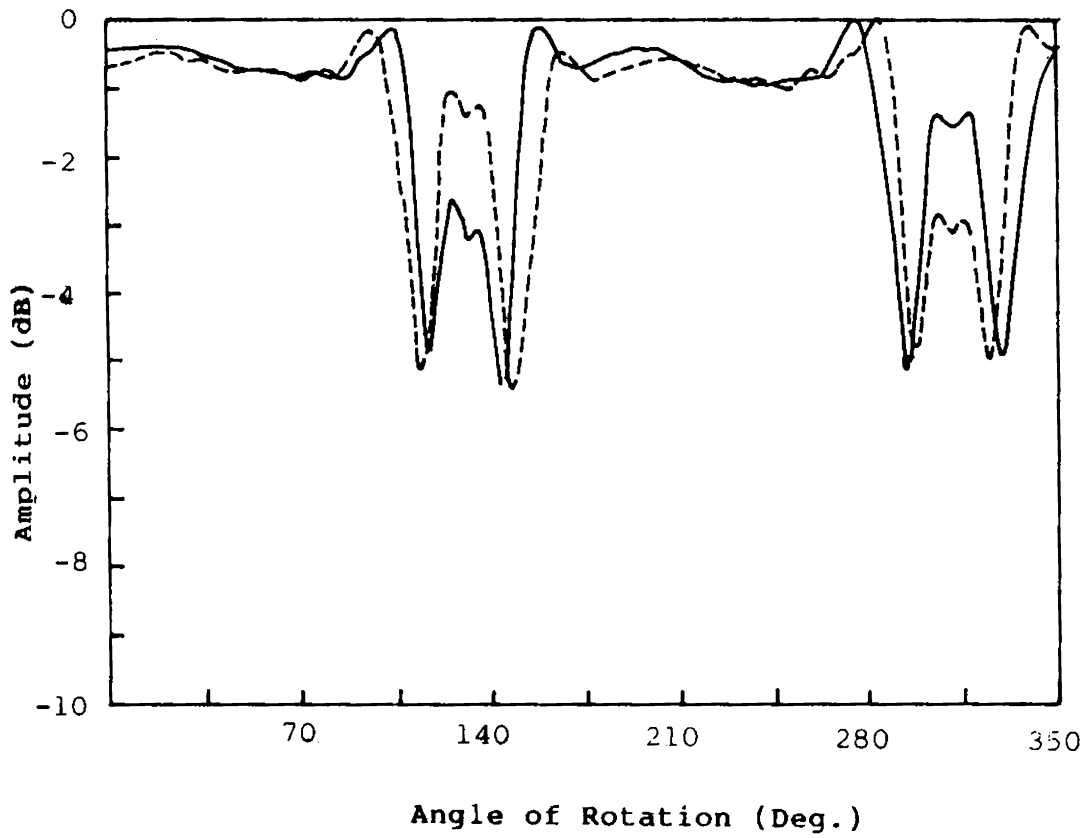


Fig.3.6(B) Amplitude pattern for a propellant sample with a cylindrical flaw of diameter 12.5 mm recorded at two different frequencies.
—— 12 GHz; - - - - 9 GHz.

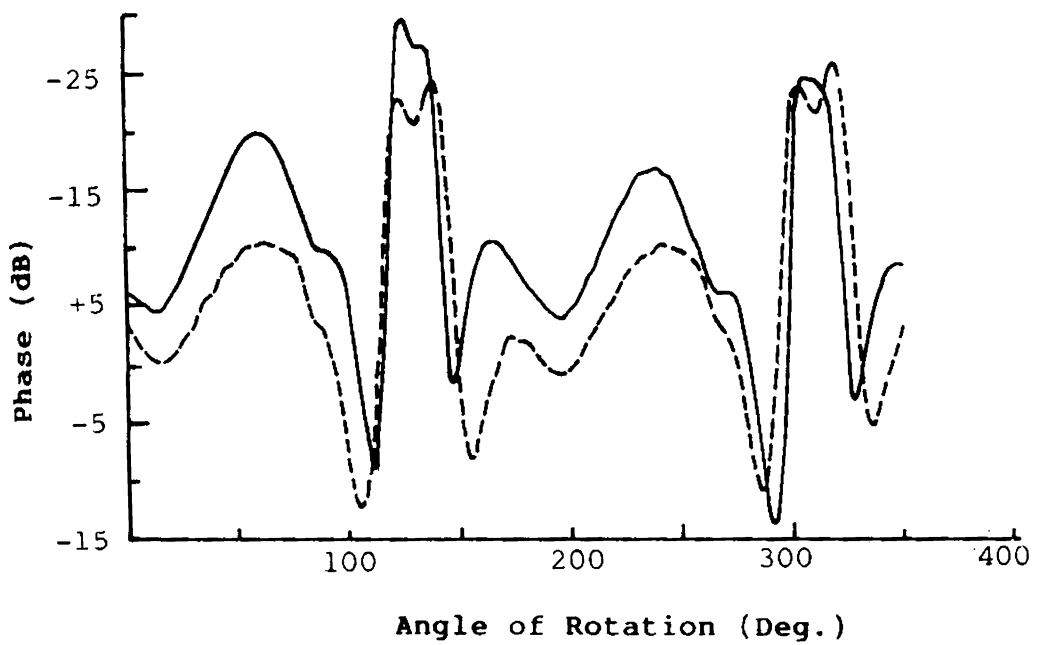


Fig.3.6(C) Phase pattern recorded for a defective sample with a cylindrical flaw of diameter 12.5 mm at two different frequencies.

———— 12 GHz; - - - - - 9 GHz

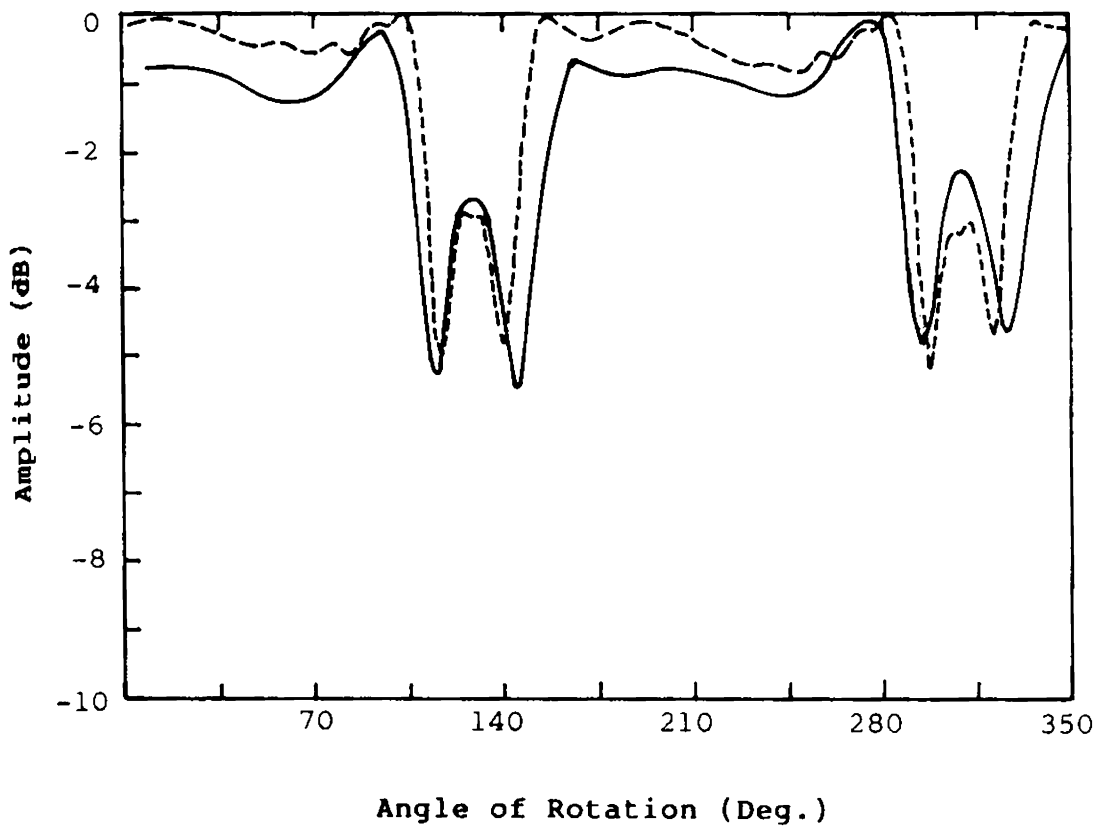


Fig.3.6(D) Amplitude pattern recorded for a defective sample at two different frequencies. The defect was a cylindrical cavity of diameter 17 mm. — 8 GHz; ---- 12 GHz

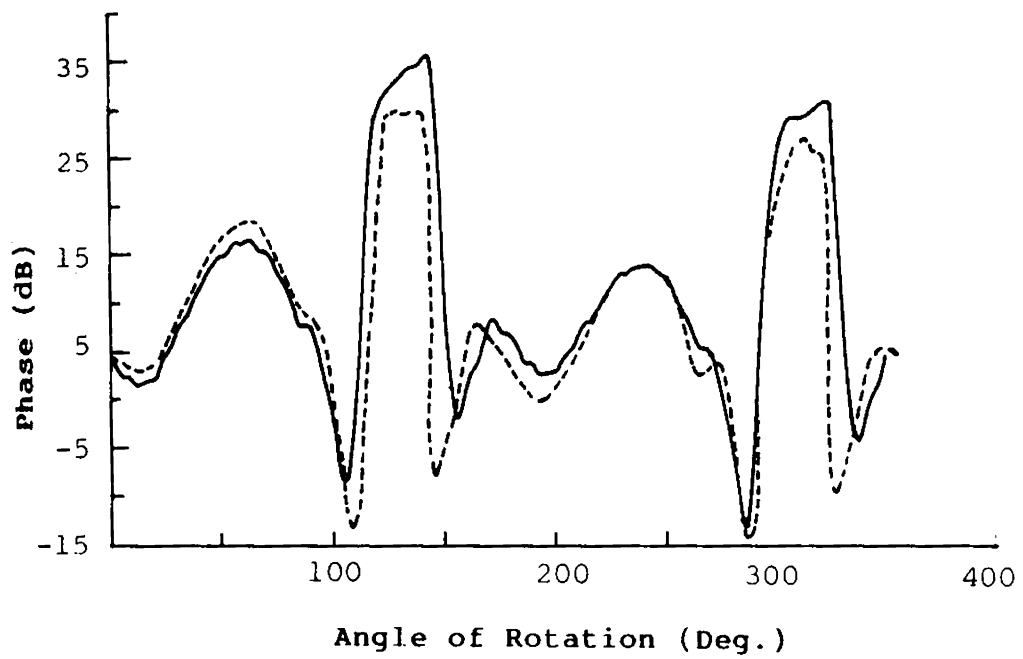


Fig.3.6(E) Phase patterns recorded at two frequencies for a defective sample with a cylindrical flaw of 17 mm diameter.

— 8 GHz ; - - - - - 12 GHz

composition II (IPP 40-Dummy). Using the theory explained earlier in chapter 2, values of dielectric constant were calculated and the same were plotted in a graph against curing time. One such graph for a sample length $d = 3.12$ cm is shown in Fig.3.7(A), for composition I.

In Figs.3.7(B) & 3.7(C) the results are plotted for different sample lengths of propellant composition I. Variation in dielectric constant with curing time for different sample lengths of composition II are presented in Fig.3.7(D) & 3.7(E). The difference in behaviour of the two curves has been explained in the next chapter.

3.8 VARIATION OF LOSS TANGENT (or $\tan \delta$)

The variation of $\tan \delta (= \epsilon' / \epsilon'')$ for the propellant composition I (IPP 40-Dummy) has also been studied. Equation (2.6) shown in chapter 2 was used for this purpose. Typical curves obtained for different sample-lengths are illustrated in figures 3.8(A) & 3.8(B).

3.9 CORRELATION BETWEEN MECHANICAL AND ELECTRICAL PROPERTIES

The property of the propellant sample which is normally used for knowing the completion of curing is its

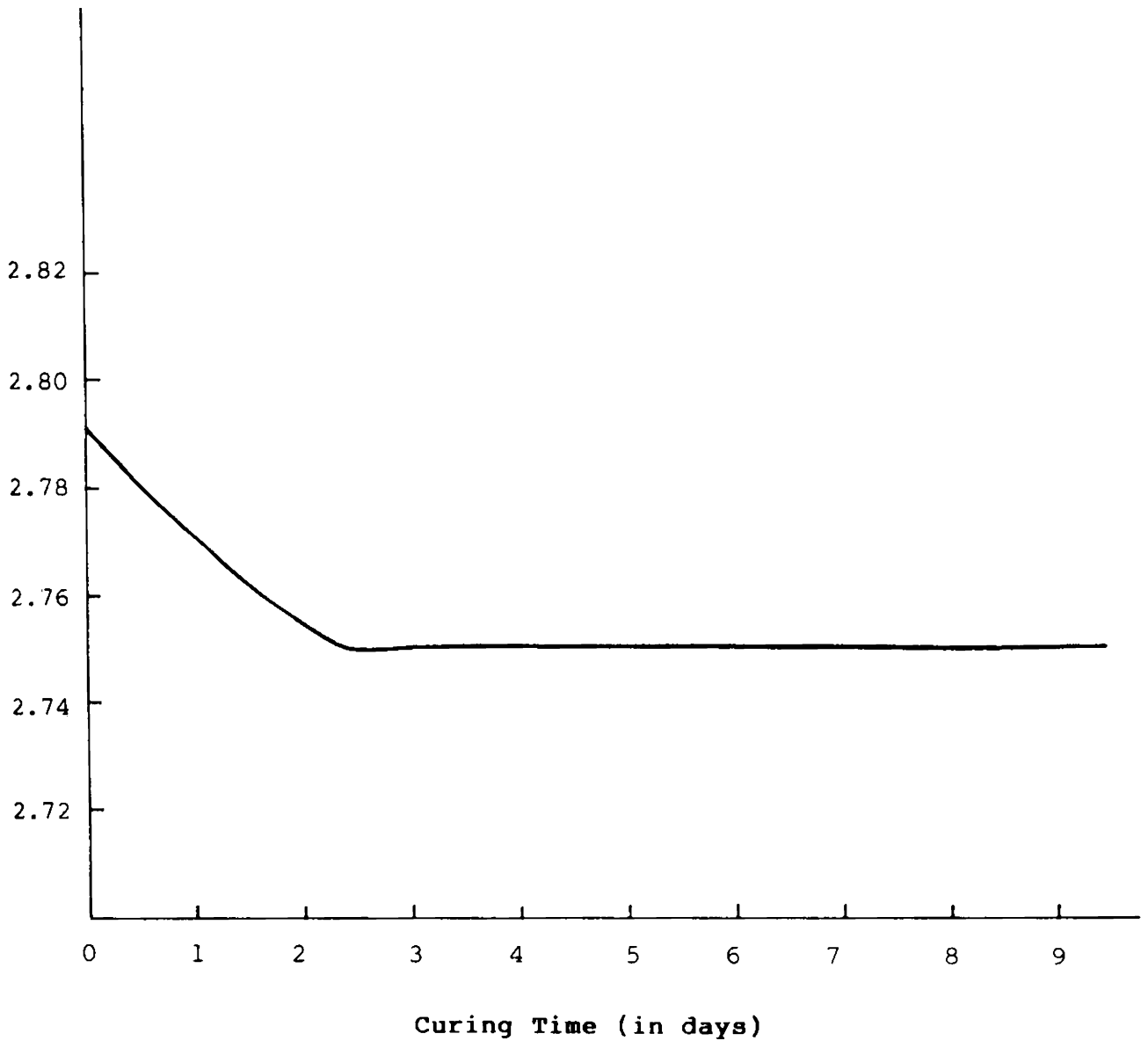


Fig 3.7(A) Variation of dielectric constant (ϵ') with curing for an IPP-40 live propellant sample. Sample length $d = 3.12$ cm.

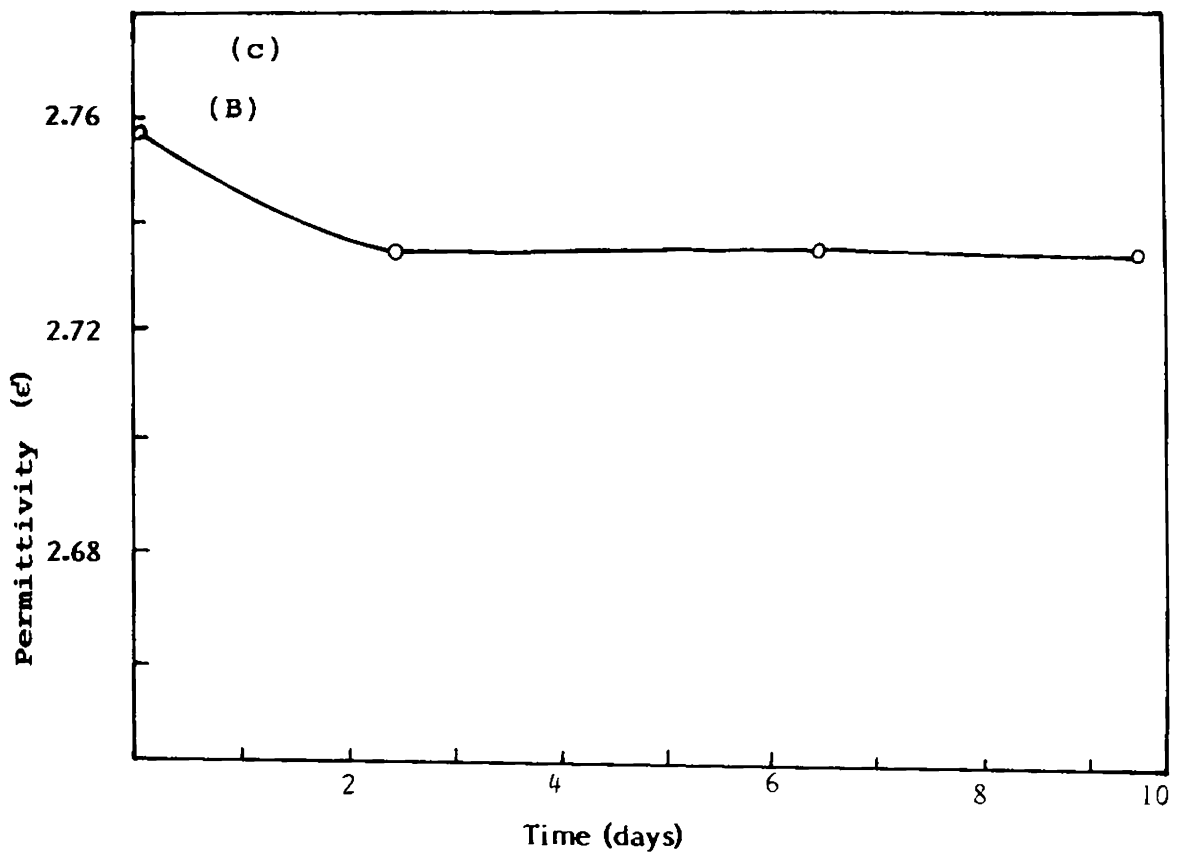


Fig.3.7(B) Variation of electrical property against curing time
Live propellant. ($d = 4.51$ cm)

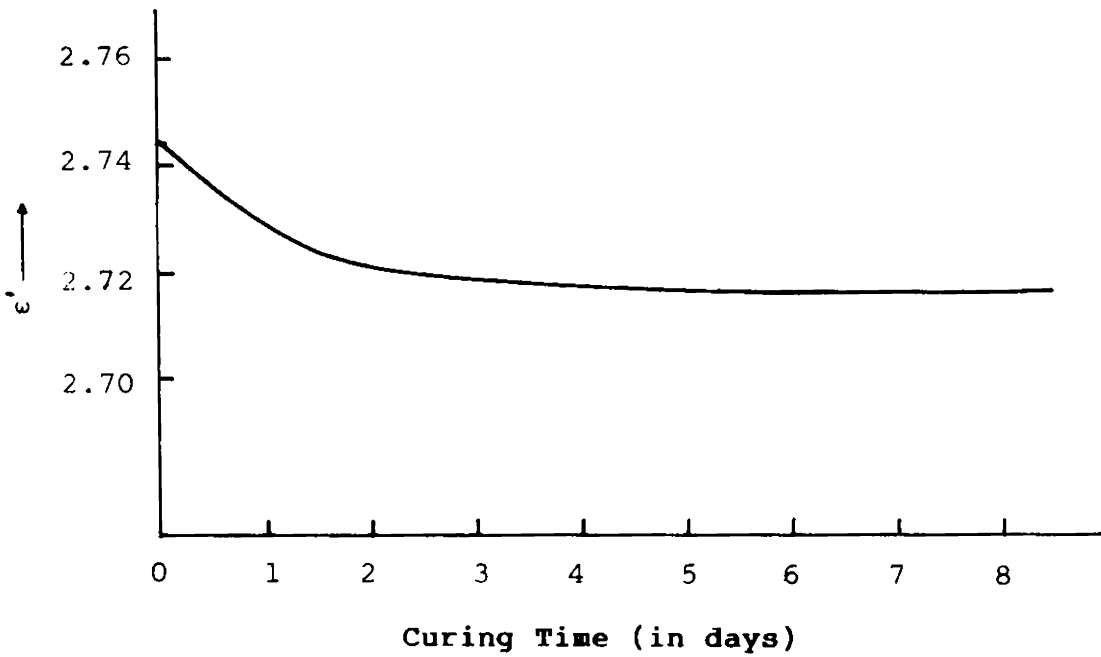


Fig.3.7(C) Variation of dielectric constant (ϵ') with curing time for an IPP-40 live propellant sample. Sample length $d = 5.12\text{cm}$.

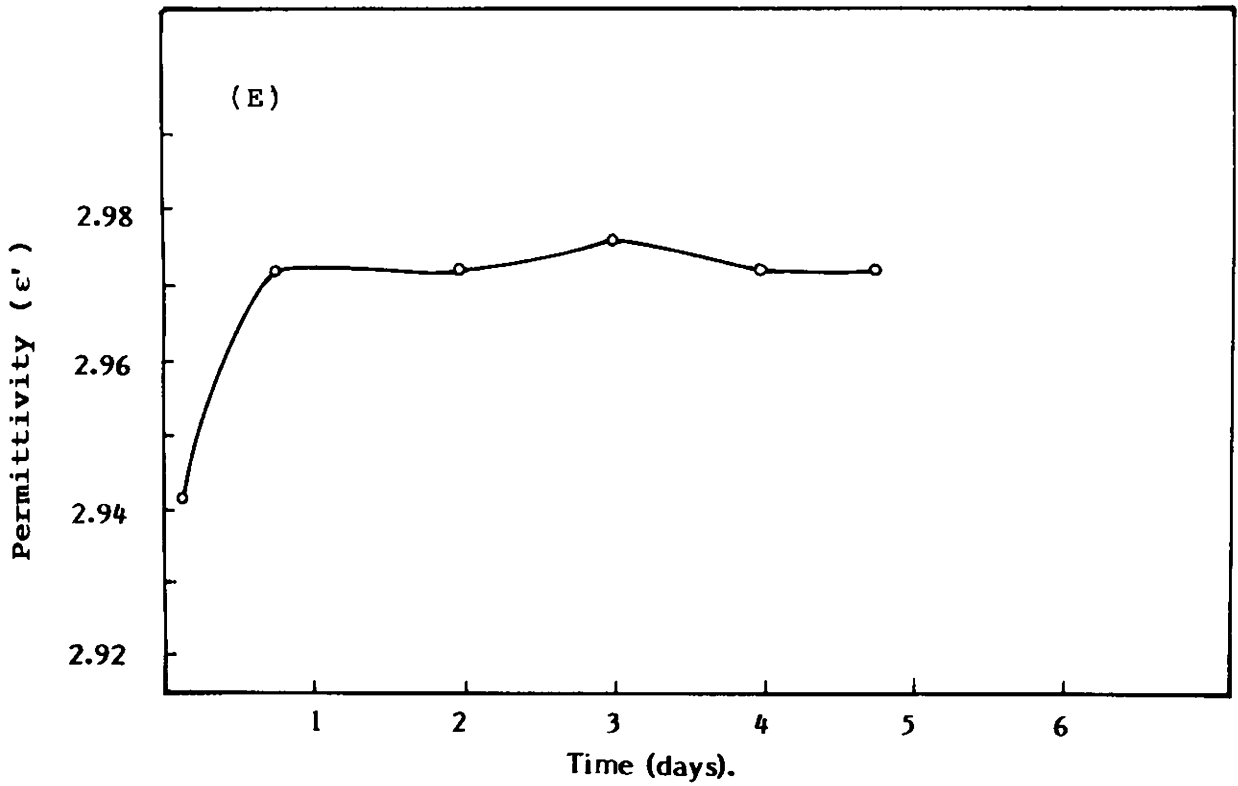
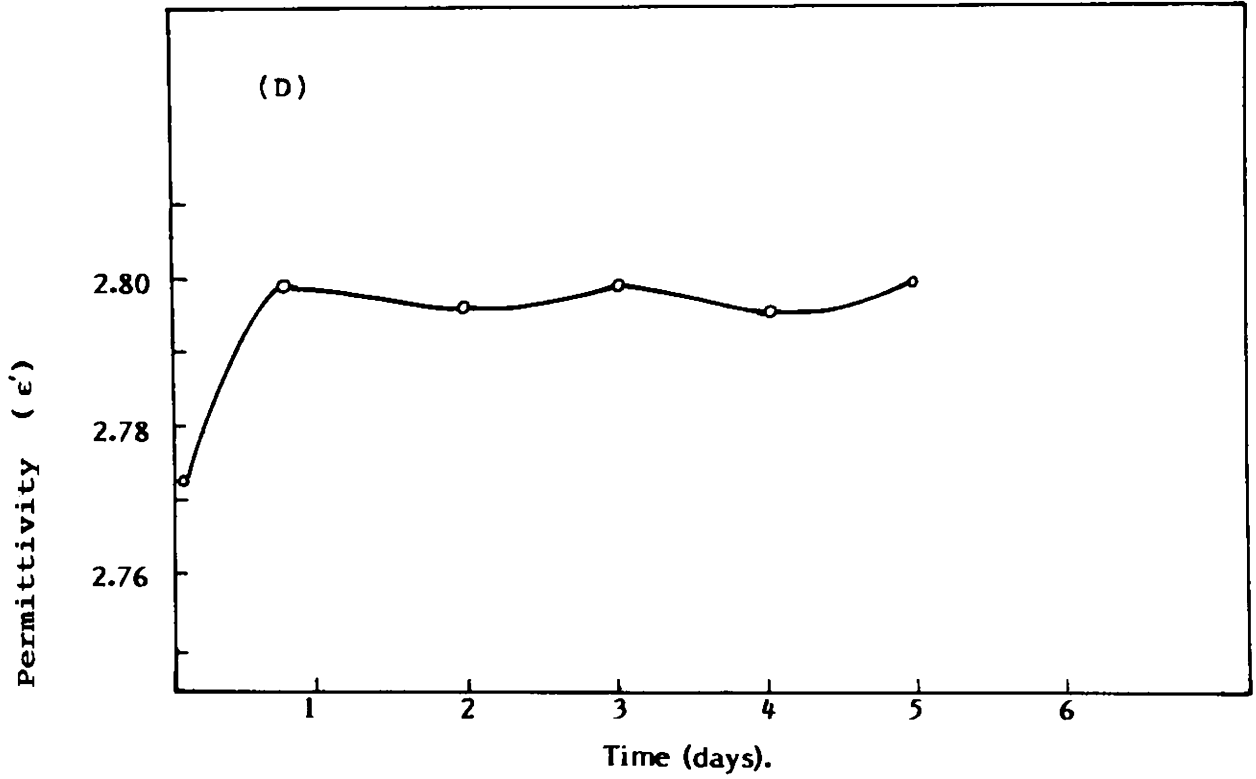


Fig.3.7(D) & (E) Variation of permittivity versus curing time: IPP-40 dummy propellant of different length d
(D) $d= 1.2$ cm; (E) $d= 5.13$ cm.

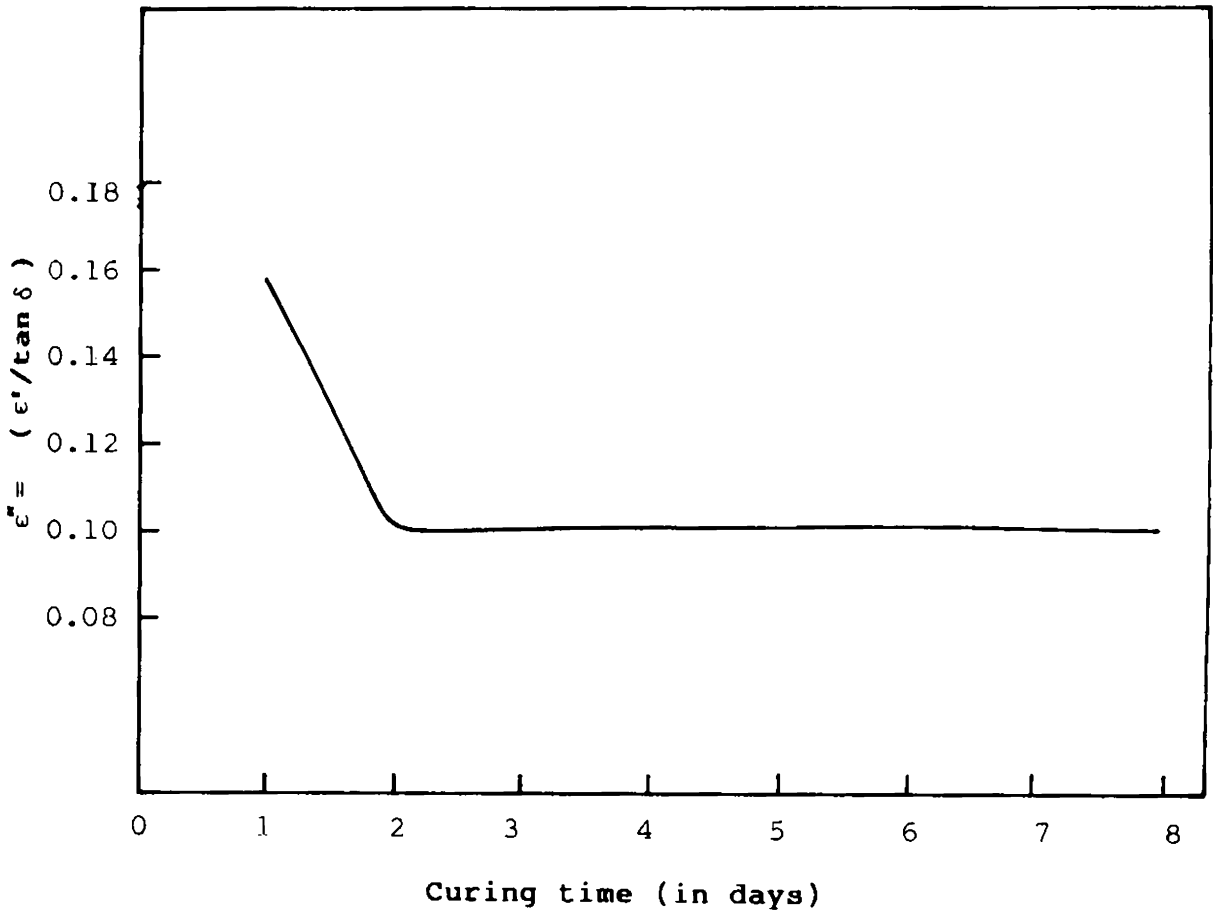


Fig.3.8(A) Variation of loss factor for an IPP-40 dummy propellant sample with curing time. Sample length 3.5 cm.

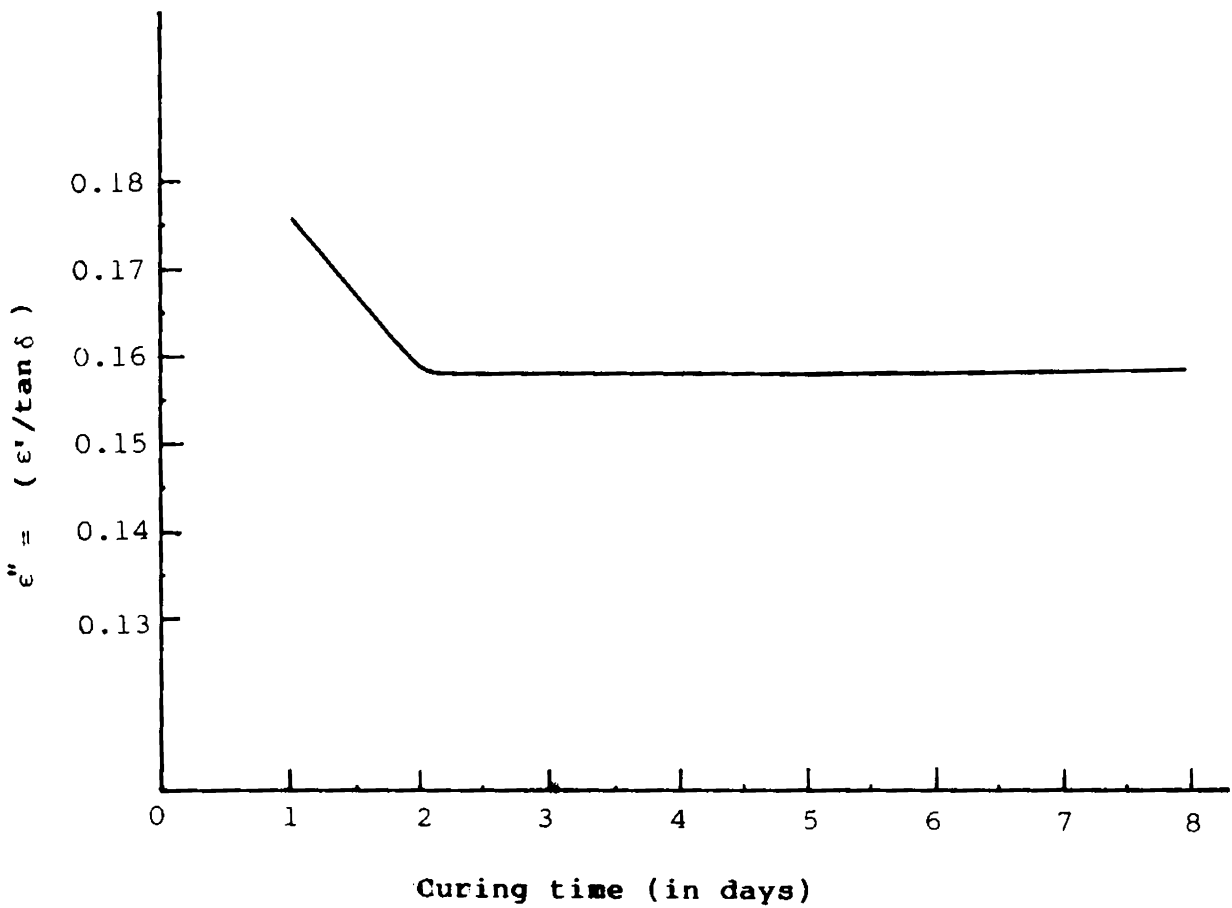


Fig.3.8(B) Variation of loss tangent with curing time for an IPP-40 dummy propellant sample. Sample length 3.12 cm

tensile strength, a mechanical property. A correlation curve relating the mechanical property and the electrical property with curing time would be helpful for comparing these properties. Hence a correlation curve is given here. The tensile strength data obtained from VSSC, Trivandrum was used for plotting the mechanical property with curing time. This is shown by a dotted line in Fig.3.9(A). The solid line in the same figure corresponds to the electrical property or dielectric constant.

Fig.3.9(B) shows similar curves for propellant composition II. Further analysis of these results are presented in the next chapter.

3.10 ATTENUATION MEASUREMENTS

Changes in the absorptive property of the propellant sample at various stages of curing were studied by attenuation measurement technique described in chapter 2. The power at the sample output was measured and plotted against the curing time. Experiments were carried out on propellant samples of two different compositions.

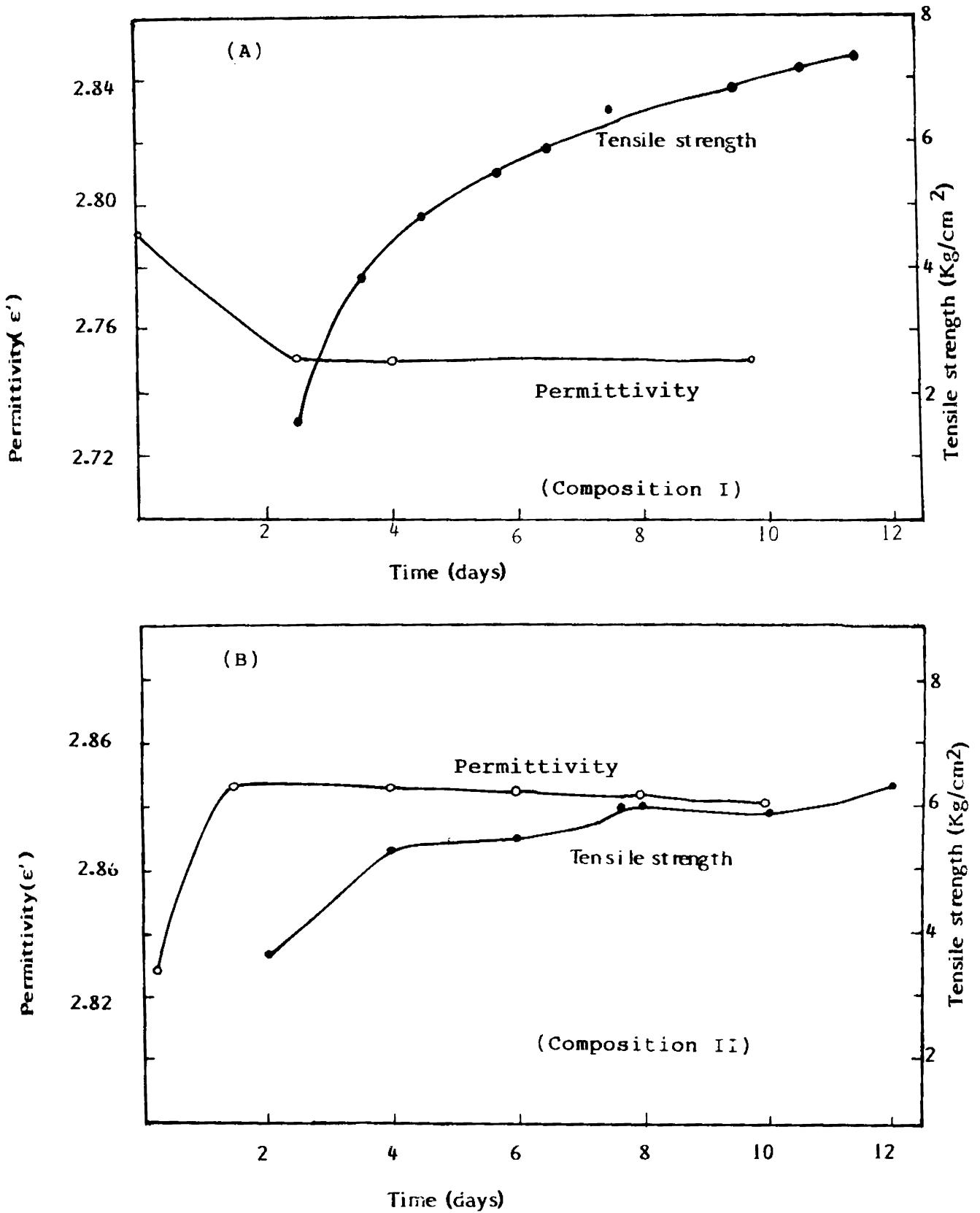


Fig.3.9 Curves co-relating the electrical and mechanical properties of the propellant samples
 (A) Live sample: (B) Dummy.

Fig.3.10(A) shows the results obtained for sample composition I (IPP 40-Live) while Fig.3.10(B) depicts the variation in output power for sample composition II. The interpretation of these results has been given in chapter 4.

3.11 VARIATION OF VSWR

Variations in the measured values of VSWR ($= E_{\max}/E_{\min}$) for the propellant composition II are illustrated in Fig.3.11(A) & 3.11(B) for two different cell lengths. The importance of this measurement will be discussed in the next chapter.

3.12 CONCLUSIONS

In this chapter the results obtained from various measurements carried out during the course of this research work have been presented. The results presented are related to detection and localization of flaws and variations in the signal characteristics with flaw size and shape. Results are presented for samples with multiple defects. The effect of changing the frequency on the pattern for a particular flaw-size is illustrated. Variations in the electrical properties of the sample

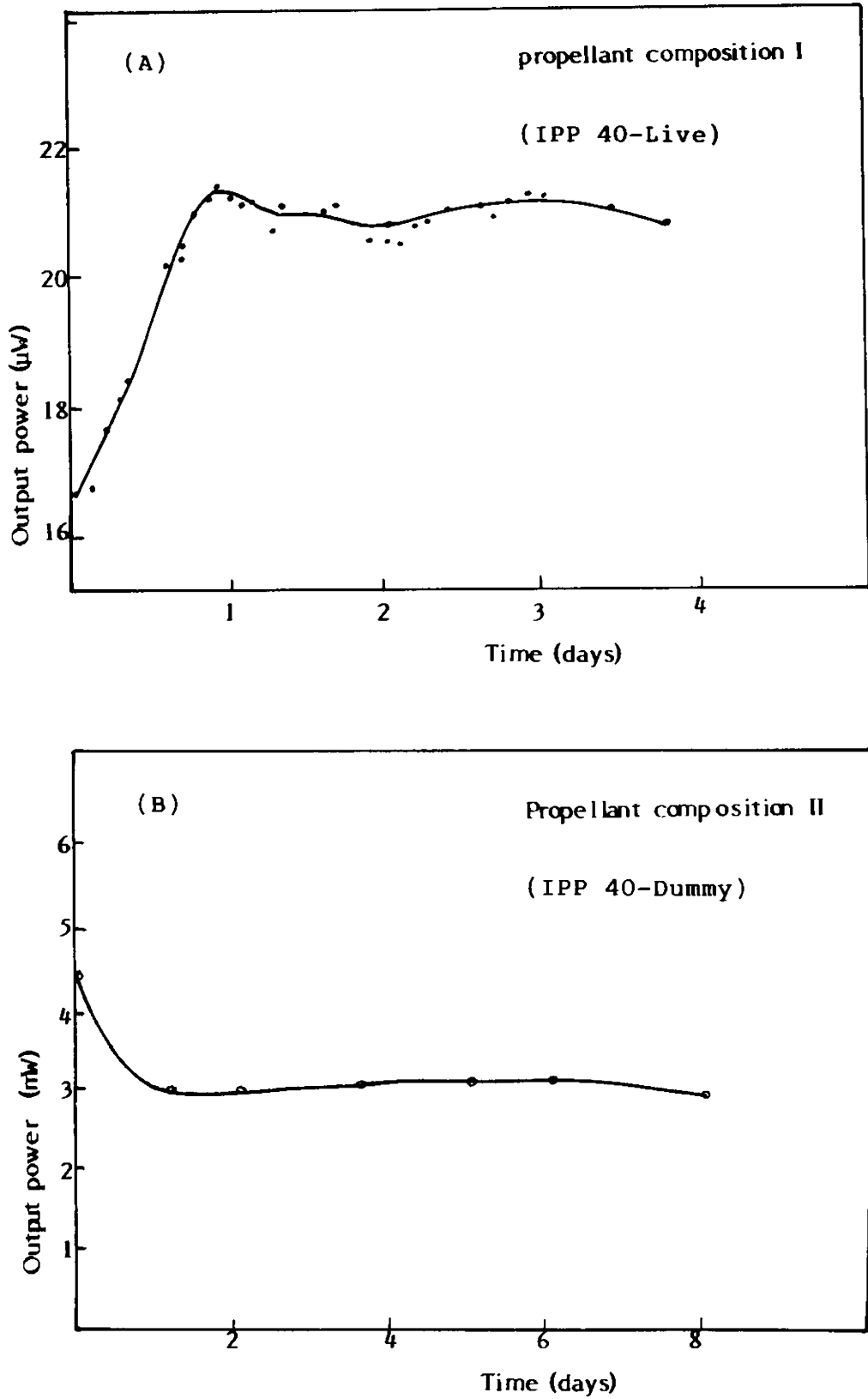


Fig.3.10 (A)&(B) Output power against curing time
 (A) for propellant composition I
 (B) for propellant composition II

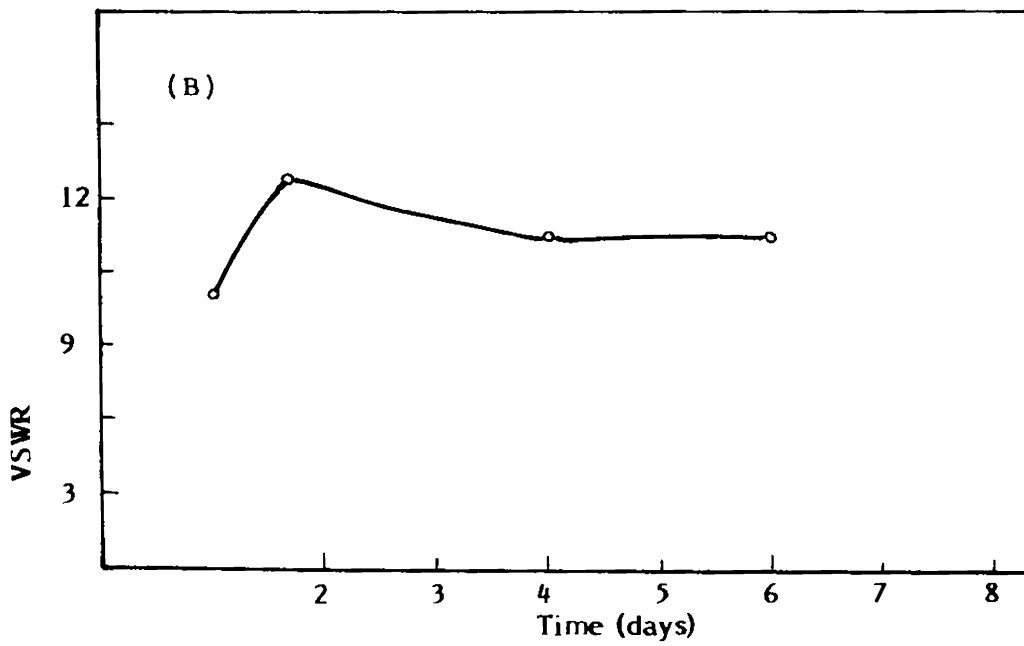
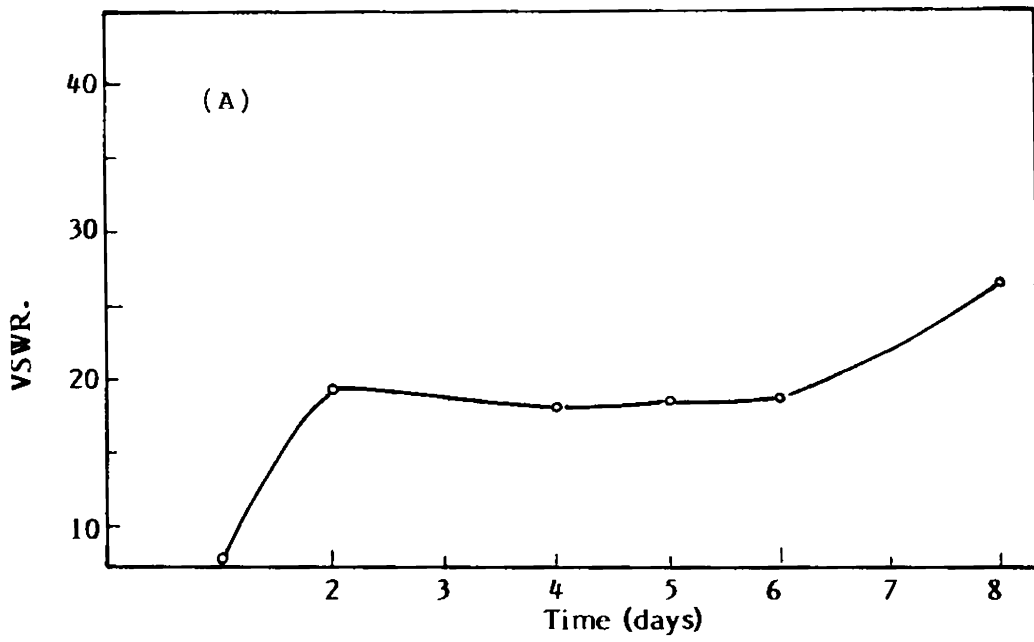


Fig.3.11(A) & (B) Variation of VSWR against curing time: IPP-40 dummy propellant
(A) for $d = 1.2$ cm
(B) for $d = 5.13$ cm.

undergoing curing are brought out. The properties studied include the dielectric constant, $\tan \delta$ and the absorptive properties. Correlation curves showing variations in the mechanical and electrical properties of the propellant sample at different stages of curing are also presented.

Chapter 4

ANALYSIS OF EXPERIMENTAL RESULTS

	<u>Page</u>
4.1 Introduction ..	120
4.2 Detection, Location and Characterization of Defects ..	120
(a) Detection ..	121
(b) Location ..	124
(c) Defect Characterization ..	125
4.3 Changes in the Electrical Properties and Predicting the State of Cure Propellant Samples ..	132
4.4 Sources of Errors and Suggestions for Improvements ..	136
4.5 Conclusion ..	138

Chapter 4

ANALYSIS OF EXPERIMENTAL RESULTS

4.1 INTRODUCTION

In this chapter the results presented in the previous chapter have been analyzed in more detail so as to arrive at certain conclusions. The first part of the analysis is concerned with detection, location and characterization of flaws or voids within a cured propellant sample. In the second part of the analysis the electrical characteristics of a propellant sample undergoing curing have been carried out so as to enable the prediction of state of cure of the material. Limitations of the techniques employed and ways of improving them have also been brought out in this chapter.

4.2 DETECTION, LOCATION AND CHARACTERIZATION OF DEFECTS

Results shown in figures from 3.2(A) to 3.6(E) in chapter 3 have been analyzed here for the purpose of identification of a defect or an inhomogeneity within a cured propellant sample.

a) Detection

For a homogeneous sample, as expected and as shown in Fig.3.2(A) and 3.2(B) almost a flat response was observed both in the amplitude and phase patterns. For a defective sample, here a sample with an artificially created void, changes were observed both in the amplitude and phase patterns as indicated in Figs.3.2(C), 3.2(D) & 3.2(E). The presence of the flaw resulted in the scattering of microwave radiation impinging on it, bringing about a reduction in the intensity level of the received signal. There are two dips in Fig.3.6(C) or two peaks in Fig.3.6(D), which are separated by 180 degrees, corresponding to a single localised flaw. The first dip (or peak) is observed when the flaw traverses the signal path near the transmitter and the second dip (or peak), corresponds to the flaw, as it crosses the receiving horn. Comparing Figs.3.2(C) & 3.2(E), it can be seen that there is a difference in the recorded amplitude patterns. The reasons for this is stated as follows:

For the first recording, two waveguide sections were used as the transmitter and receiver of microwave energy. The resulting beam cross-sections were very large and hence the fine details of diffraction effects could not

be recorded. In the second case two microwave horns with better beam concentrations were used for directing and receiving microwave energy. In this case, apart from the scattering by the inhomogeneity, diffraction effects were also prominent and hence the recorded patterns were also different from the previous one. It has also been observed that in both cases the recorded patterns were changing with the separation of transmitter and receiver. This is because of the formation of standing waves between the sample and the transmitting and receiving antennas. This problem can be eliminated by the use of matching transformers [8]. However, this does not pose any serious problem as far as detection of a flaw is concerned. The presence of an inhomogeneity is detected by comparing the curves for a test sample with those of a standard (or reference) sample recorded for the same spacings of transmitter and receiver. Results similar to those shown in Fig.3.2(C) has also been observed for a material with metallic inclusions. As microwaves are strongly reflected back by very thin metallic strips, their presence can also be seen as a reduction in the intensity of the received energy.

The dotted line in Fig.3.2(D) is obtained for a cured sample with a small portion of it is replaced by undercured paste. A small but detectable change in the phase pattern indicated the presence of inhomogeneity.

So far the analysis were based on the results obtained on solid rocket propellants without a mandrel or central cavity. In a real propellant sample, there will be a central star-shaped mandrel along its axis. The results obtained from observations on such samples are given in Figs.3.2(F) to 3.2(J). The ups and downs in these plots indicate the presence of a star-shaped structure. Fig.3.2(F) and Fig.3.2(H) are reference curves ie., curves for samples without any artificially created flaws. The amplitude patterns recorded for defective samples are shown in Fig.3.2(G) & 3.2(J) and these plots again indicate the presence of a void by a reduction in the amplitude level of the received signal. The experiments in this case have been performed at a lower frequency because as the frequency was increased the patterns were found to give too many ups and downs due to multiple reflections. The reflection at the interfaces will depend upon λ , the operating wavelength. As λ is reduced (frequency is

increased) the reflections from small discontinuity will also figure in the recorded patterns. Further the tested sample itself was not homogeneous (otherwise the alternate amplitude levels in the recorded reference patterns would have been equal and the pattern symmetric). This made identification of a defect very difficult at higher frequencies. However, if a reference plot is available for a perfect sample then the amplitude levels for the test sample can be compared with that of the reference sample and take a decision based on this observation.

The above analysis leads to the conclusion that a defective sample can be identified by the use of microwave NDT from recordings of amplitude/phase for the test sample and comparing the results with that for a reference sample.

b) Location

A precise information regarding the location is available from the previous results. That is, the diameter along which the defect lies can be marked from those results. Another piece of information, whether the defect is closer to the centre of the sample or away from the

centre, can be obtained by examining the width of the recorded amplitude (phase) trace. This is because, as a flared beam is used, defects closer to the centre will lie over a longer period within the beam and hence effects will be visible in the recorded pattern over a longer angular displacement. Thus the width of the amplitude (or phase) trace will be more in this case. For defects lying near the periphery of the sample, just the reverse arguments hold and consequently, the width of the amplitude (or phase) trace will be less. Justification of this reasoning can be found by comparing the curves given in Fig.3.2(E) & 3.4(G), for flaws located closer and away from the periphery of the sample, respectively. In the first case, the width of the amplitude trace is 60 degrees while, for the second case, the amplitude trace width is nearly 85 degrees, defect more towards the centre .

Spotting of location of single localised flaws is possible by a method described in chapter 2 and results pertaining to these are shown in Fig.3.3(A). Table 3.3 shows the actual distance of the defect from the centre of the sample and its calculated value for three different cases. The results were found to be accurate with a maximum error of 7.6%. This technique suffer from following limitations:

- i) This method is applicable only for samples of cylindrical shapes.
- ii) Only single localized flaws can be spotted.
- iii) The relation $D = d/\cos\theta$ holds good only for small displacements of the sample. The percentage of deviation is more for larger displacements.

c) Defect characterization

Figures from 3.4(A) to 3.6(E) have been analyzed here for the purpose of extracting information as to what the defect size and shape is and how does a flaw react to changes in operating frequencies. Analysis of test results on samples with multiple flaws have been carried out. The minimum detectable defect size also has been arrived at.

Referring to Figs.3.4(A) and 3.4(G) it is clear that the amplitude of the received microwave signal level decreases with increasing flaw-size. But a correlation between the scattered signal amplitude and the flaw-size could not be established. Hence actual grading of imperfections using these observations will not be possible.

An alternative will be to generate enough data of scattered signal amplitudes corresponding to flaws of different dimensions in a reference sample and then compare these data with that of unknown samples (of same size and type) and then grade the defect size. As the scattered signal levels from imperfections within a sample can vary for samples of different materials and also for different samples of the same material, the amount of data to be generated is enormous. A second way out will be to go in for microwave imaging techniques or cross-sectional measurements.

A set of interesting results are presented in Figs.3.4(C) to 3.4(F). These results are informative as regard to the dimensions of the defects in directions both perpendicular and parallel to the direction of propagation of microwave signal. For a defect of rectangular geometry, there are two directions, one parallel and the other perpendicular to the direction of the beam, which define the defect size and also the minimum detectable defect size. A close examination of the plots presented in Figs.3.4(B) to 3.4(E) show that the width of the amplitude and phase traces are more when a defect is lying with its larger dimension perpendicular to the direction of propagation

than for the same defect lying with its smaller dimension perpendicular to the direction of propagation. Another observation is that the scattered energy is less (energy received after scattering) for a defect lying with its larger dimensions along the direction of propagation. Coupling these two informations together, it is possible to get an idea of the orientation of the flaw within a cured sample. The recorded amplitude pattern corresponding to the minimum detectable defect size is shown in Fig.3.4(F). For reference, the amplitude pattern for the same sample without any artificially created flaw is also included in the plot. The defect size was 0.45 x 0.45 cm which in terms of operating wavelength is approximately $\lambda/8$. Defects of still smaller size can be detected by using much higher frequencies. But attenuation of the waves by the sample should not be too high, as it calls for more energy to be pumped in to get an output after transmission through the sample.

Figs.3.4(H) & 3.4(J) can be analyzed for the purpose of identifying the defect type ie., whether the defect is having a cylindrical geometry or rectangular geometry. The recorded amplitude patterns showed that the signal excursions corresponding to a cylindrical defect are

more compared to those of a rectangular defect. In the figures just mentioned, the first and third dip in the amplitude pattern corresponds to a cylindrical flaw while the 2nd and 4th are due to a rectangular flaw. However, drawing a conclusion based on this result is not proper as the pattern may change with transmitter-receiver spacings and hence the recorded patterns may look different from those given here. A much more reliable technique will be the radar cross-section analysis of the defects and classifying the defects based on this information.

The next set of curves analyzed are related to a propellant sample with multiple defects. The recorded plots are presented in Figs.3.5(A) to 3.5(G). The purpose of analysis of these results are to arrive at the defect-resolution, (ie., how well two closely spaced defects can be resolved) using the transmission technique. As already discussed in chapter 3, a major factor that controls the resolution is the beamwidth, which is again a function of frequency employed and the separation between the sample and the transmitting and receiving horns.

In Figs.3.5(A) & 3.5(B) the amplitude pattern recorded for a defective sample with two cylindrical voids

with an angular spacing of nearly 100 degrees (measured clockwise) between them is shown for two different frequencies. The presence of the two voids are clearly indicated in the recorded pattern and the spacing between them can be measured by measuring the angular separation between two consecutive dips. This turns out to be approximately the same as the actual value. The amplitude patterns corresponding to a sample with two closely spaced flaws (angular spacing of 30 degrees) are illustrated in Figs.3.5(C), 3.5(D) & 3.5(E) at frequencies 8 GHz, 10 GHz and 12 GHz respectively. Assuming a 'W' shaped pattern associated with each flaw, the first two plots do not resolve the flaws properly. But the plot at 12 GHz clearly shows two 'W' shaped patterns and the separation between the centres of these patterns turn out to be equal to the angular spacings between them. Thus the measured angle between the markers 1 & 2 and 3 & 4 are 30 degrees. The separation between markers 1 & 3 and 2 & 4 are both 180 degrees as the flaws have traversed the transmitter-receiver path twice. Analysis of plots given in Figs.3.5(F) & 3.5(G) indicate that for a sample with three closely spaced defects (each with an angular spacing of 30 degrees between them) the plot at 8 GHz resolves only two flaws (the first and third

separated by 60 degrees) while plot at 12 GHz resolves all the three flaws. This can be inferred from the positions of markers shown in Fig.3.5(G) and the arguments given earlier holds good here also. As a third trial, a sample with three defects, with an angular spacing of 30 degrees between the first two and a spacing of 20 degrees between the second and third, was also tried out and the recorded patterns at 8 GHz and 12 GHz are shown in Figs.3.5(H) & 3.5(J). As expected, the first plot could resolve only two flaws. But the second plot at 12 GHz also resolves only two flaws (the first two separated by 30 degrees). This is because, for the set up used, the width of beams at points where the defects intercept the beam were more than 26 degrees but less than 30 degrees.

The above results holds good only for defects lying closer to the periphery of the sample. As the defect location is moved closer to the centre of the sample, the resolution will be still poorer owing to reasons already explained in chapter 3. By employing very narrow pencil beam, the resolution can be further improved, irrespective of the position of the defect. To get such resolutions, high frequency microwaves or millimeter waves will have to be employed.

To see how a flaw react to changes in operating frequency, the results presented in Figs.3.6(A) to 3.6(E) are analyzed. An examination of these test-results reveal that, for a particular flaw-size as the frequency is varied the widths of the traces, both phase and amplitude, will be reduced. Fig.3.6(A) shows the recordings corresponding to a flaw size of 15 mm at two different frequencies. Similar plots for flaw sizes of 17.5 mm and 12.5 mm are given in Figs.3.6(B) to 3.6(E). A direct inference from these test-results is that the resolution can be improved by the use of higher frequencies, preferably millimeter waves.

4.3 CHANGES IN THE ELECTRICAL PROPERTIES AND PREDICTING THE STATE OF CURE PROPELLANT SAMPLES

Results presented in Fig.3.7(A) to 3.11(B) are analyzed in this section to see the variations in the electrical properties of a propellant sample undergoing curing and use this information to predict the state of cure of the sample. Two samples, designated as propellant composition I (IPP 40-Live) and propellant composition II (IPP 40-Dummy) were subjected to the study.

The curves given in Fig.3.7(A) to 3.7(C) indicate that the dielectric constant of IPP 40-Live sample decreases initially (as the curing progresses) and then attains a constant value at the completion of curing. In the case of IPP 40-Dummy the results observed were just the opposite. That is, the dielectric constant for this propellant composition increases with curing and finally attains a constant value. This can be understood from the curves given in Fig.3.7(D) and 3.7(E). This change of behaviour in the dielectric constant accounts for the change in composition of the two propellant samples. In IPP 40-Dummy sample marble powder was used in place of the ammonium perchlorate used in the IPP 40-Live sample.

The changes in electrical and mechanical properties (tensile strength) are compared in Figs.3.9(A) & 3.9(B) for the two propellant compositions. The idea of comparison is to see whether any correlation exists between these properties. If it exists then, instead of measuring the mechanical property, which is destructive test, the electrical property or dielectric constant can be measured to arrive at the completion of curing or to indirectly

measure the mechanical property. The later measurement can be done non-destructively. As clear from those figures, a correlation exists between the two properties for both the propellant samples. For IPP 40-Dummy propellant sample, both the mechanical and electrical property increases with curing time while for IPP 40-Live sample the electrical property varies inversely with the mechanical property. Referring to the Figs.3.9(A) & 3.9(B) it can also be seen that the electrical property attains a constant value much earlier compared to the mechanical property. This point can be explained as follows.

In a normal curing process, the propellant samples are taken in bulk quantities in plastic containers and hot air is sent through them for curing. In this case, owing to the poor conductivity of plastic containers, the process of curing is slow. In the experiments conducted, the sample in paste-form is taken in highly conducting copper waveguides surrounded by an oil jacket maintained at the curing temperature. Here, the sample attains curing temperature in no time and hence it is subjected to 'accelerated curing'. This explains why the curves for electrical property levelled off much earlier than the mechanical property.

In Figs.3.8(A) & 3.8(B) the variation of $\tan \delta$ (or ϵ'') for the propellant composition II (IPP 40-Dummy) are given. The curves show that value of ϵ'' decreases as the curing progresses and then attains a constant value indicating the completion of curing.

Analysis of results of attenuation measurements is carried out referring to Figs.3.10(A) & 3.10(B). Fig.3.10(A) shows that for IPP 40-Live sample, the output power increases as the curing progresses. Hence the material becomes more transparent to microwaves. After completion of curing the output power remains almost a constant. The curve shown in Fig.3.10(B) shows that for IPP 40-Dummy the behaviour is just opposite to that of IPP 40-Live propellant sample. This result may appear to contradict those given in 3.8(A) to 3.8(C), because, as the output power decreases with curing, the losses associated with material should go up. Hence the curves in Fig.3.8 must be reversed. But a study of changes in the VSWR (Voltage Standing Wave Ratio) with curing showed that there is no anomaly in the above curves. Referring to Figs.3.11(A) & 3.11(B) it can be seen that for the IPP 40-Dummy, VSWR increases as the curing progresses.

This implies that the power reflected from the face of the sample has increased with curing and this resulted in the reduction of output power and not by the losses associated with the sample.

The above results suggest that the state of cure of the propellant samples can be monitored either by noting the variations in the output power coming after transmission through the sample or by evaluating the variations in the dielectric constant of the sample at different stages of curing.

4.4 SOURCES OF ERRORS AND SUGGESTIONS FOR IMPROVEMENTS

In the experiments conducted there could be a number of sources of errors and the following points will be helpful in keeping these errors a minimum.

1. In the testing of cured propellant samples, the alignment of the 'motor axis' with that of the turntable is very important. Any discrepancy in this will lead to serious errors in the detection and location of localized flaws. Repetition of the experiment under

varied conditions and interpreting the results with proper care will minimize the errors. However, in fully automated systems errors due to this will be a minimum.

2. In the waveguide experiment, expansion of waveguide dimensions due to heat causes errors. However, the final reading is not affected much, since we are concerned only with relative values of transmitted power after attaining the curing temperature. Using waveguide made of alloys having minimum expansion, the errors due to this could be minimized.
3. Electrical property (ie., dielectric constant) of the sample corresponding to any curing time, when the sample is in the curing bath may be different from that at room temperature at which the mechanical property is measured. For a comparative study of the variation of these two properties, the sample temperature has to be brought down to the room temperature and then measure its electrical property.
4. The rocket propellant sample in its paste form is filled inside the waveguide initially for dielectric measurements. The waveguide cell closed with mica windows is

heated by the oil circulated through the jacket surrounding the cell. It is observed that, as the sample gets heated up, it expands and bulges out of the waveguide. Though the mass of the sample is the same, its volume changes due to changes in length and this will seriously affect the measurements of electrical parameters. To avoid this, mica windows were reinforced with the metal flanges of the waveguide cell containing the sample.

4.5 CONCLUSION

In this chapter the experimental results presented in chapter 3 have been analyzed so as to arrive at valid conclusions as regard to detection, location and characterization of flaws. Results pertaining to changes in the electrical parameters of the sample were also analyzed to predict the cure-state. Finally, the sources of errors in the experiment and ways of overcoming them were also mentioned.

Chapter 5

CONCLUSIONS AND SCOPE FOR FURTHER WORK

	<u>Page</u>
5.1 Introduction ..	140
5.2 Feasibility of Microwaves as an NDT Tool ..	140
5.3 Inspection of Vehicular Tyres ..	142
5.4 Variation of Electrical Property and Prediction of Cure State ..	144
5.5 Scope for Further Work ..	145

Chapter 5

CONCLUSIONS AND SCOPE FOR FURTHER WORK

5.1 INTRODUCTION

In this chapter the major conclusions drawn based on the investigations carried out on solid rocket propellant samples are given. The feasibility of using microwaves in a limited way for the inspection of non-metallic materials is emphasised. Eventhough the study conducted here is concentrated on solid rocket propellants, the techniques developed can be extended to other materials also. For example, NDT technique developed for testing vehicular tyres using microwaves, with a microprocessor-based instrumentation has been mentioned. Finally, the need for further work in the area has been cited so as to establish microwave inspection technique as a better NDT tool.

5.2 FEASIBILITY OF MICROWAVES AS AN NDT TOOL

The results of investigations reveal that microwaves can be used effectively for the inspection of solid rocket propellant samples. It can detect inhomogeneities within the sample, even if they are distributed.

The exact position of the flaws can be estimated for the case of single localized flaws. The experiments conducted also reveal that the orientation of flaw can also be detected by the technique developed. Estimation of flaw-location will be rather involved if the number of defects are more. Exact grading of the defects, ie., identification of defect type and estimation of its size and shape, may not be possible by this technique. However, relative grading of inhomogeneities are possible by comparison with standard or reference curves. The minimum detectable defect size is $\lambda/8$ (= 0.45 cm in this case), where λ is the operating wavelength. It is presumed that use of higher frequencies can result in detection of defects of much smaller size. A comparison with other inspection techniques like ultrasonic testing is worth mentioning here. If a defect of the same size was to be detected using ultrasonics then the frequency to be employed would have been nearly 0.5 MHz so as to keep the wavelength down to that of microwaves. The attenuation of ultrasonics by the sample would be terribly high at this frequency and hence enormous amount of energy would be required to irradiate the sample. Moreover, some form of liquid coupling would have been necessary. This spells out the advantage of using microwaves in such cases.

The technique developed here is also useful in resolving closely spaced defects provided, their angular spacing is not less than 30 degrees. The resolution can be further improved by the use of high frequency microwaves or millimeter waves and by shaping the beam into a narrow pencil beam. However, this technique cannot resolve defects lying along the same line or if the angular spacing is 180 degrees.

By the use of highly sophisticated instrumentation like the semi-automatic network analyzer test set up, each sample can be scanned in no time and the results of scanning can be displayed in the monitor. It can be either stored in the memory or a plot can be made for further analysis. Rocket motors of any size can be tested by this technique at relatively low power levels (10 dBm).

5.3 INSPECTION OF VEHICULAR TYRES

Eventhough the technique described has been developed solely for the inspection of rocket propellants, it can readily be extended to the inspection of other materials as well, with slight modification. In Fig.5.3(A)

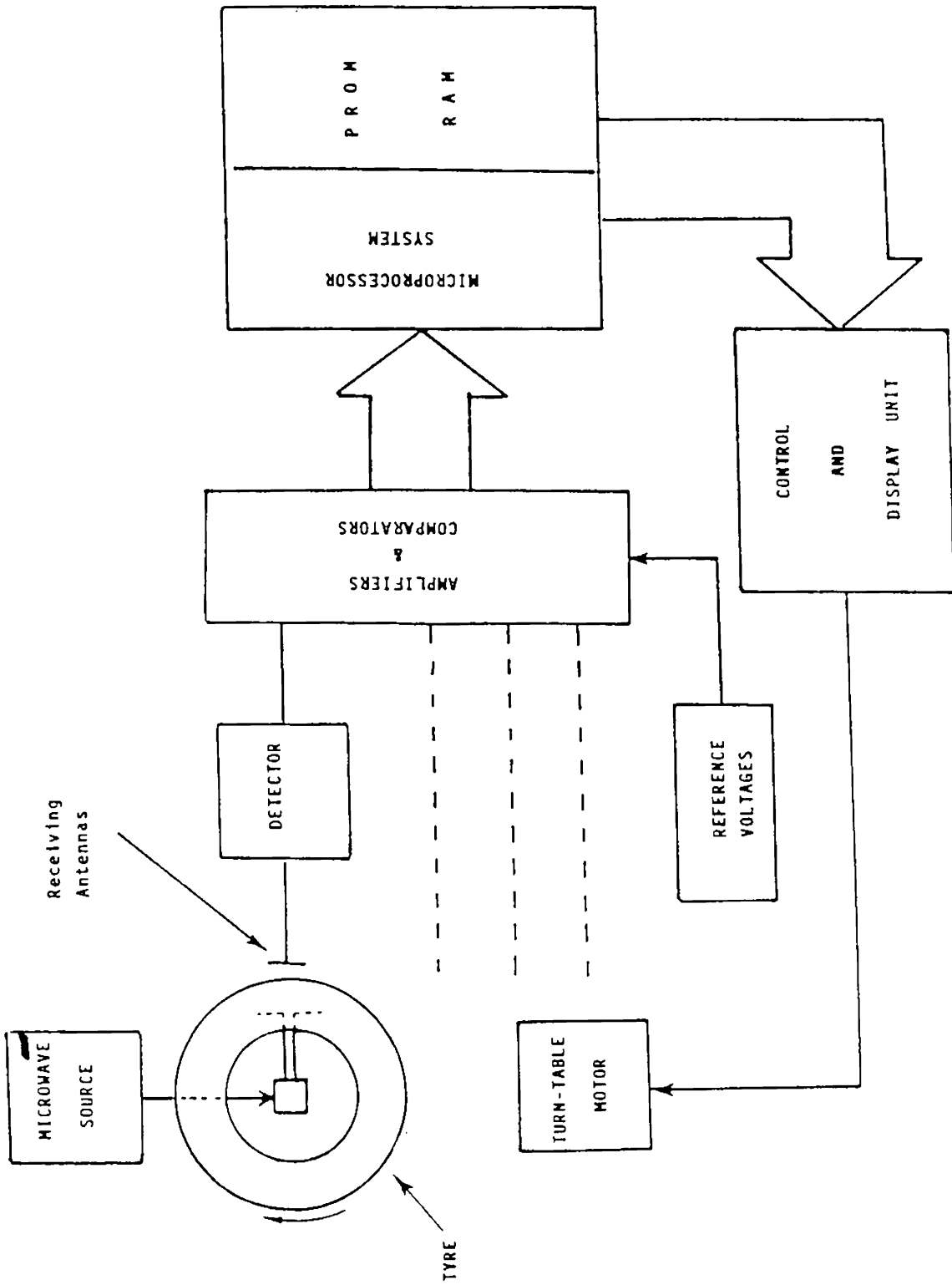


Fig.5.3(A) Microwave instrumentation for inspection of vehicular tyres.

a pp-based test set up tried out in the laboratory for testing vehicular tyres is shown. The results of investigations have shown that air-traps or other inhomogeneities within the material can be easily detected using microwaves.

5.4 VARIATION OF ELECTRICAL PROPERTY AND PREDICTION OF CURE-STATE

In the second phase of the experiments, attempts were made to see whether the changes in electrical properties of a propellant sample undergoing curing can be measured by studying the propagation characteristics of microwaves passing through it. The feasibility of this measurement has been established by adopting a waveguide technique described in chapter 2. The results showed that as the curing progresses, the dielectric constant of the sample increases or decreases depending upon the composition of the materials used. However, after curing, the dielectric constant attains a constant value in both cases. Efforts made to correlate the mechanical property (tensile strength) with the electrical property of the sample showed that eventhough there is no one-to-one correlation between the two, both property changes initially (with curing) and

attains a constant value at the completion of curing. This leads to the final conclusion that the state of cure of a material can be predicted either by monitoring the mechanical property or the electrical property of the sample. Further experiments have shown that simple attenuation measurements of microwaves passing through a propellant sample undergoing curing can give a clue to its state of cure.

5.5 SCOPE FOR FURTHER WORK

In the present work, an experimental investigation has been carried out to study the feasibility of employing microwaves as an NDT tool for inspecting non-metallic materials. The results of investigation have revealed that there are still a lot of work to be carried out to effectively use microwave technique as a good NDT tool.

1. It has been mentioned that use of millimeter waves can give a better resolution and defects of still smaller sizes can be detected by using high frequency microwaves. This has to be tried out and the results to be examined.

The precision with which the defects can be located may also be improved by the use of high frequency narrow beams of microwaves or millimeter waves.

2. In the technique developed, there is no direct way of grading the imperfections. The identification of the type of defect and estimation of its size and shape are also important in NDT applications. Radar cross-section measurements of defective samples or their microwave imaging may yield better results.
3. Dielectric measurements employing cavity technique may give more accurate results and these results may show better correlation with the mechanical properties. Work in this direction can also be taken up as an extension of these experimental observations.
4. The work described in this thesis is confined to NDT of solid rocket propellants. The adaptability of these techniques to other materials like plastics, polymers, concrete and other non-metallic materials can also be taken up for future studies.

The above studies indicate the high potentiality of microwave technique as an effective NDT tool.

Appendix I

BANDWIDTH ENHANCEMENT OF MICROSTRIP ANTENNAS BY SHUNT IMPEDANCE TECHNIQUE

	<u>Page</u>
I.1 Introduction	.. 148
I.2 Test Facilities Used	.. 149
I.3 Experimental Procedure	.. 153
I.4 Experimental Results	.. 155
I.5 Conclusion	.. 158

APPENDIX I

BANDWIDTH ENHANCEMENT OF MICROSTRIP ANTENNAS

BY SHUNT IMPEDANCE TECHNIQUE

I.1 INTRODUCTION

Microstrip antennas find wide applications due to its potential advantages like light weight, low profile, easy fabrication and flush mounting capability. But a serious drawback of these antennas is that they are highly resonant structures and hence, exhibit a narrow impedance bandwidth [31A]. The operating bandwidth of a single linearly polarized patch antenna is limited by its input VSWR and is inversely proportional to the Q-factor of the patch resonator. Typical values of fractional bandwidths are 2 to 4%. There are several techniques for improving the bandwidth of these antennas. The techniques can be generally classified as follows:

1. Decreasing Q-factor by increasing the substrate height and lowering dielectric constant.
2. Use of multiple resonators located in one plane.

3. Use of multi-layer configurations with multiple resonators stacked vertically.
4. Use of impedance matching networks.

In this section, a technique employing a lumped impedance connected between the non-radiating edge of the patch and the ground plane is described for improving the impedance bandwidth.

I.2 TEST FACILITIES USED

The main test facilities used in this study include an HP 8510 B automatic network analyzer system and an Anechoic Chamber. The experimental arrangement employed for the performance evaluation of the antenna is shown in Fig.AI(A). The impedance characteristics of the antenna were studied by setting up the network analyzer system in the reflection (or S_{11}) mode. The radiation patterns were recorded using the same set up but, in the S_{12} or S_{21} (ie., transmission mode) of the system. By the use of a software developed in the laboratory, the patterns were automatically recorded on an HP plotter. A broad-band dipole was used as the transmitting antenna while the test antenna was used as

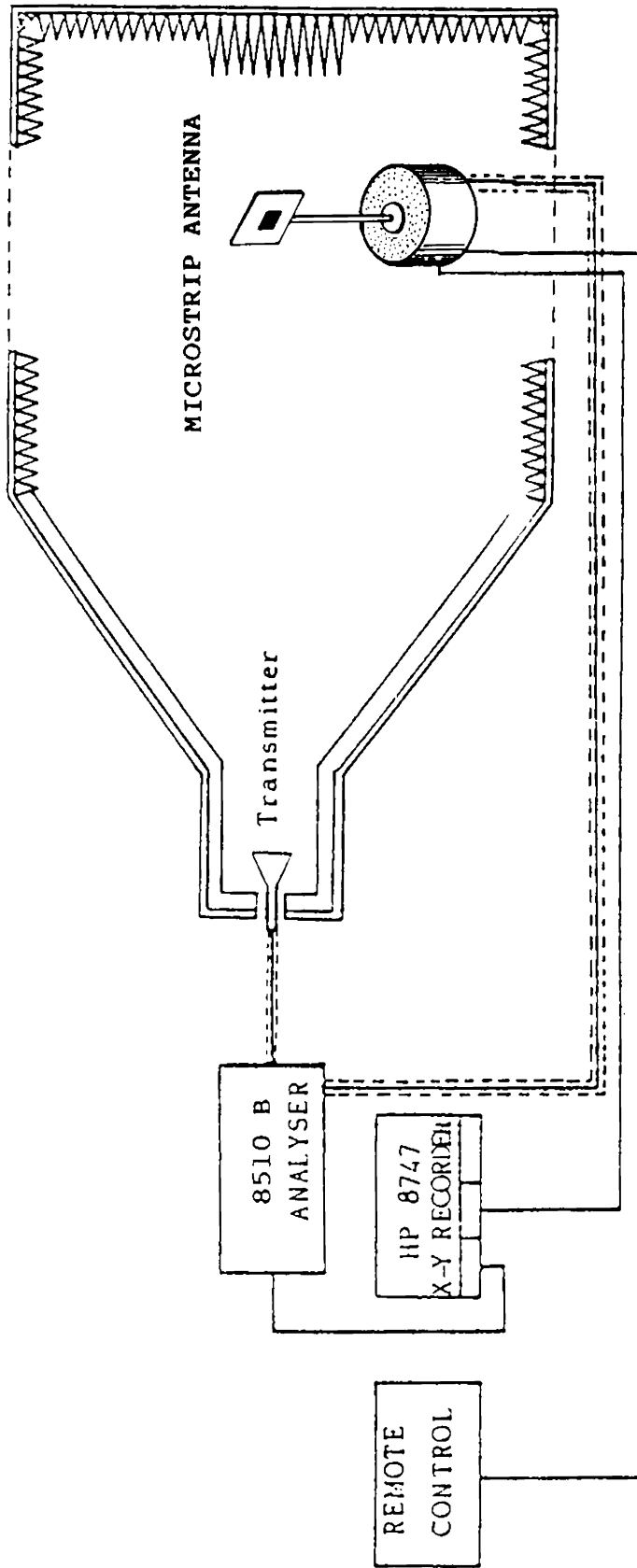


Fig. AI(A) Antenna performance evaluation test set up

the receiver. The transmitter-receiver set up was housed in an Anechoic Chamber, a short description of which is given below.

The Anechoic Chamber provides a simulated free-space environment and hence is very much helpful for accurate performance evaluation of antennas. If the patterns were taken inside an ordinary room, there may be unwanted reflections that will enter the receiving antenna (or test antenna) thus distorting the radiation patterns.

A schematic diagram of the Anechoic Chamber facility used is shown in Fig.AI(B). It is a convertible type so that for antenna radiation pattern measurements a tapered geometry can be employed while for scattering and other bistatic measurements the chamber can be configured to a rectangular type. The chamber was filled with microwave absorbing materials of pyramidal and wedge shapes. The material used was polyurethane-foam based with some microwave absorbing materials dispersed inside. The antenna positioner (or turn-table over which the test antenna is mounted) is kept at the "silent zone" or "quiet zone" of the chamber, where the reflections are a

CONVERTIBLE MICROWAVE ANECHOIC CHAMBER

[view from the top]

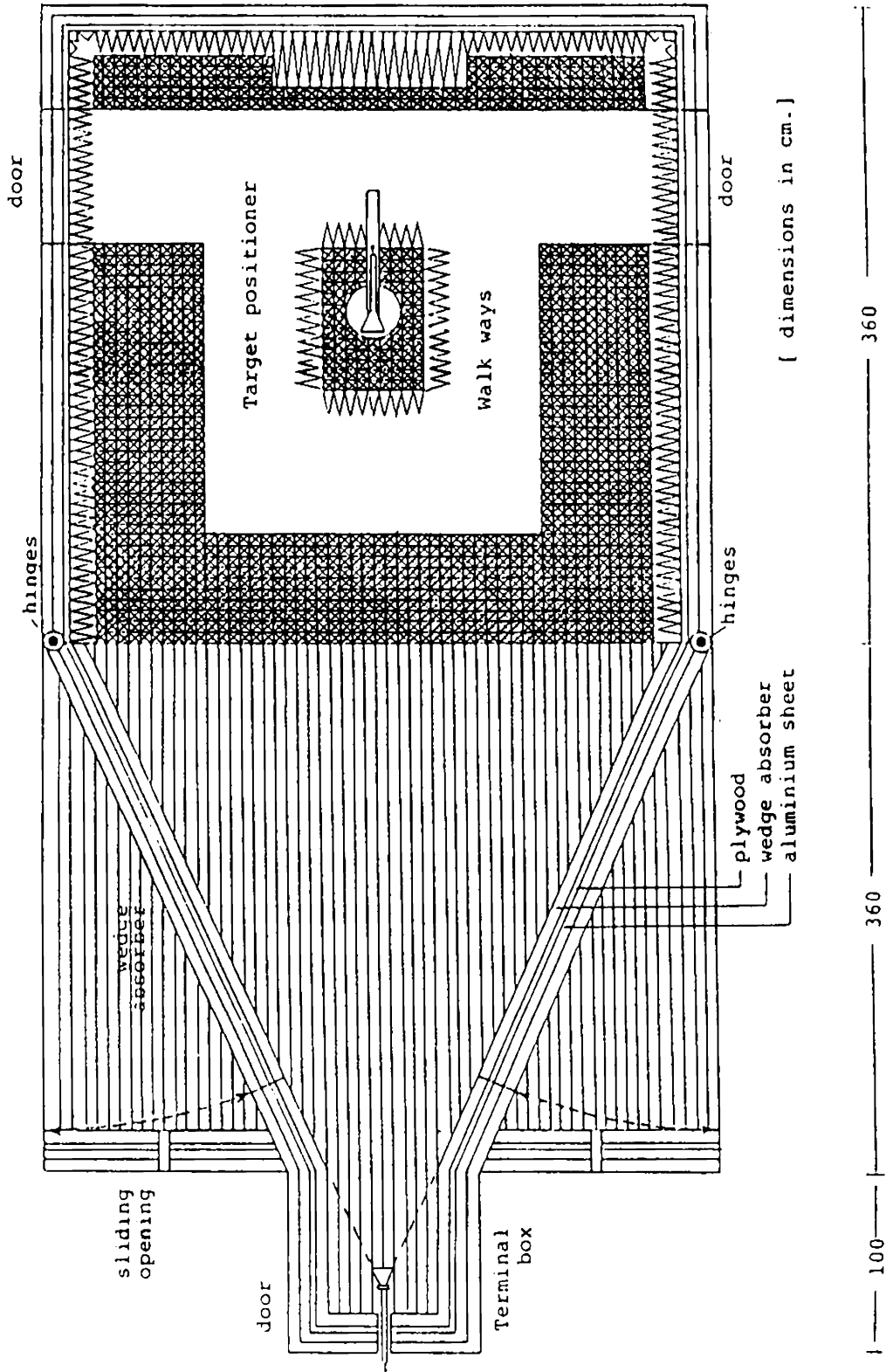


Fig.AI(B) Schematic diagram of the convertible Anechoic chamber.

minimum. The separation between the test antenna (receiver) and the standard horn antenna (transmitter) should be greater than $2D^2/\lambda$, where D is the maximum aperture dimension and λ is the operating wavelength. This implies that the quiet zone should be suitably displaced from the tapered portion to accommodate the test antennas of maximum size of interest. The height and the overall width of the chamber is chosen to be $W > R/2.75$, where R is the distance between the source and the test antenna and W , is the width or height of the chamber.

I.3 EXPERIMENTAL PROCEDURE

The geometry of the patch antenna used in the study is shown in Fig.AI(C). The patch was etched on a 0.8 mm thick RT duroid substrate ($\epsilon_r = 2.2$) and was fed by a coaxial probe. The position of the feed was adjusted to give 50Ω match at the resonant frequency. The impedance locus was plotted using the HP automatic network analyzer system. A lumped impedance was then connected between the non-radiating edge of the driven element and the ground plane. The spread of impedance curve and its location were found to be controlled by the value of lumped impedance and

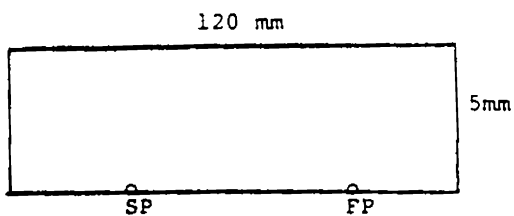


Fig.AI(C) Geometry of the Microstrip Antenna.
 FP is the feed point, SP is the Shunt location.

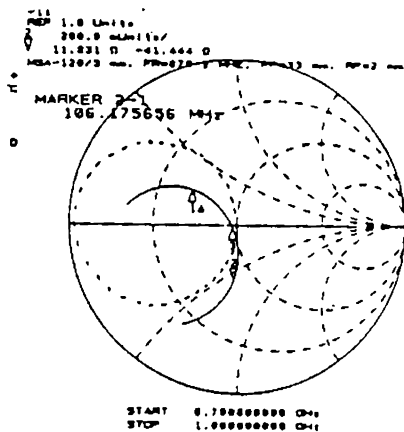


Fig.AI(D) Impedance loci of microstrip antenna.
 ——— With shunt - - - without shunt.

its position (S_p) along the non-radiating edge of the patch. By experimental iterations, it was found that an impedance value of $(100-j 45)\Omega$ gives minimum spread for the impedance curve. Hence a lumped impedance value of $(100-j 45)\Omega$ is connected. The position of the feed point F_p and S_p were then adjusted so that the impedance locus shift to the vicinity of 50Ω region. The impedance plot was again recorded using the plotter.

The experiment was repeated for a geometry shown in Fig.AI(E). This antenna structure was selected as it gives a wider bandwidth compared to a single patch of identical dimensions and its radiation patterns do not show any frequency squinting [32]. The impedance plot for this antenna was recorded with a lumped impedance connected between the non-radiating edge of the driven element and the ground plane. The antenna radiation patterns were also measured and recorded.

I.4 EXPERIMENTAL RESULTS

The impedance plot for a single antenna of the type shown in Fig.AI(A) is given in Fig.AI(E). The dotted line corresponds to the patch alone and the solid line

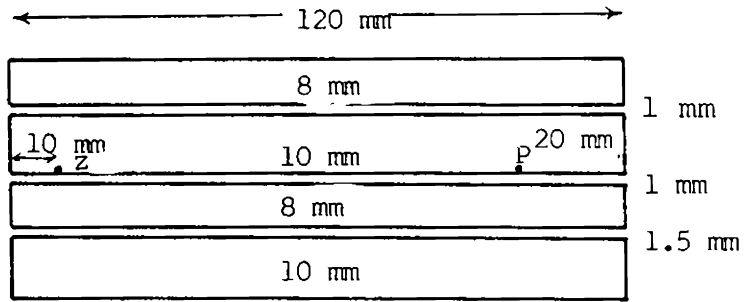


Fig.AI(E) Patch antenna with parasitic elements gap coupled
 P - Feed point, Z - Shunt point.

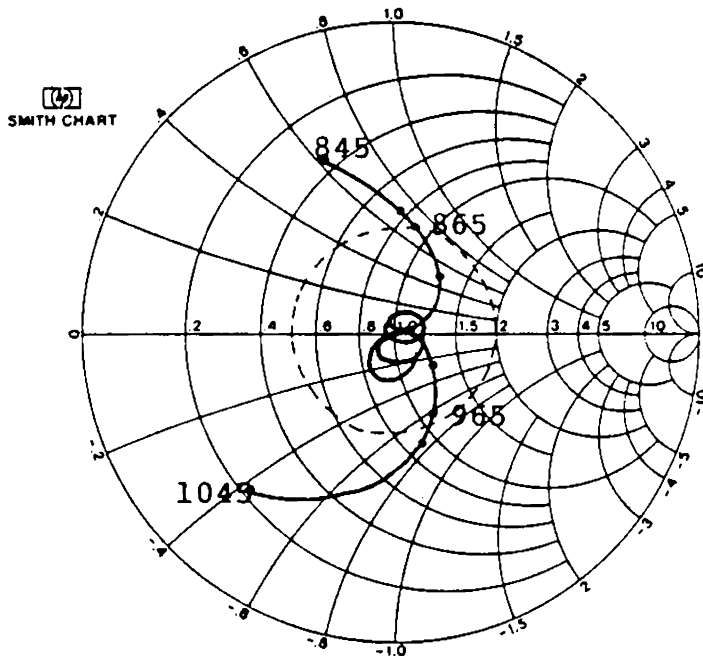


Fig.AI(F) Impedance plot for the antenna shown in Fig.AI(D).

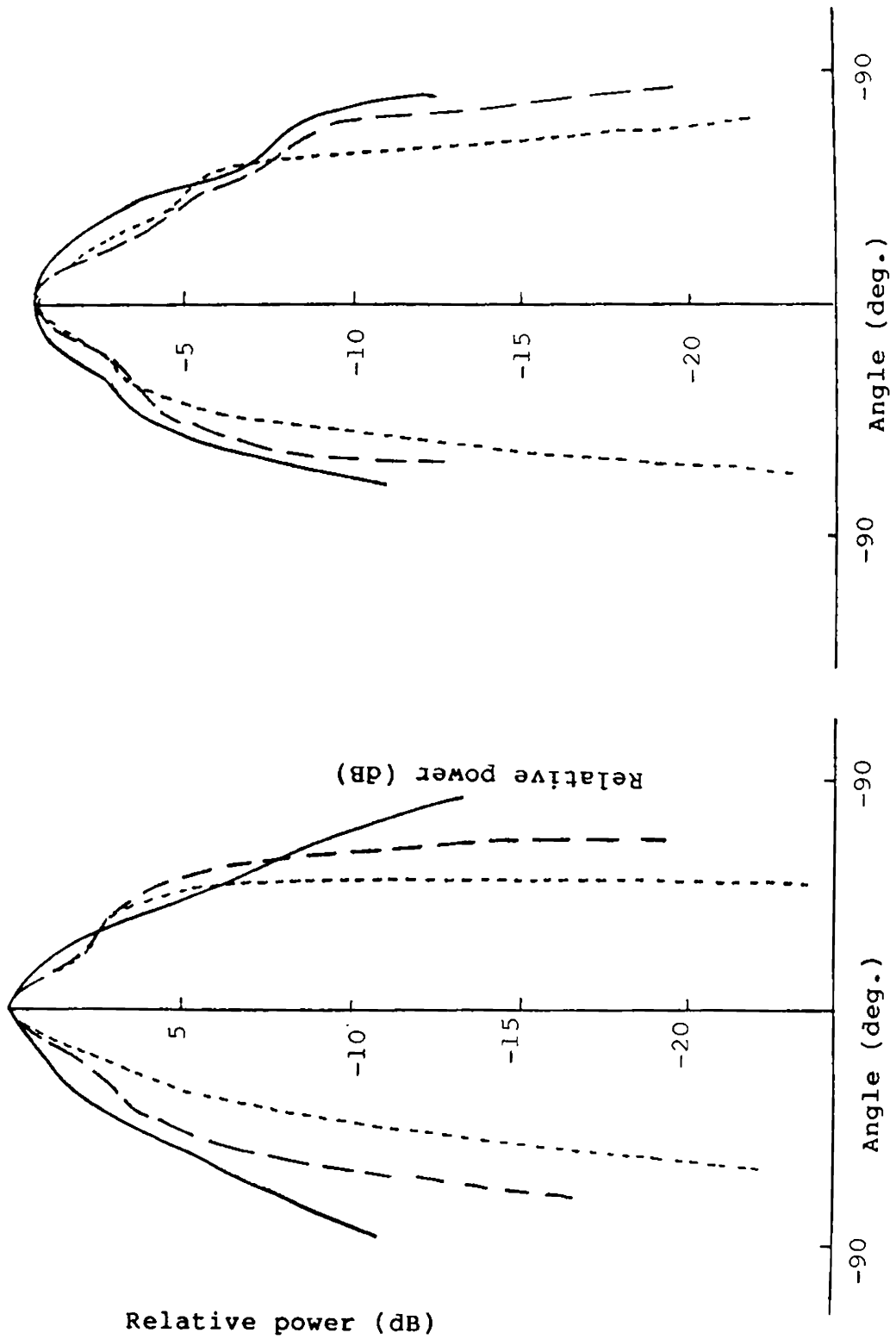


Fig.AI(G) E-plane and H-plane radiation patterns of the test antenna
 865 MHz, - - - 917 MHz, 969 MHz

corresponds to the patch with the lumped impedance connected. It can be seen that the 2:1 VSWR bandwidth of the antenna has been improved considerably i.e., from 5 MHz for the single patch to 106 MHz for the patch with shunt impedance. A similar plot for the antenna configuration shown in Fig.AI(D) is shown in Fig.AI(F). The radiation patterns recorded for this antenna system at three different frequencies is shown in Fig.AI(H). It is clear from these graphs that the patterns are not deteriorated by the use of this technique.

I.5 CONCLUSIONS

The above experimental observations suggest that the bandwidth of the microstrip antenna can be improved by nearly 10% by the use of a shunt impedance connected between the non-radiating edge of the patch and the ground plane. The resulting patterns do not show any frequency squinting. A comparison of the results with those in reference [33] show that the antenna bandwidth can be almost doubled while the antenna size could be reduced by half by adopting this technique. However, the efficiency of the antenna is slightly less owing to losses in the lumped impedance.

Appendix II

A COMPACT DUAL FREQUENCY MICROSTRIP ANTENNA

	<u>Page</u>
II.1 Introduction ..	160
II.2 Antenna Geometry and Experimental Details ..	160
II.3 Results and Discussions ..	162
II.4 Conclusion ..	164

APPENDIX II

A COMPACT DUAL FREQUENCY MICROSTRIP ANTENNA

II.1 INTRODUCTION

Dual frequency antennas are useful in systems where the antenna is required to operate at two distinct frequencies. A single patch antenna cannot often radiate efficiently at the two frequencies due to their inherent bandwidth limitation. There are different techniques used for achieving dual frequency operation of microstrip antennas. One technique is by employing stacked elements [34]. A second method is by using a single element with multiple feeds [35]. The use of tabs [36] and shorting pins [37] also aids in dual frequency operation. In this section, a new compact microstrip antenna structure for dual frequency operation is described.

II.2 ANTENNA GEOMETRY AND EXPERIMENTAL DETAILS

A sketch of the geometry studied is shown in Fig.AII(A). A rectangular ring patch with a small gap on one of its sides was etched on a RT Duroid substrate with a

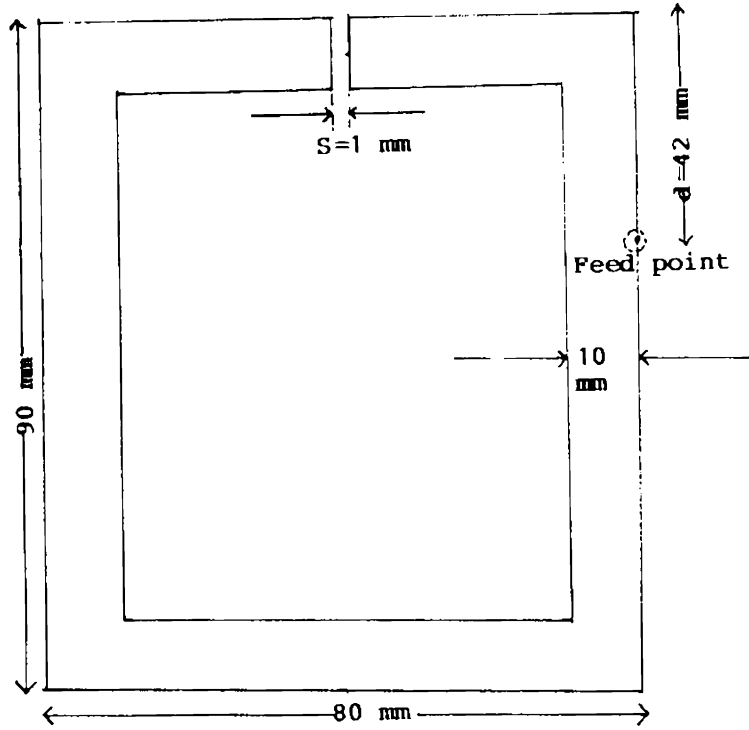


Fig.AII(A)Geometry of the Antenna Element.

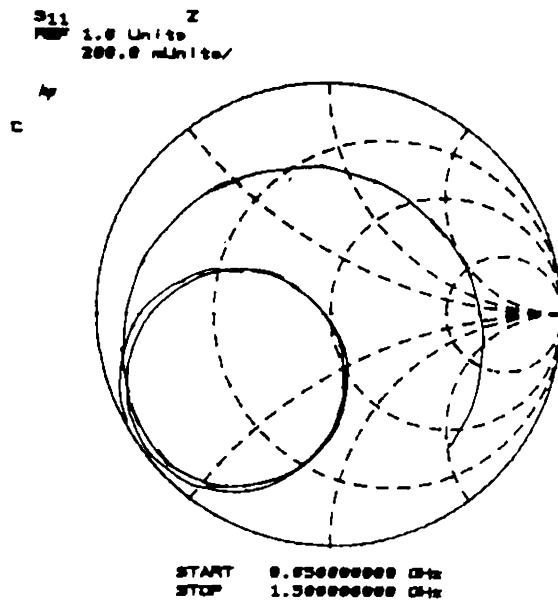


Fig.AII(B) Impedance plot of the Antenna shown in Fig(1).

dielectric constant of $\epsilon_r = 2.2$ and of thickness 0.08 cm. The dimensions of the patch has been arrived at by experimental iterations. The antenna was edge fed with a coaxial probe. Two loops were observed in the impedance chart indicating two radiating frequencies for the antenna. The position of the feed point was adjusted so that the loops are in the vicinity of 50Ω region. The results were then plotted using the automatic network analyzer and the plotter. The E-plane and H-plane radiation patterns were also plotted as explained in Appendix I.

II.3 RESULTS AND DISCUSSIONS

The impedance characteristics and the return loss of the antenna are shown in Figs.AII(B) & AII(C) respectively. It can be seen that the antenna is well matched to the two resonant frequencies, 705 MHz and 1062 MHz. The recorded E-plane patterns for the antenna at two different frequencies are shown in Fig.AII(D). The radiations at the two frequencies were orthogonally polarized. The patterns do not show any frequency squinting. The cross-polar components measured were found to be nearly 22 dB down the co-polar maxima.

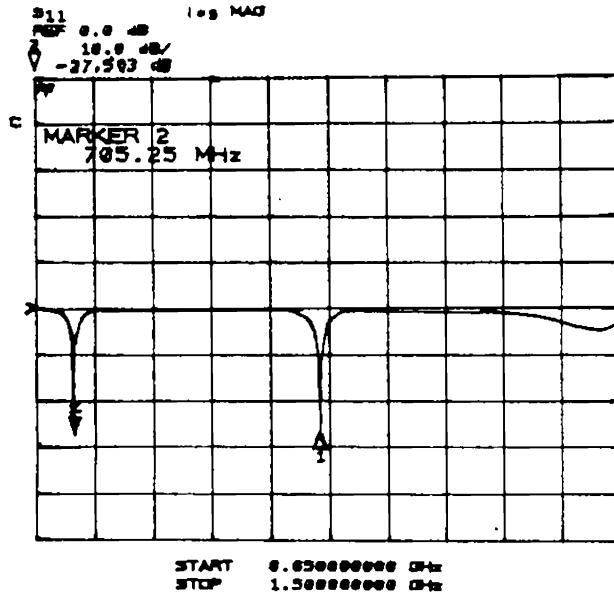


Fig.AII(C) Measured Return Loss.
Marker 1 = 1062 MHz.

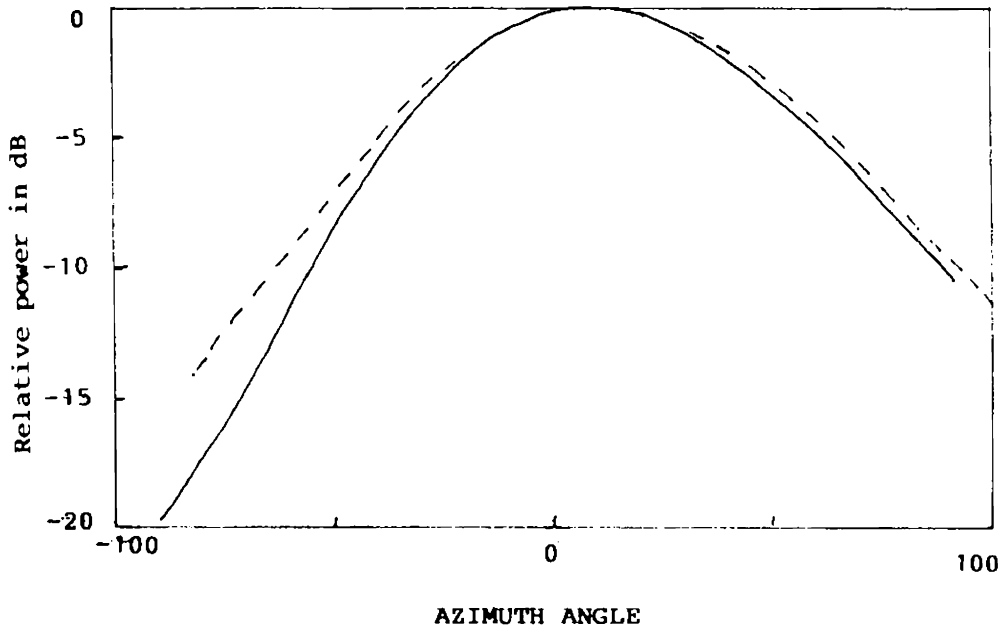


Fig.AII(D) E-plane Radiation pattern of the Antenna.
———— 1062 MHz ———— 705 MHz.

It has been observed that the width 'W' play an important role in the impedance matching of the antenna at the two frequencies. Increasing or decreasing the width from 10 mm showed that there is a mismatch at any one of two resonant frequencies. This experiment was performed at the UHF band. This dimension may change at a different band of operation. The resonant frequencies of the antenna can be selected by properly choosing the internal and external dimensions of the ring, keeping the difference between the two dimensions as 10 mm. A slight tuning of the resonance frequencies are possible by adjusting the gap width. As the gap width is increased, both resonances were found to shift to the higher frequency side. However, increasing the gap width will reduce the efficiency as the total radiation aperture is reduced.

II.4 CONCLUSIONS

Employing the microstrip antenna structure described in this section, it is possible to operate a single antenna at two distinct frequencies. The antenna is compact compared to other dual frequency antennas and the radiation characteristics do not deviate much from the

normal patterns. An additional feature of these antennas is that a lower resonant frequency can be achieved with a smaller patch size as compared to other dual frequency microstrip antennas.

Appendix III

BANDWIDTH ENHANCEMENT BY A FLARED MICROSTRIP DIPOLE ANTENNA (FMDA)

	<u>Page</u>
III.1 Introduction	.. 167
III.2 Experimental Details	.. 167
III.3 Test Results	.. 169
III.4 Conclusion	.. 171

APPENDIX III

BANDWIDTH ENHANCEMENT BY A FLARED MICROSTRIPDIPOLE ANTENNA (FMDA)

III.1 INTRODUCTION

In 1984, Bailey [38] has reported that using a half-wave dipole configuration for microstrip antennas, their impedance bandwidth can be considerably improved. The results of a detailed experimental investigation on exploring the possibility of further enhancement of impedance bandwidth are presented in this Appendix. This has been achieved by optimizing the shape of the elements and the feed positions. The new configuration do not adversely affect the efficiency of the antenna.

III.2 EXPERIMENTAL DETAILS

The schematic diagram of the Flared Microstrip Dipole Antenna (FMDA) is shown in Fig.AIII(A). It consists of two flat arms etched on both sides of a low loss dielectric substrate ($\epsilon_r = 4.2$) of thickness 0.16 cm. An arm-angle of 7° was selected after experimental iterations

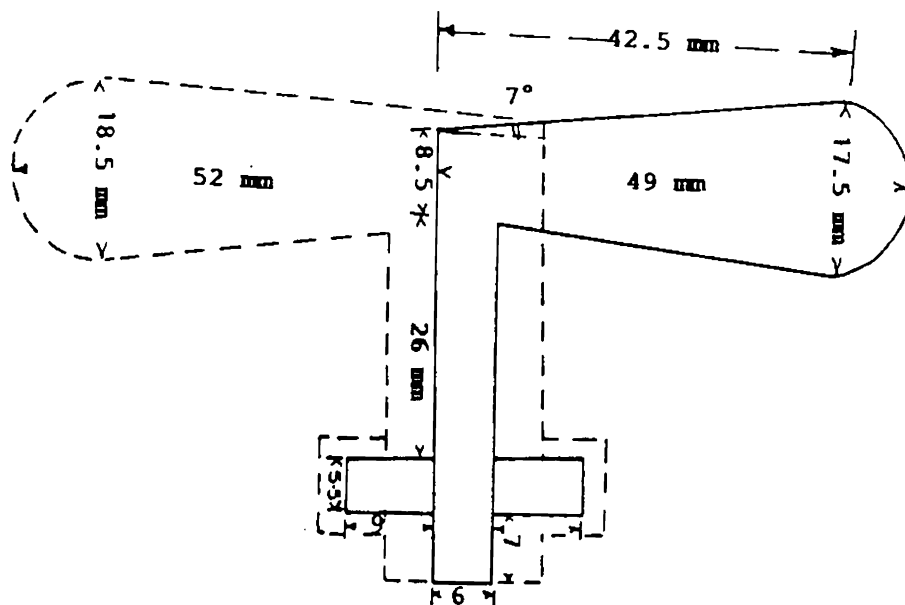
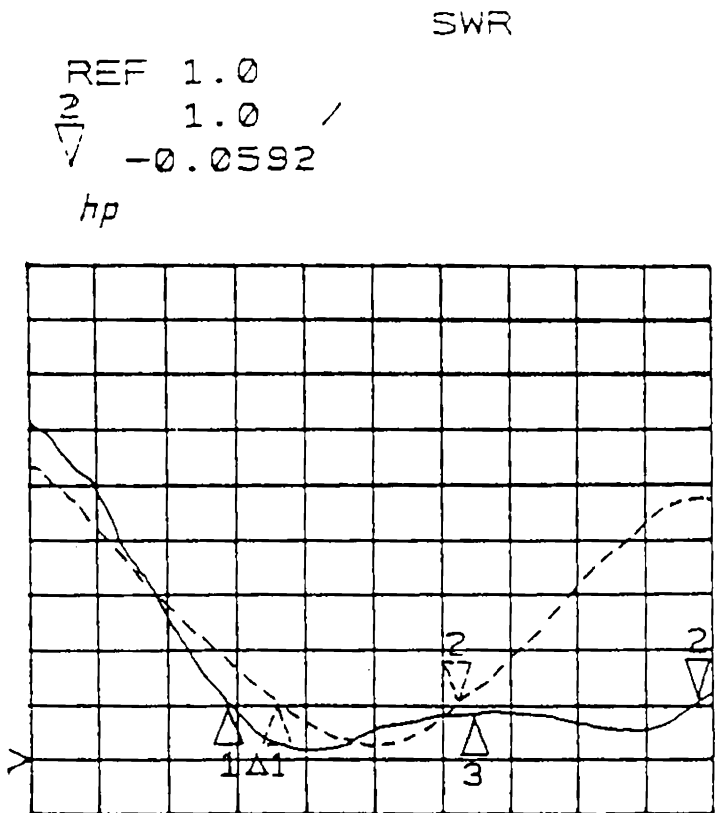


Fig.AIII(A) Geometry of the PMDA Antenna. All the dimensions are in millimeters. Dotted patr is etched on the other side of the substrate.



START 0.899000000 GHz
 STOP 1.504000000 GHz

Fig.AIII(B) Variation of SWR with frequency.
 — PMDA - - - - Ordinary Dipole.

for best performance characteristics. Experiments have shown that for better radiation efficiency, one arm has to be slightly shorter in dimension by 0.012λ . For better impedance bandwidth an open circuited stub was also used as shown in Fig.AIII(A).

The FMDA characteristics were studied using the test set up described in Appendix I. For comparing the performance a conventional stub-matched dipole was also studied. The results are presented in the following paragraph.

III.3 TEST RESULTS

In Fig.AIII(B) the impedance bandwidth of the FMDA is shown. The plot also includes the impedance bandwidth of a conventional stub-matched antenna. It is clear from the plots that the 2:1 VSWR bandwidth of the FMDA is 415 MHz while that of conventional dipole is only 150 MHz, for a centre frequency of 1200 MHz. In Fig.AIII(C) the radiation efficiency of the two antennas are compared. It can be seen that the FMDA is radiating more power in the frequency band of interest than the conventional antenna. This confirmed that the enhancement in bandwidth are not followed by losses.

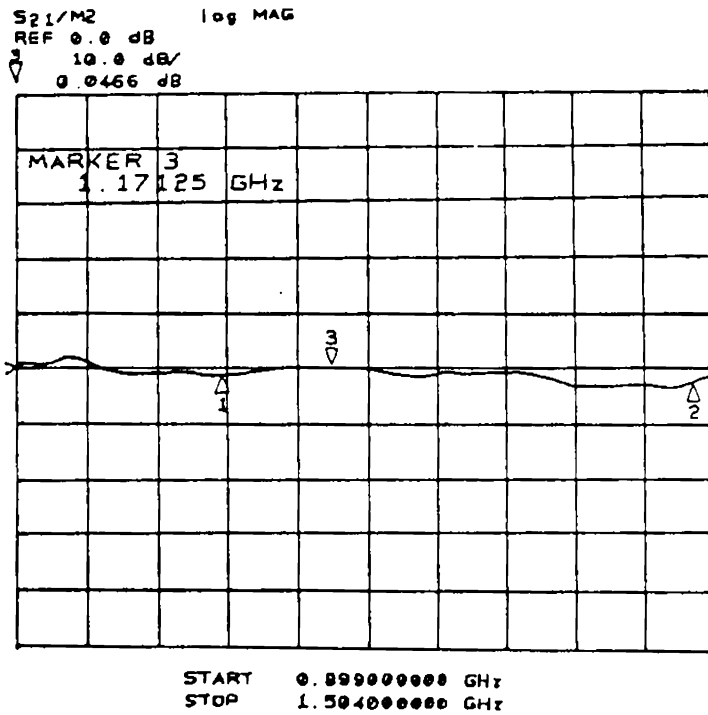


Fig.AIII(c) Difference in gain between FMDA and ordinary Dipole. S₂₁ is for ordinary Dipole and M₂ is for FMDA.

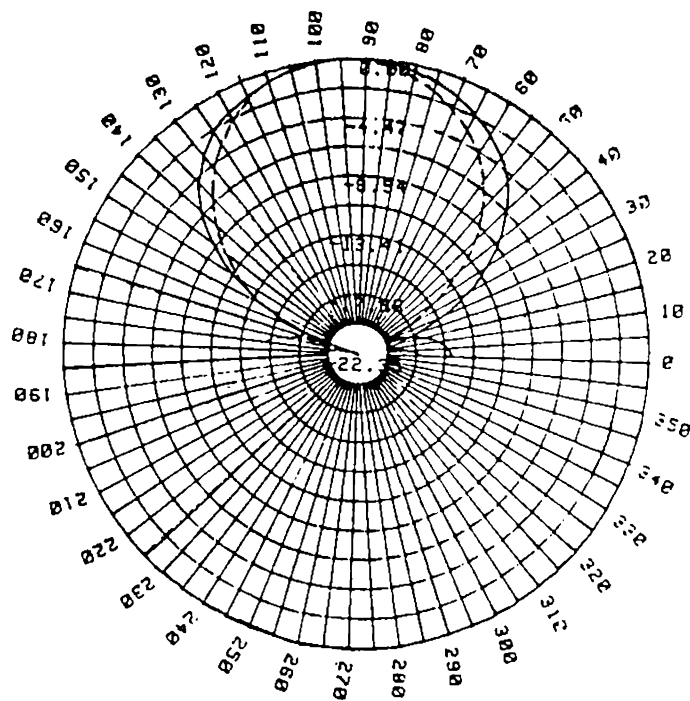


Fig.AIII(D) Typical E-plane radiation pattern of FMDA.
 ——— 1 GHz - - - - - 1.4 GHz.

Typical radiation patterns of the FMDA for two different frequencies are presented in Fig.AIII(D). As is evident from these plots the antenna is free from frequency squinting like the conventional dipole antenna. The experiments have also shown that a unidirectional pattern with enhanced gain can be obtained by placing a reflector at a distance of 0.22λ from one face of the antenna.

III.4 CONCLUSIONS

Optimized design of an FMDA is given in this Appendix. The system has broad bandwidth of conventional dipole antenna. The enhancement in bandwidth are not accompanied by any losses. The FMDA antenna will be a real substitute for conventional dipoles in phased array antennas for terrestrial applications. Further work on these types of antennas may lead to more interesting results.

REFERENCES

1. A.H.Ryan and S.D.Summers: "Microwaves used to observe commutator and slip ring surfaces during operation", *Electrical Engineering, N.Y.*, 73, (1954), 251-55.
2. M.R.E.Bichara and J.P.R.Poitevin: "Resistivity measurement of semiconducting epitaxial layers by the reflection of a hyperfrequency electromagnetic wave", *IEEE Trans. on Inst. and Measure.*, 13, (1964), 323-28.
3. Dr.S.Doraiswamy: "Microwave as an NDT tool", Report on Microwave Non-Destructive Test methods, copy of document from VSSC, Trivandrum, October, (1984).
4. C.N.Owston: "Eddy current testing at microwave frequencies", *Non-Destruct. Test.*, 2, (1969), 193-96.
5. J.B.Beyer, J.V.Bladel and H.A.Peterson: "Microwave thickness detector", *Rev.Sci.Inst.*, 31, (1960), 313-16.
6. D.J.H.Wort: "Method of measuring dynamic clearances, microwave interferometry as an NDT", *Non-Destruct. Test.*, 4, (1971), 380-81.

7. A.Husain and C.A.Ash: "Microwave scanning microscopy for NDT", 5th European microwave conference, Hamburg, 1-4, September (1975), 213-17.
8. T.M.Lavelle: "Microwaves in non-destructive testing", Mater. Evaluation, 25, (1967), 254-58.
9. D.Whistlecroft: "Microwave thickness measurement of dielectric materials", J.British Instn. Radio Engrn., 23, (1963), 151-55.
10. M.Tuiri et al.: "A microwave instrument for measurement of small inhomogeneties in supercallender rollers and other dielectric cylinders", J. of Microwave Power, 9(2), (1974), 117-21.
11. N.Rockowitz and L.McCuire: "A microwave technique for the detection of voids in honeycombed ablative materials", Mater. Evaluation, 24, (1966), 105-08.
12. R.C.Stinebring and R.H.Harrison: "Non-destructive testing of rocket components using microwaves and low frequency ultrasonics", Mater. Evaluation, January, (1965), 17-23.

13. D.S.Dean and D.T.Green: "The use of microwaves for detection of flaws and measurement of erosion rates in materials", J.Sci.Inst., 44, (1967), 699-701.
14. B.Forssell: "Non-destructive measurements of the glass fibre content in reinforced plastics by means of microwaves", 4th European microwave conference, 10-13, September, (1974), 132-36.
15. Dr.K.N.Shankara and S.Balasubramanian: "Microwave techniques in non-destructive testing", Report on a feasibility study conducted for ATIRA (Ahmedabad Textile Industries Research Association) by Space Application Centre, Ahmedabad.
16. Eiji Tanabe and William T.Joines: "A non-destructive method for measuring the complex permittivity of dielectric materials at microwave frequencies using an open transmission line resonator", IEEE Trans. on Inst. Measure., Vol.IM-25, September, (1976), 222-26.
17. M.C.Decreton and M.S.Ramachandraiah: "Non-destructive measurements of complex permittivity for dielectric slabs", IEEE Trans. on Microwave Theory and Techniques, MTT-23, (1975), 1077-80.

18. T.Itoh: "A new method for measuring properties of dielectric materials using a microstrip cavity", IEEE Trans. on Microwave Theory and Techniques, MTT-22, (1974), 572-76.
19. O.Hashimoto and Y.Shimizu: "Reflecting characteristics of anisotropic rubber sheets and measurement of complex permittivity tensor", IEEE Trans. on Microwave Theory and Techniques, Vol.MTT-34, (1986), 1201-07.
20. Reza Zoughi and Sasan Bakhtiri: "Microwave non-destructive detection and evaluation of disbonding and delamination in layered dielectric slabs", IEEE Trans. on Inst. and Measure., Vol.39, No.6, December, (1990), 1059-63.
21. Marianne Gex-Fabry, Juan R.Mosig and Fred E.Gardiol: "Reflection and radiation of an open-ended circular waveguide: Application to non-destructive measurement of materials", Electronics and Communication (AEU), Band 33, (1979), 473-78.
22. J.R.Mosig, J.E.Besson, M.Gex-Fabry and F.E.Gardiol: "Reflection of an open-ended coaxial line and application to non-destructive measurement of materials", IEEE Trans. on Inst. and Measure., IM-30, (1981), 46-51.

23. S.Summerhill: "Microwaves in the moisture measurement", Instrument Review (British), 14, (1967), 419-22.
24. H.B.Tayler: "Microwave moisture measurement", Industrial Electronics (British), February, (1965), 66-70.
25. D.S.Dean and L.A.Kerridge: "Microwave techniques; in research techniques in non-destructive testing", ed. R.S.Sharpe, Academic Press (N.Y), Chapter 13.
26. R.Hochschild: "Application of microwaves in non-destructive testing", Non-destruct. Test., 21, (1963), 115-20.
27. G.Wittig and Bam: "About antenna problems in the application of microwaves in NDT", 8th World Conference on Non-destructive testing, September, (1976), 1-8.
28. H.M.Barlow and A.L.Cullen: "Microwave measurements", Constable and Company, London, (1950).
29. S.Roberts and A.Von Hippel: "New method of measuring dielectric constant and loss in the range of centimeter waves", J.Appl.Phys., Vol.17, No.7, (1946), 610-16.

30. T.W.Dakin and C.N.Works, "Microwave dielectric measurements", J.Appl.Phys., Vol.18, No.9, (1947), 789-96.
31. H.T.Al-Hafid, B.R.Vishwakarma and H.M.Al-Rizzo: "Complex dielectric constant of sand and dust particles at 11 GHz as a function of moisture content", Ind.Jour.Radio and Space Phys., Vol.14, No.2, (1985), 21-24.
- 31(A). K.C.Gupta: "Broadbanding techniques for microstrip patch antennas--A review" - A Report (Department of Electrical and Computer Engg., University of Colarado).
32. C.K.Aanandan and K.G.Nair: "Compact broad band microstrip antenna", Elec.Lett., Vol.22, September, (1986), 1064-65.
33. C.K.Aanandan: "Compact broad-band microstrip antennas using parasitic elements", Ph.D. Thesis, Cochin University of Science and Technology, (1989).
34. S.A.Long and M.D.Walton: "Dual frequency stacked circular disc antenna", IEEE Trans., AP-27, (1979), 255-58.

35. G.Gronan, H.Moschuring and I.Wolff: "Input impedance of a rectangular microstrip resonator fed by a microstrip network on the back side of the substrate", 14th European Microwave Conference, Liege, (1984), 625-30.
36. W.F.Richards, S.E.Davidson and S.A.Long: "Dual band reactively loaded microstrip antenna", IEEE Trans., AP-33, (1985), 556-61.
37. S.S.Zhong and Y.T.Lo: "Single element rectangular microstrip antenna for dual frequency operation", Electron Lett., 19, (1983), 298-300.
38. M.C.Bailey: "Broad band half-wave dipole", IEEE Trans. Antennas Propagat., 32, (1984), 410-12.

INDEX

- Accelerated curing 134
 Amplitude pattern 42,44,70
 Anechoic chamber 151
 Angular displacement 87,88
 Antenna 13
 microstrip 148,158
 microstrip dipole 167
 Artificial flaw 42
 Ash 17
 Attenuators 10
 Attenuation constant 54

 Bailey 167
 Bam 22
 Bichara 15

 Cavity method 36
 cylindrical 70
 Crystal detectors 10
 Curing 136
 temperature 51,137
 Cylindrical void 129

 Dean 21
 Decreton 20
 Defect characterization 120
 detection 120
 location 88
 minimum size 76,82,127
 multiple 87
 Defective sample 129
 Destructive test 133
 Dielectric constant 51,52,54,
 55,59,63,136
 Dipole 149
 broadband 149
 flared microstrip 167
 Directional coupler 57
 Driven element 155

 Eiji Tanobe 19
 Electrical properties 63,113,134

 Fabry 20
 Feinstein 15
 Flanges 41
 Flaw artificial 99
 characterization 61
 cylindrical 43,62,76,82
 detection 61
 location 61
 localized 121,125,126
 rectangular 44,49,62
 size 44
 Forssell 19
 Free wave method 36
 Frequency meter 11

 Green 19,21
 Guided wave method 36
 Gunn diode 9

 Half-wave dipole 167
 Harrison 18,21
 Hashimoto 20
 Hochschild 22
 Homogenous 124
 Hruby 15
 Hussain 17

 Impedance
 bandwidth 148,167,169
 lumped 155,158
 locus 155
 shunt 158
 Inhomogeneity 122,123
 Isolators 12
 Itoh 20
 Lavelle 17,21,22
 Loss tangent 106

 Magic Tee 12,17
 Mandrel 45,63,73
 Matched load 12
 Mechanical property 63,134

- McCuire 18
 Metal 14
 Metallic inclusion 122
 Microwave imaging 127
 Millimeter waves 131,132
 Network analyzer 42,59,64
 82,140
 Non-metal 17
 Owston 16
 Phase pattern 42,44
 Poetevin 15
 Propellant
 composition I 106,132
 composition II 106,132
 mix 99
 paste 137
 Q-factor 148
 Radar cross-section 129
 Radiation efficiency 169
 pattern 149,151,155
 158,171
 Ramachandriah 20
 Reference sample 124
 Reza-Zoughi 20
 Rockowitz 18
 Ryan 15
 Sasan Bakhtiari 20
 Shimizu 20
 Silent zone 151
 Slurry form 51
 Standing wave ratio 54
 Stinebring 18,21
 Stub-matched dipole 169
 Summers 15
 Taylor 22
 Techniques
 metal reflection 14,29
 non-metal reflection 17,29
 scattering 21
 transmission 21,33
 eddy current 16
 Tensile strength 133
 Transcendental equation 54
 Turi 18
 Turn-table 42
 Unidirectional pattern 171
 von Hippel 52
 VSWR 135,158
 Waveguides 10
 Waveguide method 36
 Whistlecroft 17
 William T Joines 19
 Wittig 22
 Wort 16

LIST OF PUBLICATIONS OF THE AUTHOR

1. "A microwave method for testing inhomogenities in cured rocket propellant", NDT International, (U.K), Vol.17, No.5, pp.277-79, 1984.
2. "A microwave NDT method for locating inhomogenities in cured rocket propellant samples", NDT International (U.K), Vol.19, No.4, pp.395-97, 1986.
3. "A microwave method for monitoring the curing conditions of a solid rocket propellant", NDT International (U.K), Vol.19, No.4, pp.398-400, 1986.
4. "Location of flaws and non-uniformities inside non-metallic bodies using microwave NDT", National Symposium on NDT, BARC, DAE, Bombay, 1986.
5. "Development of a microwave NDT facility for testing curing state and other parameters of solid rocket propellants", ISRO Technical Report (RESPOND), pp.1-9, 1986.

6. "Microwave techniques for the NDT of solid rocket propellants", Quality evaluation (India), Vol.6, No.1, pp.1-3, 1986.
7. "A novel multioctave microstrip antenna", Proc. on National Conference on Electronic Circuits and Systems, NACONECS-89, Roorkee, pp.49-51, 1989.
8. "A new microstrip antenna for improved impedance bandwidth", Proc. of the National Symp. on Microwave Antennas and Propagation, APSYM-90, CUSAT, Kochi, pp.329-32, 1990.
9. "Bandwidth enhancement of microstrip antenna using shunt impedance technique" Presented in the 77th Session of Indian Science Congress, ISCA-77, CUSAT, Kochi, 1990.
10. "Bandwidth enhancement by flared microstrip dipole antenna", Accepted in 1991 IEEE AP-S International Symp., Canada, 1991.